

Mass and Isotope Selective Infrared Spectroscopy

M. Hippler, E. Miloglyadov, M. Quack, G. Seyfang

ETH Zürich, Laboratory of Physical Chemistry, Wolfgang-Pauli-Str. 10,
CH-8093 Zürich, Switzerland, Email: Martin@Quack.ch

reprinted from

“Handbook of High-Resolution Spectroscopy”

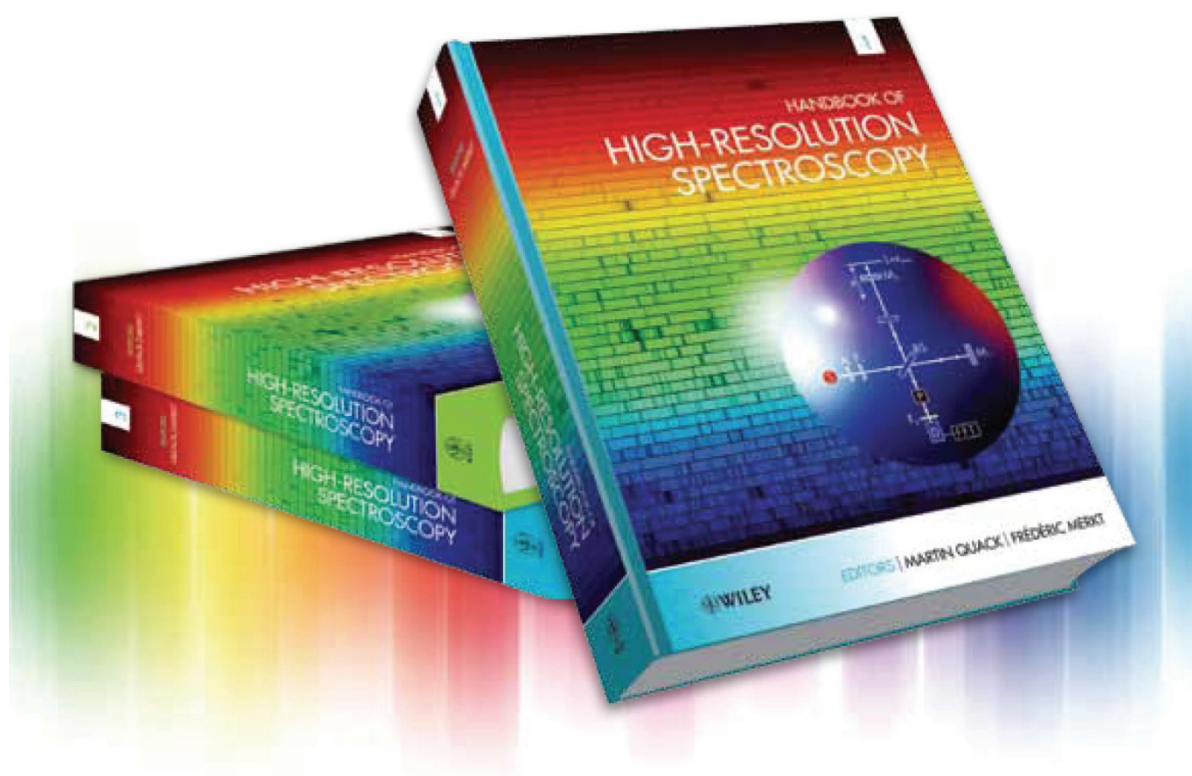
Vol. 2, chapter 28, pages 1069–1118

M. Quack, and F. Merkt, Eds. Wiley Chichester, 2011,

ISBN-13: 978-0-470-06653-9.

Online ISBN: 9780470749593,

DOI: 10.1002/9780470749593.



with compliments from Professor Martin Quack, ETH Zürich

Abstract

Recent advances in laser spectroscopic techniques make it possible to obtain mass- and isotope-selective infrared spectra of gas-phase species at high resolution and reduced hot-band spectral congestion. In these techniques, infrared excitation is coupled with ultraviolet multiphoton ionization and detection of the resulting ions in a mass spectrometer, which allows the separation of contributions of different isotopomers and, more generally, species of different mass in a mixture. In combination with jet cooling techniques, spectra are obtained for very cold molecules. These spectra can then be analyzed to extract information on dynamical processes such as intramolecular vibrational redistribution or tunneling and rearrangement processes, and on how intramolecular dynamics is influenced by vibrational excitation and isotope effects. In this review, we introduce isotope-selective infrared spectroscopic techniques and present some selected applications on isotope effects and intramolecular dynamics of vibrationally excited chloroform, aniline, and benzene obtained by isotope-selective infrared spectroscopy.

Keywords: isotopes; infrared spectroscopy; vibrations; intramolecular vibrational redistribution; tunneling; intramolecular dynamics; laser spectroscopy; mass-selective spectroscopy

Mass and Isotope-selective Infrared Spectroscopy

Michael Hippler¹, Eduard Miloglyadov², Martin Quack²
and Georg Seyfang²

¹*Department of Chemistry, University of Sheffield, Sheffield, UK*

²*Laboratorium für Physikalische Chemie, ETH Zürich, Zürich, Switzerland, martin@quack.ch*

1 INTRODUCTION

The present review deals largely with mass- and isotope-selective infrared spectroscopy as developed in our laboratory in terms of OSVADPI (overtone spectroscopy by vibrationally assisted dissociation and photofragment ionization), ISOS (isotopomer-selective overtone spectroscopy) and IRSIMS (infrared spectroscopy with isotope and mass selection) over the last two decades (Hippler and Quack 1994, 1995, 1996, 1997, Fehrensens *et al.* 1998, Hippler *et al.* 2003). In providing such a review concentrating on the work outlined above, we should, nevertheless, make it clear that high-resolution molecular spectroscopy, by its nature, is mass and isotope selective. This selectivity arises from the mass dependence of the Doppler line width and also, of course, from the dependence of the rotational line structure of the spectra upon the mass and even the mass distribution within the molecular structure. There are, however, several techniques that make very explicit use of mass selection by means of mass spectrometers in the detection step and we refer to these techniques in particular (Page *et al.* 1987, 1988a,b). We shall make a reference to some of this work in the course of our article, although we should make it clear that a complete coverage of the field is by no means intended. We also refer to the related but not identical topic of the spectroscopy of mass-selected molecular ions, reviewed by Duncan (2000).

The main goal of the present article is to make the essential contents of an earlier review more easily available

Handbook of High-resolution Spectroscopy. Edited by Martin Quack and Frédéric Merkt. © 2011 John Wiley & Sons, Ltd.
ISBN: 978-0-470-74959-3.

in the framework of the present handbook, which should provide a rather complete and compact coverage without the necessity to search for extra information in the older literature. We therefore draw large sections of the present article from our previous review (Hippler and Quack 2006), updating as appropriate. In some parts, we reduce coverage to some extent, and in other parts, we extend it. The review is structured as follows: we start with two sections providing introductory surveys of general principles of isotope effects in spectra (Section 2) and an overview of isotope-selective spectroscopy in relation to intramolecular dynamics (Section 3). In Section 4, we provide a simple introduction to the concepts of the kinetics of intramolecular dynamics as derived from spectroscopy with high frequency resolution but not time resolution. Section 5 presents details of our IR + UV two-frequency experiments for the IRSIMS. Section 6 deals with results from the OSVADPI technique and Sections 7 and 8 with ISOS.

2 PRINCIPLES OF ISOTOPE EFFECTS IN INFRARED SPECTROSCOPY AND MOLECULAR DYNAMICS

Molecular isotope effects arise from four conceptually distinct origins connected to different properties of the isotopic nuclei:

1. mass differences
2. different spins
3. different “Pauli” identities
4. different electroweak charge of the isotopes.

Although in practice the four qualities come as combinations when changing one isotope against another, one can, nevertheless, identify certain limiting situations, where one quality becomes dominant; we shall discuss these in turn in our general introduction to this article.

1. Mass differences of the isotopes are the most common source of molecular isotope effects and these are discussed in, for instance, Bauder 2011: **Fundamentals of Rotational Spectroscopy**, Albert *et al.* 2011a: **Fundamentals of Rotation–Vibration Spectra**, Albert *et al.* 2011b: **High-resolution Fourier Transform Infrared Spectroscopy**, Wörner and Merkt 2011: **Fundamentals of Electronic Spectroscopy**, Snels *et al.* 2011: **High-resolution FTIR and Diode Laser Spectroscopy of Supersonic Jets**, this handbook, as well as in many chapters in *Isotope Effects in Chemistry and Biology* (Kohen and Limbach 2006), for instance, in Bigeleisen (2006), Wolfsberg (2006), and Hippler and Quack (2006) forming, as mentioned, the basis for the present article. The difference in infrared spectra of isotopomers can be understood to lowest order by the change of harmonic wavenumber $\tilde{\omega}_e$ of a harmonic oscillator

$$\tilde{\omega}_e = \frac{\nu}{c} = \frac{1}{2\pi c} \sqrt{\frac{f}{\mu}} \quad (1)$$

and by a change of rotational constant of a rigid rotor (as wavenumber), here, for example, of a diatomic molecule:

$$B_e = \frac{h}{8\pi^2 c \mu r_e^2} \quad (2)$$

Here c is the speed of light in vacuum, and f is the force constant of the oscillator as the second derivative of the potential energy $V(r)$ at the equilibrium bond length r_e :

$$f = \left(\frac{\partial^2 V(r)}{\partial r^2} \right)_{r=r_e} \quad (3)$$

which is independent of isotopic substitution as is also the bond length r_e at equilibrium (minimum of V) in the Born–Oppenheimer approximation. On the other hand, the reduced mass μ changes strongly for different isotopomers, say in diatomic molecules with

$$\mu = \frac{m_A \cdot m_B}{m_A + m_B} = \left(\frac{1}{m_A} + \frac{1}{m_B} \right)^{-1} \quad (4)$$

with the masses m_A and m_B of the two nuclei. Through the approximate energy-level expressions of

the harmonic oscillator–rigid rotor energies

$$\frac{E_v}{hc} = \tilde{\omega}_e \left(v + \frac{1}{2} \right) \quad (5)$$

with vibrational quantum number $v = 0, 1, 2, \dots$ and

$$\frac{E_J}{hc} = B_e J(J + 1) \quad (6)$$

with the rotational quantum number $J = 0, 1, 2, \dots$, the change in the masses of isotopes of atom A or B through a change of μ , B_e , and $\tilde{\omega}_e$ leads to the obvious and, indeed, dramatic changes in the energy-level structure and the corresponding transition wavenumbers observed in infrared spectra of diatomic molecules: H/D isotope substitution often leads to wavenumber shifts of hundreds of cm^{-1} , and even $^{13}\text{C}/^{12}\text{C}$ shifts are easily several tens of cm^{-1} , whereas $^{35}\text{Cl}/^{37}\text{Cl}$ -isotope shifts are observable only at higher resolution, but nowadays in a standard way even in an undergraduate student spectroscopy laboratory. Extending these considerations from diatomic to polyatomic molecules (Herzberg 1945, 1950, Wilson *et al.* 1955, Hollas 1982, Papoušek and Aliev 1982), one frequently obtains comparable mass-dependent isotope shifts in the rigid rotor harmonic oscillator approximation. The situation can become more complex in reality, as some vibrations may show very little isotope shifts and spectral congestion may prevent their resolution, a point to which we shall return. However, the principles of the mass-dependent isotope effects are rather well understood even when including anharmonicity and nonrigidity as well as non-Born–Oppenheimer effects. The effect is generally large with large relative reduced mass differences and would vanish in the limit where $|(\mu_1 - \mu_2)/\mu_1|$ approaches zero (or μ_1/μ_2 approaches 1). Mass-dependent isotope effects are also important in reaction dynamics, particularly when tunneling or resonances become important (Fehrens *et al.* 1999b, Fernandez-Alonso *et al.* 2000, Bean *et al.* 2001, Ayers *et al.* 2003). It is well known that tunneling splittings in the spectra are extremely sensitive to the effective reduced tunneling mass both with involvement of light elements (H/D) (Bell 1980) and also heavier isotopes ($^{35}\text{Cl}/^{37}\text{Cl}$) (Quack and Willeke 2006).

2. The second isotope effect in spectra and dynamics arises from different nuclear spins of the isotopes. This is most obvious in nuclear magnetic resonance (NMR) spectra, determining even the existence (say for ^{13}C isotopes) or absence (for ^{12}C) of such spectra (Ernst 1992, Ernst *et al.* 1997), but in combination with the Pauli Principle (3) it also determines

the relative strength of spectral lines in microwave, infrared, and optical spectra via nuclear spin statistical weights and strengths of spectral lines, including also the possibility of the presence or absence of such lines (Rabi 1937, Limbach 1990, Ernst 1992, Ernst *et al.* 1997, Albert *et al.* 2011a,b). It would, in principle, occur with isotopes of different spin even in the limit where $(\mu_1/\mu_2) \rightarrow 1$. Although in practice, there will always be a mass difference, for very heavy isotopes this ratio may approach 1, whereas the spin effects remain (Limbach *et al.* 2006).

3. The third case of isotope effects in molecular dynamics is even more subtle as it would appear for isotopes with $(\mu_1/\mu_2) \rightarrow 1$ and nuclear spins $I_1 = I_2$. This arises entirely because of symmetry selection rules in spectra and because of the dynamics of different isotopomers being different. Literally, it might become dominant for nuclear isomers of almost the same mass and the same spin (say $I_1 = I_2 = 0$), a fairly exotic situation, but it may also contribute in other situations. It was apparently first postulated to be of potential importance in state-to-state chemical dynamics of heavy isotopes or nuclear isomers in 1977 (Quack 1977, 1983a) and has since then been discussed to be at the origin of certain observations of isotope effects in chemical systems (Weston 1999, 2006). To our knowledge, no firm spectroscopic example of this type has really been studied in isolation from the other two effects (1) and (2), but it is, of course, always present in combination with these in spectroscopy because of the symmetry selection rules (*see also* Quack 2011: **Fundamental Symmetries and Symmetry Violations from High-resolution Spectroscopy**, this handbook).
4. While the three isotope effects mentioned so far can be understood on the basis of quantum mechanics and physics of the first half of the twentieth century, the last molecular isotope effect to be mentioned here is related to electroweak parity violation and the electroweak nuclear force influencing molecular dynamics. These phenomena have become subject of theoretical investigations only during the last few decades, with some striking recent advances in the framework of new developments in electroweak quantum chemistry (Bakasov *et al.* 1996, 1998, 2004, Berger and Quack 2000, Quack and Stohner 2003, 2005, Quack *et al.* 2008). While the electric charge $q_e = Z_A \cdot e$ for different isotopes of the same element is the same, the electroweak charge

$$Q_w(A) = Z_A(1 - 4 \sin^2 \Theta_w) - N_A \quad (7)$$

is different for different isotopes (with proton number Z_A and neutron number N_A , Θ_w -Weinberg angle), because of the different N_A . Therefore, the electroweak electron nucleus interaction mediated by the Z-boson as a contactlike interaction is different for different isotopes with the approximate parity-violating Hamiltonian

$$\hat{H}_{pv} = \frac{\pi G_F}{hm_e c \sqrt{2}} \sum_{A=1}^N Q_w(A) \times \sum_{i=1}^n [\mathbf{p}_i \mathbf{s}_i, \delta^3(\mathbf{r}_i - \mathbf{r}_A)]_+ \quad (8)$$

with the Fermi constant G_F , electron mass m_e , its momentum \mathbf{p}_i and spin operators \mathbf{s}_i , the three-dimensional Dirac delta distribution δ^3 and positions \mathbf{r}_i of electrons and \mathbf{r}_A of the nuclei. This is perhaps the most exotic of the isotope effects in molecular spectroscopy and dynamics. Most recently, it has been quantitatively predicted to lead to a ground state energy difference between chiral isotopomers such as $\text{PF}^{35}\text{Cl}^{37}\text{Cl}$ (Berger *et al.* 2005) (and similarly $\text{HCF}^{35}\text{Cl}^{37}\text{Cl}$, etc.). This difference is predicted to be very small (about 10^{-13} cm^{-1}), but would be exactly zero for symmetry reasons if only (1)–(2) are considered. While its spectroscopic observation is possible, in principle (Quack 1986, Sieben *et al.* 2003), this has not yet been realized and should happen in the near future (*see also* the article Quack 2011: **Fundamental Symmetries and Symmetry Violations from High-resolution Spectroscopy**, this handbook).

Following this introductory survey of the principles of molecular spectroscopic and dynamical isotope effects, we shall now turn to a discussion of isotope effects as observed and used in practice in some recently developed spectroscopic techniques where the mass effect (1) is of greatest relevance (combined with (2) and (3) to some extent).

As is appropriate for use in a handbook, we provide in Table 1 a summary of the most important isotopes of interest for high-resolution spectroscopy with their relevant properties. We note that *atomic* masses are given in the table (the masses of the neutral atoms including the electrons). For some isotope effects, nuclear or ionic masses are relevant, which can be computed from these atomic masses. We note also the importance of nuclear spin, magnetic moment, and parity of the nucleus for certain isotope effects.

Table 1 Ground state properties of selected isotopic nuclei, which are important in high-resolution molecular spectroscopy^(a).

$Z_A^{(b)}$	Symbol ^(c)	$A^{(d)}$	Atomic mass, ^(e) m_a/u	Isotopic composition, ^(f) 100 x	Nuclear spin, ^(g) I^π	Magnetic moment, ^(h) m/μ_N
1	H	1	1.007 825 032	99.989	(1/2) ⁺	+2.792847
		(D)	2	2.014 101 778	0.012	1 ⁺
2	He	3	3.016 029 319	0.000 134	(1/2) ⁺	-2.127 498
		4	4.002 603 254	99.999 866	0 ⁺	0
3	Li	6	6.015 122 795	7.59	1 ⁺	+0.822 047
		7	7.016 004 55	92.41	(3/2) ⁻	+3.256 427
4	Be	9	9.012 182 2	100	(3/2) ⁻	-1.177432
5	B	10	10.012 937 0	19.9	3 ⁺	+1.800 644
		11	11.009 305 4	80.1	(3/2) ⁻	+2.688 648
6	C	12	12 (by definition)	98.93	0 ⁺	0
		13	13.003 354 838	1.07	(1/2) ⁻	+0.702 412
7	N	14	14.003 074 005	99.636	1 ⁺	+0.403 761
		15	15.000 108 898	0.364	1/2 ⁻	-0.283 189
8	O	16	15.994 914 620	99.757	0 ⁺	0
		17	16.999 131 70	0.038	5/2 ⁺	-1.893 79
		18	17.999 161 0	0.205	0 ⁺	0
9	F	19	18.998 403 22	100	(1/2) ⁺	+2.628 868
10	Ne	20	19.992 440 175	90.48	0 ⁺	0
		21	20.993 846 68	0.27	(3/2) ⁺	-0.661 797
		22	21.991 385 114	9.25	0 ⁺	0
11	Na	23	22.989 769 281	100	(3/2) ⁺	+2.217 656
12	Mg	24	23.985 041 700	78.99	0 ⁺	0
		25	24.985 836 92	10.00	(5/2) ⁺	-0.855 45
		26	25.982 592 929	11.01	0 ⁺	0
13	Al	27	26.981 538 63	100	(5/2) ⁺	+3.641 507
14	Si	28	27.976 926 533	92.223	0 ⁺	0
		29	28.976 494 700	4.685	(1/2) ⁺	-0.555 29
		30	29.973 770 17	3.092	0 ⁺	0
15	P	31	30.973 761 63	100	(1/2) ⁺	+1.131 60
16	S	32	31.972 071 00	94.99	0 ⁺	0
		33	32.971 458 76	0.75	(3/2) ⁺	+0.643 821
		34	33.967 866 90	4.25	0 ⁺	0
		36	35.967 080 76	0.01	0 ⁺	0
17	Cl	35	34.968 852 68	75.76	(3/2) ⁺	+0.821 874
		37	36.965 902 59	24.24	(3/2) ⁺	+0.684 124
18	Ar	36	35.967 545 106	0.337	0 ⁺	0
		38	37.962 732 4	0.063	0 ⁺	0
		40	39.962 383 123	99.600	0 ⁺	0
19	K	39	38.963 706 68	93.258	(3/2) ⁺	+0.39147
		40	39.963 998 48	0.012	4 ⁻	-1.298 100
		41	40.961 825 76	6.730	(3/2) ⁺	+0.214 870
20	Ca	40	39.962 590 98	96.941	0 ⁺	0
		42	41.958 618 01	0.647	0 ⁺	0
		43	42.958 766 6	0.135	(7/2) ⁻	-1.317 643
		44	43.955 481 8	2.086	0 ⁺	0
		46	45.953 692 6	0.004	0 ⁺	0
		48	47.952 534	0.187	0 ⁺	0

Table 1 continued.

$Z_A^{(b)}$	Symbol ^(c)	$A^{(d)}$	Atomic mass, ^(e) m_a/u	Isotopic composition, ^(f) 100 x	Nuclear spin, ^(g) I^π	Magnetic moment, ^(h) m/μ_N
22	Ti	46	45.952 631 6	8.25	0 ⁺	0
		47	46.951 763 1	7.44	(5/2) ⁻	-0.788 48
		48	47.947 946 3	73.72	0 ⁺	0
		49	48.947 870 0	5.41	(7/2) ⁻	-1.104 17
		50	49.944 791 2	5.18	0 ⁺	0
26	Fe	54	53.939 610 5	5.845	0 ⁺	0
		56	55.934 937 5	91.754	0 ⁺	0
		57	56.935 394 0	2.119	(1/2) ⁻	+0.090 623
		58	57.933 275 6	0.282	0 ⁺	0
27	Co	59	58.933 195 0	100	(7/2) ⁻	+4.627
28	Ni	58	57.935 342 9	68.077	0 ⁺	0
		60	59.930 786 4	26.223	0 ⁺	0
		61	60.931 056 0	1.140	(3/2) ⁻	-0.750 02
		62	61.928 345 1	3.634	0 ⁺	0
		64	63.927 966 0	0.926	0 ⁺	0
32	Ge	70	69.924 247 4	20.38	0 ⁺	0
		72	71.922 075 8	27.31	0 ⁺	0
		73	72.923 458 9	7.76	(9/2) ⁺	-0.879 468
		74	73.921 177 8	36.72	0 ⁺	0
		76	75.921 402 6	7.83	0 ⁺	0
33	As	75	74.921 596 5	100	(3/2) ⁻	+1.439 48
34	Se	74	73.922 476 4	0.89	0 ⁺	0
		76	75.919 213 6	9.37	0 ⁺	0
		77	76.919 914 0	7.63	(1/2) ⁻	+0.535 042
		78	77.917 309 1	23.77	0 ⁺	0
		80	79.916 521 3	49.61	0 ⁺	0
		82	81.916 699 4	8.73	0 ⁺	0
35	Br	79	78.918 337 1	50.69	(3/2) ⁻	+2.106 400
		81	80.916 290 6	49.31	(3/2) ⁻	+2.270 562
37	Rb	85	84.911 789 738	72.17	(5/2) ⁻	+1.352 98
		87	86.909 180 527	27.83	(3/2) ⁻	+2.751 31
44	Ru	96	95.907 598	5.54	0 ⁺	0
		98	97.905 287	1.87	0 ⁺	0
		99	98.905 939 3	12.76	(5/2) ⁺	-0.641
		100	99.904 219 5	12.60	0 ⁺	0
		101	100.905 582 1	17.06	(5/2) ⁺	-0.719
		102	101.904 349 3	31.55	0 ⁺	0
		104	103.905 433	18.62	0 ⁺	0
53	I	127	126.904 473	100	(5/2) ⁺	+2.813 27
54	Xe	124	123.905 893 0	0.095	0 ⁺	0
		126	125.904 274	0.089	0 ⁺	0
		128	127.903 531 3	1.910	0 ⁺	0
		129	128.904 779 4	26.401	(1/2) ⁺	-0.777 976
		130	129.903 508 0	4.071	0 ⁺	0
		131	130.905 082 4	21.232	(3/2) ⁺	+0.6915
		132	131.904 153 5	26.909	0 ⁺	0
		134	133.905 394 5	10.436	0 ⁺	0
		136	135.907 219	8.857	0 ⁺	0

(continued overleaf)

Table 1 continued.

$Z_A^{(b)}$	Symbol ^(c)	$A^{(d)}$	Atomic mass, ^(e) m_a/u	Isotopic composition, ^(f) 100 x	Nuclear spin, ^(g) $I \pi$	Magnetic moment, ^(h) m/μ_N
55	Cs	133	132.905 451 933	100	(7/2) ⁺	+2.582 025
74	W	180	179.946 704	0.12	0 ⁺	0
		182	181.948 204 2	26.50	0 ⁺	0
		183	182.950 223 0	14.31	(1/2) ⁻	+0.117 785
		184	183.950 931 2	30.64	0 ⁺	0
		186	185.954 364 1	28.43	0 ⁺	0
75	Re	185	184.952 955 0	37.40	(5/2) ⁺	+3.1871
		187	186.955 753 1	62.60	(5/2) ⁺	+3.2197
76	Os	184	183.952 489 1	0.02	0 ⁺	0
		186	185.953 838 2	1.59	0 ⁺	0
		187	186.955 750 5	1.96	(1/2) ⁻	+0.064 652
		188	187.955 838 2	13.24	0 ⁺	0
		189	188.958 147 5	16.15	(3/2) ⁻	+0.659 933
		190	189.958 447 0	26.26	0 ⁺	0
		192	191.961 480 7	40.78	0 ⁺	0
77	Ir	191	190.960 594 0	37.3	(3/2) ⁺	+0.1507
		193	192.962 926 4	62.7	(3/2) ⁺	+0.1637
78	Pt	190	189.959 932	0.014	0 ⁺	0
		192	191.961 038 0	0.782	0 ⁺	0
		194	193.962 680 3	32.967	0 ⁺	0
		195	194.964 791 1	33.832	(1/2) ⁻	+0.609 52
		196	195.964 951 5	25.242	0 ⁺	0
		198	197.967 893	7.163	0 ⁺	0
79	Au	197	196.966 568 7	100	(3/2) ⁺	+0.145 746
80	Hg	196	195.965 833	0.15	0 ⁺	0
		198	197.966 769 0	9.97	0 ⁺	0
		199	198.968 279 9	16.87	(1/2) ⁻	+0.505 886
		200	199.968 326 0	23.10	0 ⁺	0
		201	200.970 302 3	13.18	(3/2) ⁻	-0.560 226
		202	201.970 643 0	29.86	0 ⁺	0
		204	203.973 493 9	6.87	0 ⁺	0
81	Tl	203	202.972 344 2	29.52	(1/2) ⁺	+1.622 258
		205	204.974 427 5	70.48	(1/2) ⁺	+1.638 215
82	Pb	204	203.973 043 6	1.4	0 ⁺	0
		206	205.974 465 3	24.1	0 ⁺	0
		207	206.975 896 9	22.1	(1/2) ⁻	+0.592 583
		208	207.976 652 1	52.4	0 ⁺	0
83	Bi	209	208.980 398 7	100	9/2 ⁻	+4.1103
92	U	234	234.040 952 2	0.005	0 ⁺	0
		235	235.043 929 9	0.720	(7/2) ⁻	-0.38
		238	238.050 788 2	99.274	0 ⁺	0

(a) After Cohen *et al.* 2007.

(b) Charge number.

(c) Element symbol.

(d) Mass number $A = Z_A + N_A$ with neutron number N_A .(e) Atomic mass (in atomic units of Dalton). $1u = 1Da$, see Stohner and Quack (2011)

(f) Natural abundance as mole fraction (%).

(g) Nuclear angular momentum ("spin") I with parity π as exponent.(h) Magnetic moment m in the units of the nuclear magneton (μ_N).

3 INTRAMOLECULAR DYNAMICS AND ISOTOPE-SELECTIVE SPECTROSCOPIC TECHNIQUES: AN OVERVIEW

Information on mechanisms and timescales of ultrafast intramolecular dynamic processes is encoded in homogeneous structures of high-resolution infrared spectra. By an analysis of homogeneous splittings and line widths, the rovibrational Hamiltonian and time evolution operators, which contain this relevant information, can be extracted (Quack 1990, 1993, 1995b, 2001, Beil *et al.* 1997, Hippler 2001, *see also* Snels *et al.* 2011: **High-resolution FTIR and Diode Laser Spectroscopy of Supersonic Jets**; Marquardt and Quack 2011: **Global Analytical Potential Energy Surfaces for High-resolution Molecular Spectroscopy and Reaction Dynamics**; and Quack 2011: **Fundamental Symmetries and Symmetry Violations from High-resolution Spectroscopy**, this handbook). This allows a detailed study of dynamic processes on sub-femtosecond to picosecond timescales, for example, of intramolecular vibrational redistribution (IVR), predissociation, or tunneling processes. In this context, it is particularly interesting to investigate the influence of vibrational excitation on intramolecular dynamics, since vibrational mode selectivity allows one to influence reactions by selective vibrational excitation, perhaps also after further electronic excitation (Rizzo *et al.* 1983, Crim 1993). To understand isotope effects in chemical reactions, it is also important to investigate the influence of different isotope compositions of a molecule (isotopomers) on intramolecular dynamics. The ultimate aim of such studies is a better understanding of intramolecular primary processes and unimolecular reactions in polyatomic molecules at the fully quantum dynamical level, a level which goes far beyond simplifying statistical theories. This aim remains one of the most challenging in research in physics and chemistry, with applications also in biology and environmental sciences.

In our approach to extract detailed molecular dynamics, a high-resolution analysis of complex and often weak band structures of rovibrational spectra is required (Quack 1990, 1993, 1995b, 2001, Beil *et al.* 1997, Hippler 2001). Unfortunately, infrared spectra are often congested by hot-band transitions and because of the mixture of isotopomers, and thus reliable assignments were often not possible in the past: Extensive hot-band congestion in room-temperature spectra of polyatomic molecules requires jet cooling to obtain vibrationally resolved spectra. The resulting low number densities in conjunction with low absorption cross sections will therefore necessitate very sensitive detection of the IR excitation. Some of these aspects can be dealt with successfully by supersonic jet FTIR (Fourier transform infrared)

and laser spectroscopy (Quack 1990, Snels *et al.* 2011: **High-resolution FTIR and Diode Laser Spectroscopy of Supersonic Jets**, this handbook). In addition, molecules often exist as a mixture of different isotopomers at natural abundance. The resulting congestion of rovibrational spectra then often prevents a detailed analysis; in many cases, isotopically pure samples are not available. It is thus desirable to use experimental techniques that allow the separation of spectral contributions from different isotopomers and that, at the same time, help to reduce the spectral congestion, for example, by supersonic jet cooling.

During the last 15 years, we successfully developed new experimental techniques for the IR spectroscopy of gas-phase molecules, where the selective ionization of vibrationally excited molecules in IR + UV double-resonance schemes allows indirect, but extremely sensitive, detection of the IR excitation (Hippler and Quack 1994, 1995, 1996, 1997, Fehrensens *et al.* 1998, Hippler *et al.* 2003, Hippler 2001). Overtone transitions are intrinsically very weak. Instead of directly monitoring the IR absorption, one can couple IR excitation with further UV photon absorption steps leading finally to ionization. This allows indirect but much more sensitive detection of infrared excitation, since molecules are not ionized efficiently without vibrational excitation, as resonance enhancement. The ionization yield thus mirrors the vibrational excitation. Ionization detection of IR excitation may increase the sensitivity and selectivity of IR spectroscopy, since electrostatic fields can extract all ions and, in principle, even single ions can be detected in a mass spectrometer. The technique has been applied to overtone spectroscopy in supersonic jet expansions, where the cooling of vibrational and rotational degrees of freedom greatly reduces hot-band congestion and simplifies spectra. Ionization detection of the IR excitation can be coupled very efficiently with a time-of-flight (TOF) mass spectrometer, which allows the separation of spectral contributions of different components in a mixture. Mass spectrometry is thus added as a second dimension to IR spectroscopy, which greatly increases the selectivity. The IR excitation also increases the selectivity of mass spectrometry, since it allows the separation of species that have nearly (or exactly) the same masses (isobars), making use of the isotope effects (2)–(4) mentioned above in the case of isotopomers. Two different IR + UV double-resonance schemes are reviewed here; they are distinguished by the nature of the intermediate, electronically excited state: if it is dissociative, then overtone spectroscopy by OSVADPI allows the detection of the IR excitation in the parent molecule by observing fragment ions (Hippler and Quack 1994, 1995, 1996, 1997, Hippler 2001). With a bound intermediate state, resonantly enhanced two-photon ionization (RE2PI) of vibrationally excited molecules is very efficient via hot-band transitions of the excited state, which represents a quasi-continuum

due to its high vibrational density of states (Fehrensens *et al.* 1998, Hippler 2001, Hippler *et al.* 2003). In both schemes, synchronous tuning of the UV laser during an IR spectral scan is not required to retain the resonance condition. Employing these techniques, we have studied isotope effects in infrared spectroscopy and intramolecular dynamics of Cl-isotopomers of some aliphatic chlorides, such as chloroform, CF₂HCl, and tert-butyl chloride (Hippler and Quack 1994, 1995, 1996, 1997, Hippler 2001), of H/D-isotopomers of aniline (Fehrensens *et al.* 1998, Hippler 2001), and of ¹²C/¹³C-isotopomers of benzene (Hippler 2001, Hippler *et al.* 2003); we review some selected examples here.

We also review some recently developed alternative spectroscopic techniques, which are somewhat related to our own original developments. In infrared resonance enhanced multiphoton ionization (IR-REMPI), molecules are vibrationally excited and then ionized by multiphoton absorption in the intense IR laser field of one tightly focused laser beam. This vibrational preionization technique was demonstrated by us on C₆₀ (Hippler *et al.* 1997) and later applied by others to the IR spectroscopy of fullerenes and other molecules (von Helden *et al.* 1997, 1999). It is confined, however, to special cases where the ionization limit is low and comparable to the dissociation threshold (or lower); otherwise, dissociation would predominate over ionization. In another technique, vibrationally excited molecules are ionized by one-photon ionization of a vacuum ultraviolet (VUV) laser (Antonov and Letokhov 1981, Putter *et al.* 1996). In general, however, it may be difficult to select a suitable VUV wavelength that allows sufficient discrimination between the ionization of ground state and excited state molecules (Antonov and Letokhov 1981): the additional IR energy is rather small compared to the VUV energy, and the ionization cross section does often not change enough with energy, except at a sharp ionization threshold. In addition, the use of involved VUV laser systems may also not always be convenient. Alternatively, vibrationally excited molecules could be ionized by UV two-photon ionization, which is resonantly enhanced by an intermediate electronically excited state (Antonov and Letokhov 1981). Convenient frequency-doubled dye lasers can then be used. In previous implementations, distinct rovibrational levels of the resonance-enhancing intermediate state were selected (Antonov and Letokhov 1981, Page *et al.* 1988a, Bahnmaier *et al.* 1992). Because of the increased selectivity owing to the additional selection rules imposed by the intermediate level, this double-resonance technique may aid the assignment of selected infrared absorption features (Page *et al.* 1988a). As the UV ionization is via distinct, separated transitions, the UV laser has to be scanned simultaneously to retain the resonance during an IR scan. This is difficult to achieve, however, and no IR spectra obtained in this

manner have been reported. Another IR + UV absorption scheme was presented, where vibrationally excited phenol was ionized by nonresonant two-photon ionization (Omi *et al.* 1996, Ishiuchi *et al.* 1998). As discussed below, however, ionization presumably also occurred in these cases by RE2PI, as in the present scheme, which is based on the original earlier development of OSVADPI (Hippler and Quack 1994, 1995, 1996, 1997, Fehrensens *et al.* 1998, Hippler 2001, Hippler *et al.* 2003).

In another scheme based on photofragment spectroscopy, an IR laser promotes molecules to predissociating vibrational levels, and the fragments of this vibrationally mediated dissociation are probed by fluorescence detection, for example, by laser-induced fluorescence (LIF) of a second UV laser (Rizzo *et al.* 1983, Butler *et al.* 1986, Ticich *et al.* 1987, Crim 1993). Since the yield of fragments mirrors the IR excitation, infrared spectra are obtained indirectly, but very sensitively, by scanning the IR laser while monitoring the photofragment yield. The scheme can also be applied to the IR spectroscopy of bound vibrational states. Vibrationally excited molecules are then dissociated by the further absorption of one IR or UV photon (Butler *et al.* 1986, Ticich *et al.* 1987, Luo *et al.* 1992, Crim 1993), or alternatively by multiphoton absorption of several CO₂ laser photons by infrared laser-assisted photofragment spectroscopy (IRLAPS) (Settle and Rizzo 1992, Lubich *et al.* 1995, Boyarkin and Rizzo 1996, Boyarkin *et al.* 1997, 2002), which can also be used as a scheme for increasing selectivity in laser isotope separation (Kowalczyk 2000, Boyarkin *et al.* 2003). Besides allowing infrared spectroscopy, vibrationally mediated dissociation also provides insight into the dynamics of the dissociation process (Andresen *et al.* 1985, Brouard *et al.* 1988, Wal *et al.* 1991, Crim 1993). However, a limitation of these schemes is that they require fragments that can be probed by LIF.

Dip spectroscopy is a double-resonance technique, where a UV laser is tuned to an electronic transition of ground state molecules, which is monitored either by LIF or resonantly enhanced multiphoton ionization (REMPI) detection. If an IR laser depopulates ground state levels by rovibrational transitions first, a dip in the fluorescence or ionization signal is observed, which mirrors the IR excitation (Page *et al.* 1987, 1988a,b, Pribble and Zwier 1994, Frost *et al.* 1996, Sugawara *et al.* 1996, Ebata *et al.* 1998). The main advantage of dip spectroscopy is the added selectivity provided by the UV excitation: UV transitions of specific isomers, isotopomers, clusters, or species in a mixture can be selected, and the IR dip spectrum then corresponds to the selected species. Since dip signals are observed against a strong background, these methods suffer from poor signal-to-noise ratios. Nevertheless, dip spectroscopy has found frequent use recently (Fujii *et al.* 2000, Fujimaki *et al.* 2000, Gerhards and Unterberg 2001,

Reimann *et al.* 2001, Minejima *et al.* 2002, Sakai *et al.* 2003, Seurre *et al.* 2003, Frey *et al.* 2004, Cho *et al.* 2005, Gerhards *et al.* 2005, Chowdhury 2006, Donaldson *et al.* 2007, Shubert and Zwier 2007, Busker *et al.* 2009, Mahjoub *et al.* 2009, Ottiger *et al.* 2009, Stanca-Kaposta and Simons 2011: **High-resolution Infrared–Ultraviolet (IR–UV) Double-resonance Spectroscopy of Biological Molecules**, this handbook).

For one-photon IR absorption, the selection rules of electric dipole transitions within the electronic ground state allow only transitions changing several vibrational quanta due to anharmonicity, and these transitions are very weak. Many experimental studies in overtone spectroscopy are thus concerned with combination and overtone levels involving anharmonic hydride stretching vibrations, for example. In a different approach, vibrational levels of the electronic ground state are reached by two-photon excitation by stimulated transitions via excited electronic states (stimulated emission pumping, SEP) (Reisner *et al.* 1984, Hamilton *et al.* 1986, Suzuki *et al.* 1988, Quack 1990, Crane *et al.* 1998, Herman *et al.* 1999) or virtual levels (stimulated Raman excitation, SRE) (Esherrick and Owyong 1983, Bronner *et al.* 1984, Bar *et al.* 1990, Quack 1990, Chadwick and Orr 1992, Brown *et al.* 1997). Since different electronic states are involved in the two-photon excitation, different selection rules apply; the transition strength is then mainly governed by the Franck–Condon principle, and thus different vibrational levels can be reached compared to direct one-photon IR absorption. SEP and SRE have been combined with photoacoustic spectroscopy (Brown *et al.* 1997), photofragment spectroscopy by vibrationally mediated dissociation (Bar *et al.* 1990, Brown *et al.* 1997), ionization gain (Esherrick and Owyong 1983) and loss (dip) spectroscopy (Bronner *et al.* 1984, Suzuki *et al.* 1988), LIF detection (Chadwick and Orr 1992), and fluorescence dip spectroscopy (Crane *et al.* 1998), for example.

Double-resonance schemes, where two sequential IR absorption steps are involved to reach highly vibrationally excited levels, are also employed to increase sensitivity and selectivity (Luo and Rizzo 1990, Lehmann *et al.* 1994, Lubich *et al.* 1995, Boyarkin and Rizzo 1995, 1996, Boyarkin *et al.* 1997, Callegari *et al.* 1997, 1999). Since fundamental bands often show resolved rotational structure, a first IR photon may excite a selected rovibrational level via a fundamental transition, and a second IR photon of different wavelength then promotes to a high overtone level, which allows rotational state selected vibrational overtone spectroscopy (Luo and Rizzo 1990, Lubich *et al.* 1995, Boyarkin and Rizzo 1995, 1996, Callegari *et al.* 1997, 2000, 2001). By the selection of the first absorption step, inhomogeneous congestion can be removed. To take advantage of the resolution obtainable with microwave

spectroscopy, microwave transitions may also be included into the absorption chain (Jones 1979, Lehmann *et al.* 1994, Merker *et al.* 1999, Muentner *et al.* 1999). For example, a microwave transition can provide the last increment of energy required for dissociation in photofragment spectroscopy (Muentner *et al.* 1999). A disadvantage is that double-resonance schemes do not directly measure absolute absorbances. Besides, in general, the more laser systems are involved in a setup, the more complex and less robust the experiment will become.

This short introduction to some recent developments of sensitive and selective infrared spectroscopic techniques was meant to establish some concepts and to stress that each technique has its own merits and limitations. Ideally, an experimental technique would be as generally applicable as possible, provide high resolution, and combine high sensitivity with selectivity, and yet not be too involved. We think that our mass- and isotope-selective IR + UV schemes, which are presented in this review, have distinct advantages in this regard.

4 INTRAMOLECULAR REDISTRIBUTION PROCESSES: FROM HIGH-RESOLUTION SPECTROSCOPY TO ULTRAFAST INTRAMOLECULAR DYNAMICS

4.1 Intramolecular Quantum Dynamics and Molecular Spectroscopy

The time-dependent quantum dynamics of molecules, as of other quantum systems, is governed by the time (t)-dependent Schrödinger equation (*see also* Merkt and Quack 2011: **Molecular Quantum Mechanics and Molecular Spectra, Molecular Symmetry, and Interaction of Matter with Radiation**, this handbook)

$$i\frac{\hbar}{2\pi}\frac{\partial\Psi(q,t)}{\partial t}=\hat{H}\Psi(q,t) \quad (9)$$

where q represents the whole set of particle coordinates and spins and $\Psi(q,t)$ is the corresponding time-dependent wavefunction. The molecular Hamiltonian is time independent in the absence of external fields, but may become time dependent in their presence. The general solution is given with the time evolution operator $\hat{U}(t,t_0)$

$$\Psi(q,t)=\hat{U}(t,t_0)\Psi(q,t_0) \quad (10)$$

which satisfies an equation similar to equation (9):

$$i\frac{\hbar}{2\pi}\frac{\partial\hat{U}}{\partial t}=\hat{H}\hat{U} \quad (11)$$

which is solved with a time-independent Hamiltonian \hat{H} by

$$\hat{U}(t, t_0) = \exp(-2\pi i \hat{H}(t - t_0)/h) \quad (12)$$

In this latter case, one can write the solution for $\Psi(q, t)$ explicitly in terms of the time-independent molecular Schrödinger equation

$$\hat{H}\varphi_k(q) = E_k\varphi_k(q) \quad (13)$$

with the stationary state eigenfunctions $\varphi_k(q)$ depending only on q (not on t) and the corresponding eigenenergies E_k . The general $\Psi(q, t)$ takes then the form

$$\Psi(q, t) = \sum_k c_k \varphi_k(q) \exp(-2\pi i E_k t/h) \quad (14)$$

with time-independent complex coefficients c_k determined by the initial conditions. With time-dependent \hat{H} , the c_k in this solution would become time dependent as well. In principle, high-resolution molecular spectroscopy provides relevant information on $\varphi_k(q)$ and E_k and thus on the time-dependent molecular quantum dynamics (Quack 1990). In practice, a first spectroscopic analysis relates to an effective Hamiltonian

$$\mathbf{Z}^T \mathbf{H}_{\text{eff}} \mathbf{Z} = \text{Diag}(E_1, \dots, E_n) \quad (15)$$

where \mathbf{Z} is the eigenvector matrix of H_{eff} in some unknown basis $\chi = (\chi_1 \dots \chi_n)^T$. In order to obtain the time variational molecular Hamiltonian in an eigenstate basis φ_k , which can be described in ordinary coordinate space for the molecule, we have to find an appropriate transformation

$$\varphi = \mathbf{Z}^T \chi \quad (16)$$

The differences $E_k - E_j$ are directly measurable by spectroscopy. The scheme shown in Figure 1 illustrates the path from molecular spectra to molecular dynamics by the intermediate steps of the effective and true molecular Hamiltonians (Quack 1990, 1993, 1995b, 2001, Beil *et al.* 1997). A careful analysis of these steps was carried out by our group only in the years 1980–1990, the difference between the “true” and effective Hamiltonian analysis not having been taken into account previously by practicing spectroscopists. This point turns out to be particularly important for dynamical isotope effects, which are properly accounted for only in the case when true molecular Hamiltonians or proper transformations are used (Quack 1990, Beil *et al.* 1996, *see also* Albert *et al.* 2011a: **Fundamentals of Rotation–Vibration Spectra**, this handbook).

The general time evolution operator approach encoded in equation (11) is useful in dealing with the most general aspects of the problem (Quack 1995c, 2001, Quack

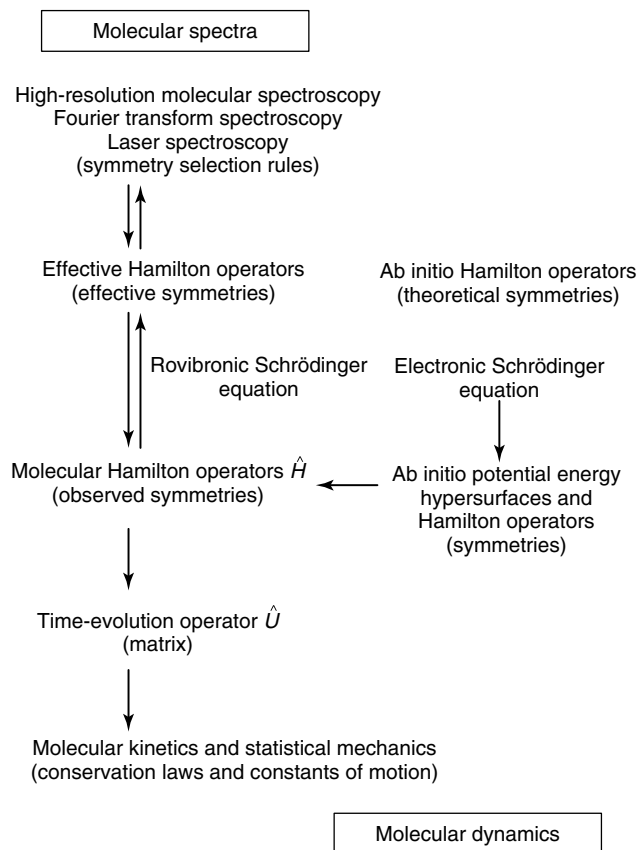


Figure 1 Scheme of the combined experimental–theoretical approach for the determination of molecular dynamics from molecular spectra (from Quack 2001).

2011: **Fundamental Symmetries and Symmetry Violations from High-resolution Spectroscopy**, this handbook). Rather than pursuing these more formal aspects, we provide here a much simplified but instructive and intuitive perspective.

4.2 Spectroscopic States and Intramolecular Dynamics: an Intuitive Perspective

4.2.1 General Aspects

Time-independent, molecular states are eigenstates of the time-independent Hamiltonian operator in the Schrödinger equation, equation (13) with the time-dependent wavefunction for an eigenstate,

$$\Psi_k = \varphi_k \exp(-2\pi i E_k t/h) \quad (17)$$

The square of the wavefunction of such stationary states is time independent, and therefore nothing moves in the molecule; only the phase is time dependent. These eigenstates are the spectroscopic states, which are observable by high-resolution spectroscopy of isolated molecules

(neglecting the natural lifetime and width due to spontaneous emission) (Quack 1981a, 1990, 1993, 1995b, 2001, Beil *et al.* 1994, Nesbitt and Field 1996, Beil *et al.* 1997, Hippler 2001, Gruebele and Bigwood 1998). A spectrum at highest resolution consists, in principle, of discrete lines having the natural line width corresponding to these eigenstates. The lines are overlapping in most cases, giving rise to homogeneous and inhomogeneous structures (Dübal and Quack 1980, 1981, Quack 1990). Homogeneous structures arise by absorption from one initial energy eigenstate. Inhomogeneous structures result from overlapping transitions from different initial quantum states, where the Doppler width of rovibrational lines, hot-band transitions, or transitions from different species, isotopomers, or isomers are examples. Using special techniques to remove spectral congestion (double-resonance experiments, supersonic jet cooling), “eigenstate-resolved” spectra have been obtained in the past for some simple molecules (Lewerenz and Quack 1988, Quack 1990, Luckhaus and Quack 1992, Lehmann *et al.* 1994, Hollenstein *et al.* 1994, Snels *et al.* 1995, Lubich *et al.* 1995, Boyarkin and Rizzo 1996, Callegari *et al.* 1999, Merker *et al.* 1999, Boyarkin *et al.* 1999). For vibrational states with small amplitudes, the harmonic approximation in the potential energy function is appropriate, and the normal modes resulting from a harmonic analysis correspond then to a good degree of approximation to the molecular eigenstates. This will, in general, be true for fundamental vibrations, except for large-amplitude motions. For overtone and combination states at higher vibrational excitation, anharmonicity in the potential energy becomes more and more important, invalidating the harmonic approximation. The molecular eigenstates are then a mixture of the formal, “zeroth-order” normal mode overtone and combination states. The mixing of idealized normal mode vibrations, which are based on a harmonic approximation, is due to anharmonicity—hence the name “anharmonic resonances”—between normal mode states of similar energy (Herzberg 1945, 1950, Wilson *et al.* 1955, Hollas 1982, Papoušek and Aliev 1982). The coupling or mixing coefficients can be calculated approximately by perturbation theory. They are frequently determined by the matrix elements of the perturbing, anharmonic potential terms in the basis of harmonic oscillator wavefunctions (Papoušek and Aliev 1982). Distinct anharmonic resonances, in particular Fermi resonances with an exchange of one quantum of excitation in one vibrational mode with two quanta in another mode, or Darling–Dennison resonances with an exchange of two quanta of vibrational excitation in one mode with two quanta in another mode, are important for very fast relaxation processes (Fermi 1931, Darling and Dennison 1940, Papoušek and Aliev 1982, Dübal and Quack 1984, Peyerimhoff *et al.* 1984, Segall *et al.* 1987, Lewerenz and Quack 1988, Mills 1988, Dübal *et al.* 1989,

Hollenstein *et al.* 1990a, Duncan and Law 1990, Quack 1990, Marquardt and Quack 1991, Luckhaus and Quack 1992, Holland *et al.* 1992, 1993, Luckhaus *et al.* 1993, Marquardt *et al.* 1995, Lubich *et al.* 1995, Boyarkin and Rizzo 1996, Hippler and Quack 1996, Boyarkin *et al.* 1997, 1999, Luckhaus 1997, Fehrensens *et al.* 1998). Fermi resonances were first observed and interpreted in the CO₂ spectrum (Fermi 1931) (*see also* Herzberg 1945, 1966), and have since then been extensively studied in the IR spectra of the CH-chromophore, for example (Peyerimhoff *et al.* 1984, Dübal and Quack 1984, Segall *et al.* 1987, Carrington *et al.* 1987, Mills 1988, Halonen *et al.* 1988, Halonen 1988, Lewerenz and Quack 1988, Dübal *et al.* 1989, Hollenstein *et al.* 1990a, Duncan and Law 1990, Quack 1990, Marquardt and Quack 1991, Luckhaus and Quack 1992, Hollenstein *et al.* 1993, Luckhaus *et al.* 1993, Marquardt *et al.* 1995, Nesbitt and Field 1996). Higher order anharmonic resonances account for a further mixing and redistribution of vibrational excitation. All resonances become particularly effective if the zeroth-order energies arising from the idealized, normal mode vibrations involved are similar (resonance condition). In addition, rovibrational Coriolis resonances from the coupling of rotation with vibrational motions may also be present (Herzberg 1945, 1950, Wilson *et al.* 1955, Hollas 1982, Papoušek and Aliev 1982). The wavefunctions of highly excited eigenstates are, in general, spread over the entire molecule and not localized, and they are thus also known as *global vibrational states* (Quack 1981a). Time-dependent states, where the atoms in the molecule are moving, are described as the superposition of time-independent eigenstates (equation 14) (Quack 1990, 1995b, Beil *et al.* 1994, 1996, 1997, Lehmann *et al.* 1994, Nesbitt and Field 1996, Gruebele and Bigwood 1998).

The time dependence arises from the spreading of phases (equation 14) of the vibrational eigenstates, from a concerted ordering of phases to give rise to an initial state $\Psi(t = 0)$, to essentially a “random” superposition. In this way, vibrational energy originally located in an initial vibrational state is distributed among other vibrational modes as a function of time—time-dependent IVR; this is the complement of the time-independent picture of IVR, visible in the nonseparability of the φ_k in a set of coordinates (normal modes) (Quack 1990, Beil *et al.* 1997). In principle, the time dependence in equation (14) allows recurrences of occupation probability of the initial state, but if the time-dependent state is composed of many eigenstates, equation (14) basically describes a relaxation process. High-resolution spectroscopy identifies eigenstates, and from their analysis and assignment, an effective Hamiltonian and, finally, the true complete molecular Hamiltonian of the molecule can be constructed, perhaps supported by *ab initio* calculations (Quack 1990, 1993, 1995b, Beil *et al.* 1997, Herman *et al.* 1999). Zeroth-order states in perturbation

theory are usually harmonic normal mode vibrations. Their energies provide the diagonal elements in a matrix representation; perturbation energies give the off-diagonal elements. Matrix diagonalization yields the energies and the vector composition of the true, perturbed states with respect to the basis functions used. Since the perturbation treatment is, in general, limited to a low-order approximation, the corresponding model Hamiltonian derived from the spectra is not the true molecular Hamiltonian, but an effective Hamiltonian (Quack 1990, 1993, 1995b, Beil *et al.* 1997). The diagonal and off-diagonal elements in the matrix representation are usually considered as fit parameters to the observed spectrum. In general, the effective Hamiltonian describes the observed spectrum very well, since mathematically it originates from a transformed molecular Hamiltonian with similar or the same eigenvalues as the true Hamiltonian. The basis functions, however, are also transformed and are then, in general, not known explicitly. Full knowledge of the true wavefunctions is only possible if the important step from an effective model Hamiltonian with unknown basis to the complete molecular Hamiltonian with known wavefunctions is made (Quack 1990, 1993, 1995b, Beil *et al.* 1997). This will finally allow the prediction of how an arbitrary, initially created state will evolve in time in full detail, not only providing the timescale of decay of the initial state but also the mechanisms of intramolecular redistribution processes. This approach of extracting dynamic information is summarized in Figure 1; it is much more than just “Fourier-transforming” spectra, as it invokes a crucial analysis step for the wavefunction (Quack 1995b). Among the initial steps in the analysis of spectra, we can mention the distinction of homogeneous and inhomogeneous structures illustrated in Figure 2.

The simple analysis in terms of dynamics refers only to homogeneous structures. However overall appearance of a spectral “band” consisting of many lines can be very similar for homogeneous and inhomogeneous structures. Frequently, one assumes that inhomogeneous structures arise from hot-band congestion (see Figure 2) and can be removed by supersonic jet cooling, for instance. However, such cooling can also remove certain homogeneous structures labeled *Reverse* in Figure 2. Furthermore, even after the purely homogeneous structures have been identified in a spectrum, only an analysis of the true wavefunctions underlying the spectral lines allows one to identify coupling pathways and schemes in appropriate molecular Hamiltonians. Similar homogeneous spectral structures can result from different coupling schemes. Often, a complete analysis is possible only by a combination of several experimental and theoretical methods. It is in this context that development of new techniques such as OSVADPI/IRSIMS/ISOS becomes important. We shall illustrate now the analysis of

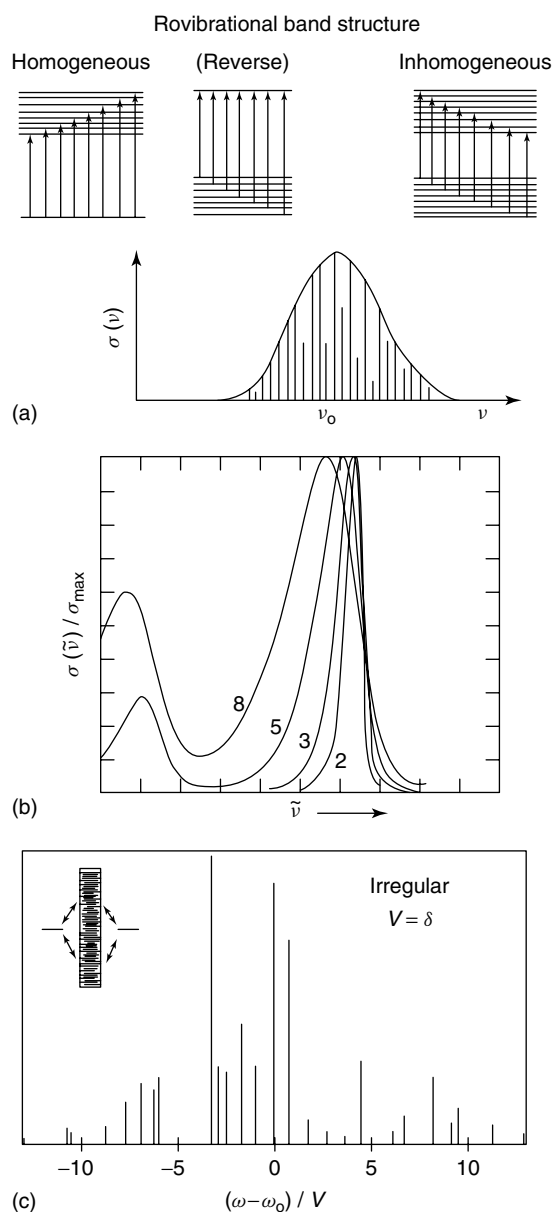


Figure 2 Illustration of “homogeneous” and “inhomogeneous” spectral structures (after von Puttkamer *et al.* 1983b, Quack 1990). (a) Schematic representation indicating transitions and levels as well as the absorption structure, σ , which may be similar for both types. Note that the role of upper and lower levels could be inverted (denoted by “Reverse”), resulting in temperature dependence for homogeneous structure or an emission band structure. (b) Model calculation for inhomogeneous structure of the CH-stretching band in $(\text{CF}_3)_3\text{C}-\text{C}\equiv\text{C}-\text{H}$ (discrete structures under continuous envelope (von Puttkamer *et al.* 1983b)). (c) Model calculation for discrete homogeneous (envelope not drawn). The coupling scheme for the upper level shown in the insert corresponds to two local mode states coupled to a dense spectrum (Quack 1981a).

the simplest spectral structures for some quite different but typical model-coupling schemes.

4.2.2 An Example of Two-level Dynamics

As the simplest case, one may consider two states φ_1^0 and φ_2^0 with energy E_1^0 and E_2^0 , respectively, coupled by an off-diagonal matrix element (perturbation energy) $-W$. The matrix representation of the effective Hamiltonian is therefore (see Albert *et al.* 2011a: **Fundamentals of Rotation–Vibration Spectra**, this handbook)

$$\mathbf{H}_{\text{eff}} = \begin{pmatrix} E_1^0 & -W \\ -W & E_2^0 \end{pmatrix} \quad (18)$$

The energy levels E_1 and E_2 corresponding to the eigenfunctions φ_1 and φ_2 given in equation (19) are observable by high-resolution spectroscopy:

$$E_{1,2} = \frac{E_1^0 + E_2^0}{2} \mp \sqrt{\left(\frac{E_1^0 - E_2^0}{2}\right)^2 + W^2} \quad (19)$$

If the unperturbed states are degenerate (or nearly degenerate), $E_1^0 = E_2^0 = E^0$, the solution is especially simple, $E_{1,2} = E^0 \mp W$, and the corresponding wavefunctions can be chosen as $\varphi_{1,2} = \frac{1}{\sqrt{2}}(\varphi_1^0 \pm \varphi_2^0)$. The eigenfunctions φ_1 and φ_2 are the symmetric and antisymmetric superpositions of the unperturbed states. By a coherent laser pulse, which has, owing to its time dependence, a frequency distribution covering both transitions to the spectral eigenstates φ_1 and φ_2 , a time-dependent coherent superposition state Ψ can be created, which corresponds to the unperturbed state φ_1^0 (equation 20) provided that it is the one state φ_1^0 that carries the electric dipole transition strength, a typical Fermi-resonance situation, if φ_2^0 corresponds to an overtone with a small or zero dipole strength.

$$\Psi(t=0) = \frac{1}{\sqrt{2}}(\varphi_1 + \varphi_2) = \varphi_1^0 \quad (20)$$

As can be seen from equation (14), $\Psi(t) = (\varphi_1 - \varphi_2)/\sqrt{2} = \varphi_2^0$ after $t = h/(2\Delta E)$, and after $t = h/\Delta E$, it recurs to φ_1^0 . Ψ thus oscillates with a period

$$\tau = \frac{h}{\Delta E} \quad (21)$$

between the two states φ_1^0 and φ_2^0 . In practice, further couplings not considered in the simple two-state model damp the oscillation and eventually transfer vibrational excitation out of these two states.

A typical example, where such a two-state model would be adequate, is provided by the classic Fermi resonance (1931), observed in Raman excitation, however. Another use is the local mode resonance, that is, a relatively weak resonance, which becomes apparent because of an (accidental) frequency match of two vibrational states corresponding to local oscillators, not normal modes. Two

equivalent, isolated oscillators provide an example for two-state coupling, for example, the hydride stretchings in the NH_2 or CH_2 group. This “local mode” coupling can be the consequence of an entirely harmonic Hamiltonian and would not be apparent in a normal mode picture. At high vibrational excitation, one often observes two nearly degenerate pairs of spectral states, which correspond to the symmetric and antisymmetric combinations of localized vibrations in one of the two bonds. By coherent excitation of these two eigenstates, a time-dependent, localized state can be created, which will oscillate between the two equivalent localized vibrational modes with period τ (Quack 1981a, 1990, 1993). In all these examples, time-independent spectroscopy measures the energy difference ΔE , which allows the conclusion by quantum mechanics that a time-dependent state can, in principle, be created by coherent excitation by laser pulses, which will oscillate with period $\tau = h/\Delta E$.

The nature of the migration of excitation between these two local modes or bond modes is of some interest. While it certainly corresponds to a migration of vibrational energy from one bond to the other, it is not necessarily linked to IVR (Quack and Kutzelnigg 1995). Indeed, in a normal mode picture, the excitation energy would remain localized and conserved within one normal coordinate (or separately within each normal coordinate) and thus separability excludes true IVR (Beil *et al.* 1997). The excitation of the two spectral lines corresponds to the excitation of two normal modes with corresponding Lissajous motion (Herzberg 1945).

An apparently similar, but in fact quite different, type of two-state coupling leads to true IVR: anharmonic Fermi resonances or Darling–Dennison resonances. If such resonances occur as two-level resonances, which is the simplest case, then they are again described by equations (18)–(21) with a periodic oscillation. In a Fermi resonance, the two coupled states correspond to an excitation of one normal mode with one quantum and another normal mode with two quanta, both levels of about the same energy, coupled by anharmonic potential terms. Here the separability of the dynamics in the normal modes is destroyed and the time dependence corresponds to a flow of energy between different vibrational normal modes. In a Darling–Dennison resonance, the two coupled levels correspond both to an excitation of two different normal vibrations, each with two quanta, the coupling being again anharmonic and nonseparable. These are just two examples where the observation of some splitting leads to an interpretation in terms of time-dependent processes but very different ones, indeed. Another very different type of two-level dynamics is related to tunneling splittings (to be discussed below) and a further one relates to spin–spin couplings. The mere observation of some splitting ΔE does not define the observed process, yet.

4.2.3 *Coupling Many Levels in a Multistate Dynamics*

In a more complex case, one state may be coupled to another state, which is coupled to a third state, and so on, leading to a chainlike coupling structure with a tridiagonal effective Hamiltonian matrix representation (Dübal and Quack 1984, Quack 1990, 1993, 1995b, Beil *et al.* 1997). A particularly well-studied example of this type is given by the Fermi resonance between stretching modes s and bending modes b in isolated hydride bonds, e.g., the alkyl-CH-chromophore. By this resonance, $3\nu_s$ is coupled to the combination band $2\nu_s + 2\nu_b$, which is coupled to $\nu_s + 4\nu_b$, which in turn is coupled to $6\nu_b$, for example. All vibrational states of a given symmetry species with common polyad number $N = \nu_s + 0.5 \cdot \nu_b$ are thus coupled together, where the ν denote vibrational quantum numbers. Off-diagonal coupling matrix elements are given as functions of a parameter k_{sbb} , which would correspond at a low order of perturbation theory to the cubic anharmonic potential term C_{sbb} . In practice, k_{sbb} is just a fit parameter to the observed spectrum and may differ markedly from C_{sbb} (Quack 1990, 1993, 1995b, Beil *et al.* 1997). Matrix diagonalization yields the energies of the molecular eigenstates. It is often assumed that only the zeroth-order state with the most stretching quanta carries noticeable transition strength (“bright state”), since hydride stretching modes are, in general, very anharmonic. The perturbed states then gain their transition strength through the admixture of bright state character in this simple model, which allows the prediction of transition energies and relative intensities within one polyad. With a very short laser pulse exciting all polyad members coherently, the pure hydride stretching mode can be prepared, in principle, which will then redistribute vibrational energy over time to the stretching/bending manifold, due to the Fermi-resonance couplings.

With increasing vibrational excitation, the density of vibrational states becomes very high, especially for molecules with low-frequency vibrational modes. In aniline, for example, the density of vibrational state is estimated to be about 1.7×10^5 per cm^{-1} in the first NH-stretching overtone region. All these background states might be coupled at least weakly with the chromophore state giving rise to homogeneous spectral structures. The weak couplings typically govern the dynamics on timescales of picoseconds to nanoseconds. Although an exhaustive analysis of these couplings and thus of all details of the redistribution process may be very difficult, except perhaps for some simpler cases employing double-resonance experiments at very high resolution, a simplified interpretation on the basis of a statistical model is often still possible. Assuming a statistical coupling with some average coupling strength, one expects, and

often observes in experiments, a Lorentzian envelope over the homogeneous structure, or even an apparent Lorentzian line width due to the overlapping of lines composing the homogeneous structure. In such a statistical model, which is similar to the Bixon–Jortner model of electronic relaxation processes (Bixon and Jortner 1968), the full width at half maximum (FWHM) Γ of the Lorentzian distribution indicates an exponential decay of the initial vibrational chromophore state to the background states with relaxation time $\tau = h/(2\pi\Gamma)$ (Quack 1981a, *see also* Merkt and Quack 2011: **Molecular Quantum Mechanics and Molecular Spectra, Molecular Symmetry, and Interaction of Matter with Radiation**, this handbook). An analogous interpretation applies to the special case of vibrational predissociation or preionization (Herzberg 1966, Jungen and Raoult 1981, Hippler *et al.* 1997, Merkt 1997, Hollenstein *et al.* 2001), where the initial vibrational state decays exponentially to a true continuum of background states with relaxation time τ , which can be again inferred from the Lorentzian line width Γ (Quack 1981a, von Puttkamer and Quack 1989).

In all cases, the accuracy of description of time-dependent and time-independent states involved depends on the level of theory on which the effective Hamiltonian was derived. In general, several mechanisms may be active for intramolecular redistribution processes of an initially prepared time-dependent state, and the interaction of different mechanisms can be studied (Fehrensens *et al.* 1998). Sometimes, a distinct ordering of coupling strengths and thus also of mechanisms can be observed, leading to a hierarchy of timescales in IVR (Dübal and Quack 1981, Segall *et al.* 1987, Lubich *et al.* 1995, Boyarkin and Rizzo 1996, Hippler and Quack 1996, Boyarkin *et al.* 1999). The understanding of spectra and the dynamics of highly excited vibrational states through overtone spectroscopy (Quack 1990) is among the most exciting current research subjects, since it is intimately related to primary processes in laser chemistry and reaction dynamics (Quack 1993, 1995a,b,c). It may appear at first glance that IVR is a molecule-specific process, which cannot be controlled, and that therefore mode-specific laser chemistry is impeded by the very fast IVR processes. This is, however, not necessarily true. The knowledge of IVR timescales suggests first the use of very short (femtoseconds to pico seconds) laser pulses to overcome the effects of IVR and thus to control the outcome of laser-driven chemistry on short timescales. Furthermore, the molecular Hamiltonian derived from a detailed analysis of experimental spectra allows the prediction of very special initial time-dependent states with “unusual” properties, showing, for example, particularly slow IVR or leading to IVR processes, which proceed in a very special way, breaking selected chemical bonds (Quack 1983b, von Puttkamer *et al.* 1983b, Lehmann *et al.* 1994, Gruebele and Bigwood

1998). Such “designed” initial states can be prepared, in principle, by the coherent superposition of eigenstates by laser pulses with specific amplitude and phase relationship between frequency components. Although at its very beginnings, this new approach to mode-specific laser chemistry is a “hot topic” of current research (Warren *et al.* 1993, Gerber *et al.* 1995, Baumert *et al.* 1997, Meshulach and Silberberg 1999, Shapiro and Brumer 2003, Witte *et al.* 2003). In principle, an appropriate spectroscopic analysis at very high resolution can be the starting point for many applications in these fields of research.

5 THE EXPERIMENTAL APPROACH TO INFRARED SPECTROSCOPY WITH MASS AND ISOTOPE SELECTION (IRSIMS)

Our experimental setup for mass-selective infrared spectroscopy is shown schematically in Figures 3 and 4. In short, IR radiation from a Ti:sapphire laser system or from an optical parametric amplifier (OPA) is focused into the core of a skimmed molecular beam within an ultrahigh vacuum (UHV) chamber. After a suitable time delay, the counterpropagating UV radiation is also focused to the same focal spot. Ions generated after IR + UV absorption by OSVADPI or by RE2PI of vibrationally excited molecules are mass analyzed in a time-of-flight (TOF) mass spectrometer. Since the ionization yield mirrors the IR excitation, mass analysis of the ions allows separation of the spectral contributions of different isotopomers or, more generally, of different components in a mixture.

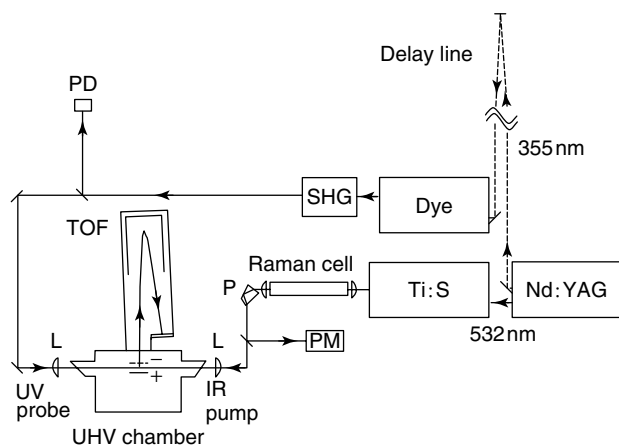


Figure 3 Experimental setup with Ti:sapphire laser and Raman shifter (after Hippler and Quack 1994). SHG, second harmonic generation of UV radiation; PD, photo diode to monitor the UV pulse energy; PM, pyroelectric monitor of the IR pulse energy; P, Pellin–Broca prism; L, lenses to focus UV and IR radiation, respectively; TOF, time-of-flight mass spectrometer.

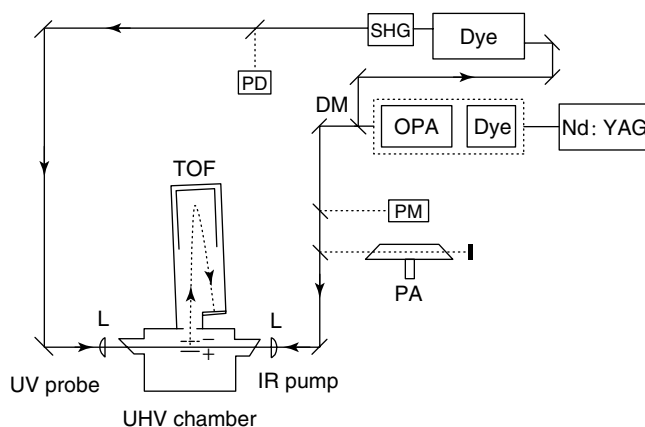


Figure 4 Scheme of the experimental setup with OPA as IR laser source (after Hippler and Quack 1997). SHG: second harmonic generation, PD: UV photodiode, L: lens, OPA: optical parametric amplifier, DM, dichroic mirror to separate the 355-nm pump radiation; PM, pyroelectric IR power monitor; PA, photoacoustic reference cell; TOF, time-of-flight mass spectrometer.

For some experiments (e.g., to observe CHCl_3 overtone spectra, see below), near-infrared light around $11\,500\text{ cm}^{-1}$ is created by a Ti:sapphire laser (STI Optronics, HRL-100) pumped by the first harmonic output (532 nm, typically 500 mJ per pulse at 10 Hz) of a pulsed Nd:YAG laser (Continuum, NY82-10) (see Figure 3). The Ti:sapphire laser has single longitudinal mode output with an essentially Fourier-transform-limited Gaussian beam with specified bandwidth of less than 500 MHz (0.017 cm^{-1}) with ca 20–40 mJ energy per 4.5 ns pulse at a 10 Hz repetition rate. The IR radiation is focused with a 20-cm focal length lens into the TOF vacuum chamber with a focal spot diameter of $100\ \mu\text{m}$ (FWHM). At a pulse energy of 40 mJ, the power density in the focal spot is thus approximately 100 GW cm^{-2} . With the Ti:sapphire laser system, the 710–910 nm ($11\,000\text{--}14\,100\text{ cm}^{-1}$) red and near-infrared spectral region is accessible. To extend this region further into the infrared, a Raman shifting cell is inserted after the Ti:sapphire laser (Figure 3). The 70-cm-long high-pressure cell is made of stainless steel and equipped with sapphire windows. It is filled with H_2 at a pressure of 20–30 bar as Raman-active medium. A 40-cm focus lens focuses the pump radiation from the Ti:sapphire laser, and after the cell, the Raman shifted radiation is made parallel again with another 40-cm focus length lens. Stimulated Raman scattering on the Q(1) line in $\nu = 1$ of H_2 with $\Delta E = 4155\text{ cm}^{-1}$ creates several Stokes and anti-Stokes lines from the pump radiation (Minck *et al.* 1963, Bischel and Dyer 1986, White 1987, Bespalov *et al.* 1991, Duncan *et al.* 1991). With 60 mJ pulse energy at 790 nm as pump source, ca 15 mJ of first Stokes radiation at 8500 cm^{-1} is obtained. The first Stokes line is separated from the fundamental pump light and other Stokes lines by a Pellin–Broca prism,

and then focused into the TOF vacuum chamber with a measured spot diameter of 500 μm (FWHM). In this case, a power density of roughly 1.5 GW cm^{-2} is estimated. Time delayed and counterpropagating to the IR radiation, ca 0.1–0.5 mJ of UV laser light from a frequency-doubled dye laser around 240 nm (Lumonics, HD-500) is also focused into the vacuum chamber with a 20-cm focal length quartz lens. The dye laser is pumped with the third harmonic output (ca 50 mJ pulse energy at 355 nm) from the same Nd:YAG laser that is used to pump the Ti:sapphire laser system. A fixed time delay of ca 30 ns between the IR and the following UV laser pulses in the vacuum chamber is achieved by optically delaying the pump light for the dye laser by several meters (Figure 3).

In other experiments (e.g. to observe aniline and benzene overtone spectra, see below), IR idler radiation is generated in an OPA of a narrow-bandwidth dye laser operating at the signal wavelength (Figure 4). A frequency-tripled, injection-seeded Nd:YAG laser (Continuum, Powerlite 9010) pumps the OPA system (Lambda Physik, modified SCANMATE OPPO). In order to improve the conversion efficiency, two β -barium borate (BBO) crystals are employed for the optical parametric amplification. The laser system is tunable from 410 to 2500 nm, delivering typical IR pulse energies between 30 mJ at 800 nm and 10 mJ at 2000 nm and some millijoules at 2500 nm after pumping the dye laser and the BBO crystals with 300 mJ per pulse of 355 nm radiation from the injection-seeded Nd:YAG laser. The temporal pulse profile is nearly Gaussian with 4 ns FWHM. The spectra displayed here are recorded with an IR laser bandwidth of 0.15 cm^{-1} , since no additional structures are apparent with the improved bandwidth of 0.02 cm^{-1} achieved using an intracavity etalon in the dye laser in a series of control experiments at higher resolution. The remaining 355 nm pump light (typically 70 mJ per pulse), which is not converted in the OPA, is separated from the signal and idler radiation by a dichroic mirror (Figure 4). After a suitable, short optical delay, it is used to pump a dye laser, which is then frequency doubled generating typically 200 μJ per pulse of UV radiation around 240–300 nm (Lumonics, HD-500). The OPA IR idler radiation is separated from the visible signal radiation by a glass filter (Schott, RG715) and focused by a 25-cm lens into the UHV chamber. In order to avoid saturation of the aniline or benzene overtone transitions by IR excitation, the focus of the IR radiation is pulled slightly out of exact overlap with the jet region (by ca 1–2 cm). Signals are then linearly dependent on the IR pulse energy. The UV laser is also focused into the vacuum chamber counterpropagating to the IR by a 30-cm quartz lens. The time delay between the IR pump and the UV probe beams is 20 ns. Both IR and UV laser radiation are linearly polarized within the same plane. In order to obtain IR + UV double-resonance

signals, it is necessary to overlap both foci very carefully. The ionization signal is found to be proportional to the IR absorption, and by scanning the IR laser while monitoring the ionization yield, overtone spectra are obtained. Double-resonance ionization signals depend linearly on the IR pulse energy, and ionization signals are normalized accordingly to correct for laser pulse to pulse energy fluctuations. Simultaneously with the IR + UV ionization spectra, reference spectra are taken with a small photoacoustic cell filled with the sample vapor or a reference gas (e.g. methane or water vapor) typically at a pressure of 100 mbar. After a quadratic fit to reference lines known from literature (Rothman *et al.* 1992, 2005, Toth 1994) or by comparing the photoacoustic spectrum with a corresponding room-temperature spectrum obtained separately with an FTIR spectrometer (BOMEM, DA-002) (Amrein *et al.* 1985, Quack 1990) or the Bruker 125 HR ZP 2001 Zurich prototype (Albert and Quack 2007, Albert *et al.* 2011b: **High-resolution Fourier Transform Infrared Spectroscopy**, this handbook), an absolute wavenumber accuracy of 0.1 cm^{-1} is estimated for the IR spectra presented below.

Sample substances are, in general, purified by distillation and degassed by several freeze–pump–thaw cycles, and the purity is checked with gas chromatography. Partially N-deuterated aniline is prepared by hydrogen exchange in a stoichiometric mixture with CH_3OD (Cambridge Isotope Laboratories, 99% D), which is then distilled off. The sample vapor is typically diluted into 1 bar of Ar, e.g., for the chloroform experiments, by preparing a mixture of saturated chloroform vapor (ca 210 mbar, Fluka puriss. p.a.) in 1 bar argon or for the aniline experiments by bubbling 1 bar of the seed gas Ar or N_2 through liquid aniline (Fluka), which has a vapor pressure of 0.74 mbar at room temperature (Fehrensens *et al.* 1999a). The gas mixture then expands through a pulsed solenoid nozzle with 1-mm circular orifice (General Valve, with Iota One pulse driver) into the first vacuum chamber. After passing a 0.5-mm skimmer (Beam Dynamics, model 2) at a distance of 3 cm from the nozzle orifice, the skimmed molecular beam enters the second UHV chamber. Ions created by IR + UV absorption are guided by electric fields through a small aperture to the UHV chamber with the TOF mass spectrometer. All vacuum chambers are pumped differentially by turbomolecular pumps. Room-temperature spectra are obtained by flowing ca 10^{-4} mbar of sample vapor through the second chamber. Differential pumping keeps the pressure in the TOF chamber always below 10^{-6} mbar. In a test run, NO seeded into 1 bar argon was probed by (1+1) REMPI via the $A^2\Sigma(v'=0) \leftarrow X^2\Pi_{1/2}(v''=0)$ transition at 226 nm (Hippler 1993, Hippler and Pfab 1995) (without the IR laser operating). In the ($R_{11} + Q_{21}$)- and R_{21} -branches, only transitions from the lowest rotational state of NO with $J = 0.5$ were observed; transitions from $J = 1.5$ or higher

J were not apparent. This indicates a rotational temperature of the skimmed molecular beam below 3 K, and a similar or perhaps somewhat higher rotational temperature is expected for expansions of chloroform or aniline seeded into Ar in the present experiment. Vibrational cooling in a supersonic expansion is frequently less effective than rotational cooling. Typical vibrational temperatures can be of the order of 100–200 K, depending on the molecule and type of vibration (Miller 1988, Gentry 1988, Demtröder 1981, Amrein *et al.* 1988, Amirav *et al.* 1980).

The custom-built TOF mass spectrometer in our experiments is a Wiley–McLaren type reflectron (Kaesdorf, Munich) (Wiley and McLaren 1955, Karataev *et al.* 1972, Mamyrin *et al.* 1973, Gohl *et al.* 1983, Boesl *et al.* 1992) combining double-stage ion extraction with a double-stage ion reflector. With this TOF, the benzene ion parent peak with $m = 78$ u is observed after a flight time $\Delta t = 27.89$ μ s with an FWHM of the ion peak of ca $\Delta t_{\text{FWHM}} = 8$ ns, which is mainly caused by the UV pulse length. With the resolving power R of a TOF mass spectrometer defined as $R = m/\Delta m = \Delta t/(\Delta t_{\text{FWHM}} \times 2)$ (Boesl *et al.* 1992), $R = 1743$ at $m = 78$ u is calculated for the present setup. Ion signals are processed by boxcar integrators (Stanford Research, SR 250) and an oscilloscope (Tektronix, TDS 520A), where time windows for integrating ion signals are defined, corresponding to selected flight times of different masses. In this way, separated ion yields of different components are recorded simultaneously, which allows for mass spectroscopy and ISOS.

6 MASS-SELECTIVE OVERTONE SPECTROSCOPY BY VIBRATIONALLY ASSISTED DISSOCIATION AND PHOTOFRAGMENT IONIZATION: OSVADPI

In this section, a variant of infrared photofragment spectroscopy is introduced and evaluated; this technique was developed by us by 1994 as overtone spectroscopy by vibrationally assisted dissociation and photofragment ionization (OSVADPI) (Hippler and Quack 1994, 1995, 1996, 1997, Hippler 2001). In this scheme, IR excitation is coupled with UV dissociation and ionization of photofragments, which allows indirect, but extremely sensitive, IR spectroscopy. Since ionization detection can be conveniently coupled with a mass spectrometer, mass- and isotopomer-selective infrared spectroscopy is possible for studying isotope effects in intramolecular dynamics. This new technique allows the separation of spectral contributions arising from naturally occurring isotopomers, or of different components in a mixture: ISOS or, more generally, IRSIMS.

The combination of sensitive infrared spectroscopy with mass spectrometry greatly increases the selectivity, which is important for both fundamental and analytical applications of spectroscopy. The decomposition of overlapping spectra from different components reduces inhomogeneous congestion; in many cases, it will allow for the first time a secure assignment, as in the examples discussed below. After a discussion of the excitation mechanism and scheme of absorption, we introduce, as an exemplary application, the overtone spectroscopy of Cl-isotopomers of chloroform, revealing isotope effects and a hierarchy of timescales of IVR after excitation of the CH-chromophore (Hippler and Quack 1996).

6.1 Mechanism of Vibrationally Assisted Dissociation and Photofragment Ionization

Without the IR laser operating, a weak ion current is observed, if UV radiation between 235 and 240 nm is focused into a cell or a molecular beam containing vapor of some aliphatic chlorides, such as chloroform, tert-butyl chloride, or CF_2HCl . The ion current increases, but is still very small, if the UV laser is tuned to one of the several $(2 + 1)$ REMPI transitions of Cl ($^2P_{3/2}$) or Cl ($^2P_{1/2}$) in this region (Arepalli *et al.* 1985). Aliphatic chloride compounds have a characteristic first UV absorption band below 200 nm (Tsubomura *et al.* 1964, Russell *et al.* 1973, Hubrich and Stuhl 1980). In this $n \rightarrow \sigma^*$ transition, electron density is transferred from a nonbonding to an antibonding orbital around the C–Cl bond, which causes the bond to break, releasing Cl ($^2P_{3/2}$) or Cl ($^2P_{1/2}$) fragments. Apparently, UV radiation between 235 and 240 nm dissociates molecules on the very edge of this absorption band with low cross section, or by a two-photon transition to a higher electronic dissociative state. Nascent Cl fragments are then ionized by the same UV laser beam in a $(2 + 1)$ REMPI process. Other heavier fragments might also be ionized by REMPI via broad absorption bands. Since the UV laser wavelength is unfavorable for the first dissociation step in the absorption sequence, ionization signals are only weak.

If the IR laser operates in addition and excites molecules first, a distinct increase of the resonant ionization yield is observed. Two possible schemes of excitation suggest themselves and need to be discussed: first, IR multiphoton absorption could lead to electronic ground state dissociation. Nascent Cl fragments would then be ionized by the UV laser by $(2 + 1)$ REMPI, for example. IR multiphoton dissociation, however, does not appear to apply in the present case. In CF_2HCl or CHCl_3 , the energetically lowest dissociation channel via the electronic ground state is α, α -elimination of HCl (Schug *et al.* 1979, Duperré and

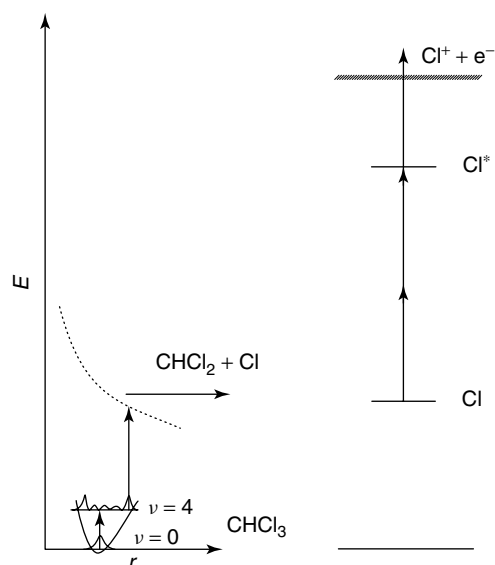


Figure 5 OSVADPI scheme of excitation with CHCl_3 serving as example (after Hippler and Quack 1994).

van den Bergh 1979, Quack *et al.* 1980, Yang *et al.* 1994). Scanning the UV laser through known HCl (2 + 1) REMPI transitions did not reveal any HCl, however. Further, the ionization yield depends linearly on the IR pulse energy, indicating that only one IR photon is absorbed. The presence of Cl fragments finally points to dissociation via an excited electronic state (Yang *et al.* 1994). This leads to the scheme of excitation summarized in Figure 5, OSVADPI: After the absorption of one IR photon, vibrationally excited molecules are UV photodissociated. Cl fragments are then ionized by (2 + 1) REMPI, and possibly also some heavier fragments. The first IR absorption step effectively limits the ionization yield. Ionization detection in this scheme allows indirect, but very sensitive, infrared spectroscopy.

The combined IR and UV radiation excites the dissociative electronic state much more efficiently than one-photon UV absorption alone. This is partly due to the higher total energy of IR + UV photons: The absorption cross section of the first UV absorption band increases by several orders of magnitude at the higher total energy of the IR + UV photons compared to the UV photon alone. Another, essential enhancing mechanism is provided by the Franck–Condon principle: by vibrational excitation, the molecular wavefunction extends over a larger region, which allows a more efficient transition to the electronically excited state. This is indicated in the scheme of Figure 5, but the real multidimensional situation is, of course, much more complex than shown. Similar explanations are invoked to explain the enhanced absorption in vibrationally mediated dissociation of other molecules, where photofragments have been probed by LIF detection (Crim 1993). In this respect, the dissociation mechanism of OSVADPI is analogous

to vibrationally mediated dissociation spectroscopy. The proposed mechanism of excitation is corroborated by studying the dependence of the ionization yield on the IR and UV pulse energies with CHCl_3 as example (Hippler and Quack 1994). At a UV wavelength that corresponds to a (2 + 1) REMPI transition of Cl, the ionization yield depends linearly on the IR intensity and fluence, consistent with vibrational one-photon IR excitation as the first step in the absorption scheme. The dependence on the UV intensity and fluence is quartic at low intensity, cubic at intermediate levels, and finally quadratic at pulse energies over $40 \mu\text{J}$ per pulse, corresponding to peak intensities of about 40 MW cm^{-2} or fluences of about 0.4 J cm^{-2} . This is consistent with four UV photons being involved in the absorption sequence. The first photon induces vibrationally assisted photodissociation, and the remaining ionize Cl fragments formed in their spin–orbit split ground state via (2 + 1) REMPI. With increasing UV pulse energy, first the dissociation and the ionization step are saturated, leaving finally the quadratic dependence of the two-photon Cl excitation, which has a low absorption cross section. At UV wavelengths not coinciding with a Cl atomic resonance, the ionization yield depends also linearly on the IR intensity. Again, the first step in the absorption sequence is the IR one-photon excitation. The dependence of the ionization yield on the UV intensity is found to be cubic at low and quadratic at intensities over 50 MW cm^{-2} . The first absorbed UV photon causes vibrationally assisted photodissociation of CHCl_3 , followed presumably by two-photon ionization of fragments, possibly CHCl_2 .

One important aspect in the OSVADPI scheme presented is that the electronically excited state is a dissociation continuum. This intermediate state in the ionization sequence does not show any apparent structure within the small energy range encompassed by scanning the IR laser to obtain an overtone spectrum. It was therefore in all cases entirely adequate to leave the UV laser at a fixed frequency while scanning the IR laser, which greatly simplifies the experiment. This is a very important advantage compared to other schemes with ionization detection of infrared excitation via discrete electronically excited rovibrational states. The experimental setup is also less involved than comparable schemes: The UV photons required for dissociation and REMPI detection of photofragments are all derived from one laser system operating in the UV range around 250 nm, which is conveniently accessible by standard frequency doubling of a dye laser. Both IR and UV laser systems are pumped by one single Nd:YAG pump laser, and an optical delay line achieves the synchronization of the laser systems (Figures 3 and 4). Ion detection is extremely sensitive; OSVADPI is thus a very sensitive indirect technique for IR spectroscopy. Because low sample pressures are required and the absorption path is the focus region only,

the OSVADPI technique is ideally suited to study overtone spectroscopy of samples having low vapor pressure or of jet-cooled samples in supersonic jet expansions. Compared to the much higher sample pressure required for FTIR or photoacoustic spectroscopy to get spectra of comparable quality, the low sample pressure greatly reduces the unwanted effect of pressure broadening. Coupling ionization detection with a TOF mass spectrometer finally allows mass- and isotope-selective infrared spectroscopy of different components in a mixture, for example, Cl-isotopomers of chloroform at natural abundance. Although it would be, in principle, possible to chemically prepare isotope-pure Cl-isotopomers of chloroform, this would be very expensive and not very practical; with the present scheme, however, this is not necessary, since the different Cl-isotopes are separated in the mass spectrometer.

Figure 6 shows the TOF mass spectrum after IR excitation at $11\,384.6\text{ cm}^{-1}$ and UV photodissociation and ionization. The UV wavelength at 235.32 nm corresponds to the $(2 + 1)$ REMPI transition of Cl, $3p^4 4p\ (^3P)\ ^2D_{3/2}^o \leftarrow 3p^5\ ^2P_{3/2}^o$ (Arepalli *et al.* 1985). The dominating ions are thus ^{35}Cl and ^{37}Cl . As shown below, the IR excitation corresponds to a transition of $\text{CH}^{35}\text{Cl}_2^{37}\text{Cl}$. The observed $^{35}\text{Cl}/^{37}\text{Cl}$ -isotope ratio does therefore not reflect the natural abundance of Cl-isotopes; it is rather about 2:1 as in the particular IR-excited isotopomer. ^{12}C , $^{12}\text{C}^{35}\text{Cl}$ and $^{12}\text{C}^{37}\text{Cl}$ ions and a small fraction of the corresponding ^{13}C containing ions are also observed. Possibly, the second photofragment CHCl_2 is ionized by $(1 + 1)$ REMPI, and further fragmentation leads to the appearance of CCl and C ions. Alternatively, secondary photodissociation of CHCl_2 may yield CCl and HCl fragments (as for the

193 nm photodissociation of CHCl_3 (Yang *et al.* 1994)), and CCl is then ionized and further fragmented. Since the UV radiation cannot ionize C atoms efficiently, C ions result from the fragmentation of an ionic precursor. Mass gating the ion detection to ^{35}Cl and ^{37}Cl will not allow isotopomer-selective spectroscopy of CHCl_3 directly, since there are four Cl-isotopomers: $\text{CH}^{35}\text{Cl}_3$ (43.5% natural abundance), $\text{CH}^{35}\text{Cl}_2^{37}\text{Cl}$ (41.7%), $\text{CH}^{35}\text{Cl}^{37}\text{Cl}_2$ (13.3%), and the minor component $\text{CH}^{37}\text{Cl}_3$ (1.4%). ^{13}CH - and ^{12}CH -chromophore absorptions are well separated with ^{13}CH -transitions outside the range discussed below (Hollenstein *et al.* 1990a). Mass-selective detection of ^{35}Cl and ^{37}Cl ions in OSVADPI allows a simple manipulation to assign spectral features to the three major Cl-isotopomers: if twice the yield of ^{37}Cl is subtracted from the yield of ^{35}Cl fragments, the influence of $\text{CH}^{35}\text{Cl}_2^{37}\text{Cl}$ on the total yield of ^{35}Cl fragments is approximately subtracted, since for every ^{37}Cl , two ^{35}Cl appear for this isotopomer. Spectral features, which remain unaffected under this operation, are thus identified to belong to $\text{CH}^{35}\text{Cl}_3$ whereas features, which disappear, belong to $\text{CH}^{35}\text{Cl}_2^{37}\text{Cl}$. The influence of the third important isotopomer $\text{CH}^{35}\text{Cl}^{37}\text{Cl}_2$, however, would be overestimated. “Negative” features after the subtraction are thus due to $\text{CH}^{35}\text{Cl}^{37}\text{Cl}_2$. This subtraction scheme allows secure assignments, especially for resolved spectral features (Hippler and Quack 1996, 1997, Hippler 2001).

6.2 Isotopomer-selective Overtone Spectroscopy (ISOS) of the $N_j = 4_2$ CH-chromophore Absorption of CHCl_3

Because of the presence of four Cl-isotopomers, CHCl_3 overtone spectra have a very complex structure, which is also affected by vibrational hot-band transitions: at room temperature, the vibrational ground state of chloroform has only a population of 38%. ν_6 (the degenerate C–Cl₃ bending vibration at 260 cm^{-1} (Ruoff and Bürger 1970)) and $2\nu_6$ have a population of 22 and 10%, respectively, and ν_3 (the C–Cl₃ “umbrella” vibration at 367 cm^{-1} (Ruoff and Bürger 1970, Hippler and Quack 1997, Pietilä *et al.* 1999)) a population of 7%. This inhomogeneous congestion is especially apparent in the central part of parallel vibrational bands with sharp Q -branches of Cl-isotopomers and of hot-band transitions. Without means to simplify spectra, secure assignment of features to genuine, anharmonic local resonances would be exceedingly difficult. The $N_j = 4_2$ CH-chromophore absorption (corresponding approximately to the $3\nu_1 + 2\nu_4$ combination band) is part of the $N = 4$ polyad; in the order of descending wavenumbers, it is the second band after $N_j = 4_1$. The very weak band has only about 5% of the peak intensities compared to $N_j = 4_1$

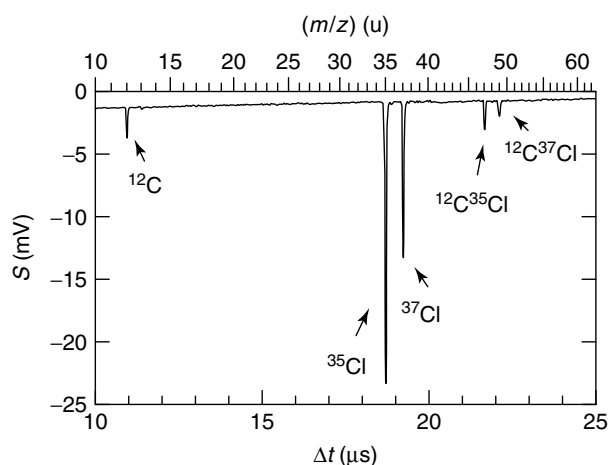


Figure 6 Fragment mass spectrum after dissociation of vibrationally excited CHCl_3 and ionization with UV radiation at 235.32 nm (from Hippler and Quack 2006). S denotes the ion signal, Δt the flight time in the time-of-flight mass spectrometer; m/z is the corresponding nonlinear mass scale.

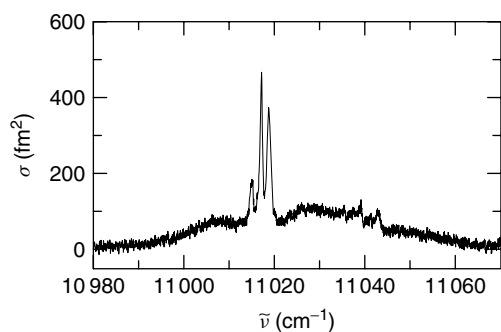


Figure 7 $N_j = 4_2$ CH-chromophore absorption of chloroform at room temperature, recorded by FTIR spectroscopy in a multipass absorption cell, $l = 49$ m, 100 mbar CHCl_3 , 0.1 cm^{-1} experimental bandwidth (recorded by H. Hollenstein, Zürich group; from Hippler and Quack 2006).

(see Figure 7). In a simple intensity model for the $N = 4$ polyad, the $\nu_1 = 4$ CH-stretching overtone carries all of the absorption intensity. All polyad states acquire absorption intensity according to the admixture of this CH-stretching overtone due to the Fermi resonance between CH-stretching and bending modes. The $N_j = 4_2$ band has been observed before in an investigation of this strong Fermi resonance, but only an approximate band position at 11019 cm^{-1} was reported without any further details, for example, discussing the position of different Cl-isotopomers (Wong *et al.* 1987, William *et al.* 1987). Since a secure assignment of $N_j = 4_2$ is essential to corroborate the identification of the local perturber in the $N_j = 4_1$ overtone (see the next section), this band was reinvestigated in detail (Hippler 2001). The room-temperature spectrum recorded by FTIR in a multipass absorption cell corresponds to the natural Cl-isotopomer mixture of 100 mbar chloroform (Figure 7). The spectrum shows the parallel band with sharp Q -branch features and typical broad contours of the P - and R -branches located around the Q -branch at lower and higher wavenumbers, respectively. In addition, there are very weak features around 11040 cm^{-1} that cannot be assigned at present. Presumably, they are due to a different combination band.

In Figure 8, the Q -branch region of $N_j = 4_2$ is shown in more detail. In (b), the room-temperature FTIR spectrum (as in Figure 7) is shown and in (a) the corresponding OSVADPI spectrum (without mass selection) is shown. OSVADPI spectra of ca 10^{-4} mbar chloroform vapor (leaking through the vacuum chamber) were obtained with the OPA system and with the UV laser at 235.32 nm corresponding to a $(2 + 1)$ REMPI transition of Cl. Both spectra are essentially identical, which indicates that OSVADPI is a faithful mirror of IR excitation. In the Q -branch, three features are apparent, which are labeled “A”, “B”, and “C” for convenience. Whether they correspond to the Q -branches of

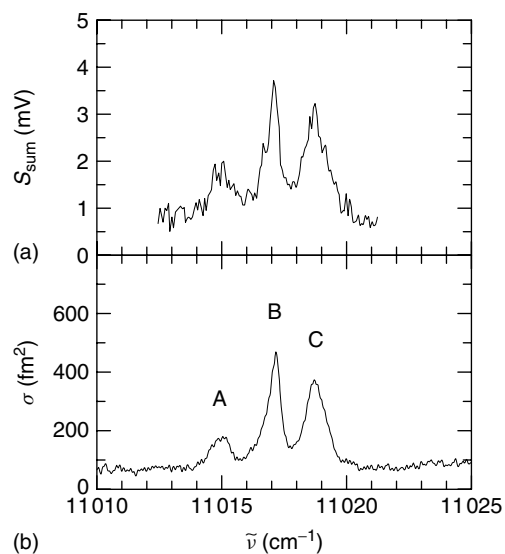


Figure 8 Q -branch region of the chloroform $N_j = 4_2$ CH-chromophore absorption at room temperature (from Hippler and Quack 2006). (a) An OSVADPI spectrum of ca 10^{-4} mbar chloroform vapor (without isotopomer selection, S_{sum} corresponding to the sum of all ions). (b) The FTIR reference spectrum (as in Figure 7). The three distinct spectral features have been labeled A, B, and C; they are discussed in the text.

the three major Cl-isotopomers, to hot-band transitions, or perhaps to the homogeneous structure of a local anharmonic resonance, however, cannot be decided and assigned on the basis of the room-temperature spectrum without decomposition of the spectrum into Cl-isotopomers. Mass gating the fragment ion detection in the OSVADPI scheme to the yield of ^{35}Cl and ^{37}Cl ions with the TOF mass spectrometer, ISOS spectra have been obtained after application of the subtraction scheme introduced before (see Figure 9). It is clearly seen that feature “C” belongs to the $\text{CH}^{35}\text{Cl}_3$ isotopomer, since it does not contribute to the ^{37}Cl fragment yield. Feature “B” has a $^{35}\text{Cl}/^{37}\text{Cl}$ -isotope ratio of 2 : 1 and is therefore due to $\text{CH}^{35}\text{Cl}_2^{37}\text{Cl}$. Feature “A” corresponds to an isotope containing more ^{37}Cl than ^{35}Cl , since the peak is “negative” after the subtraction; it is therefore assigned to $\text{CH}^{35}\text{Cl}^{37}\text{Cl}_2$. The relative peak areas of features “A”, “B”, and “C” (normalized to the sum 100) are 15, 41, and 44, respectively, which, in this assignment, corresponds closely to the relative abundance of isotopomers. Q -branch maxima at 11015.0 cm^{-1} , 11017.2 cm^{-1} , and 11018.7 cm^{-1} are thus found by ISOS for the isotopomers $\text{CH}^{35}\text{Cl}^{37}\text{Cl}_2$, $\text{CH}^{35}\text{Cl}_2^{37}\text{Cl}$, and $\text{CH}^{35}\text{Cl}_3$, respectively, with an estimated accuracy of 0.1 cm^{-1} . The maxima are good estimates for the band origins of $N_j = 4_2$. Relative to the position of $\text{CH}^{35}\text{Cl}_3$, Cl-isotopomer shifts are thus 1.5 cm^{-1} for $\text{CH}^{35}\text{Cl}_2^{37}\text{Cl}$ and 3.7 cm^{-1} for $\text{CH}^{35}\text{Cl}^{37}\text{Cl}_2$. These experimental shifts may serve as benchmark results for theoretical calculations (Hollenstein *et al.* 1993, Pietilä *et al.* 1999).

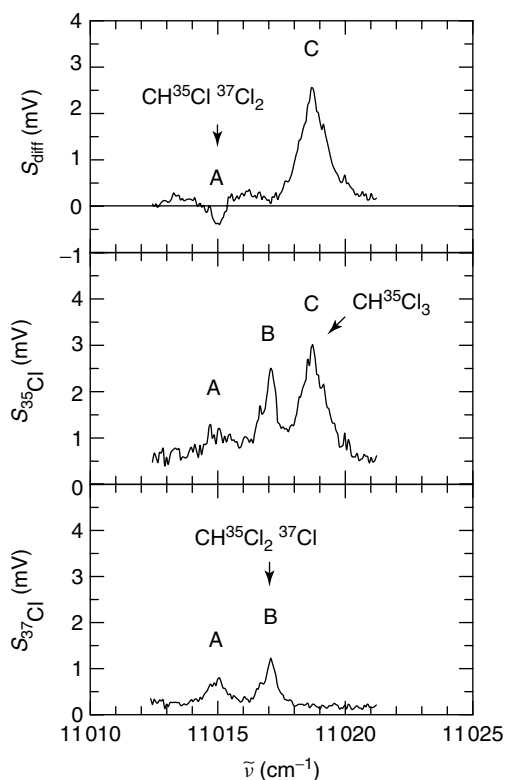


Figure 9 Isotopomer-selective OSVADPI spectra (ISOS) of the Q -branch region of the $N_j = 4_2$ CH-chromophore component of chloroform at room temperature (from Hippler and Quack 2006). The peaks A, B, and C are assigned to the three major Cl-isotopomers (see text).

Since lighter isotopomers appear at higher wavenumbers, the order of band origins is as expected if no perturbations are effective. Vibrational hot-band transitions are probably hidden in the Q -branch contours, which have an FWHM of about $0.5\text{--}1\text{ cm}^{-1}$ at room temperature.

6.3 Isotopomer-selective Overtone Spectroscopy (ISOS) of the $N_j = 4_1$ CH-chromophore Absorption of CHCl_3 : A Hierarchy of Timescales and Isotope Effects in Intramolecular Vibrational Energy Redistribution (IVR)

The $N_j = 4_1$ CH-overtone level of chloroform (approximately the third CH-stretching overtone) has a complex structure, which could not be assigned prior to our work (Hippler and Quack 1996). Figure 10 shows the central structure with the Q -branches of the different isotopomers of chloroform at room temperature. Outside the range displayed, the overtone has, in addition, broad P - and R -branches with the typical contour of a parallel transition. With the Ti:sapphire IR laser system and the UV laser

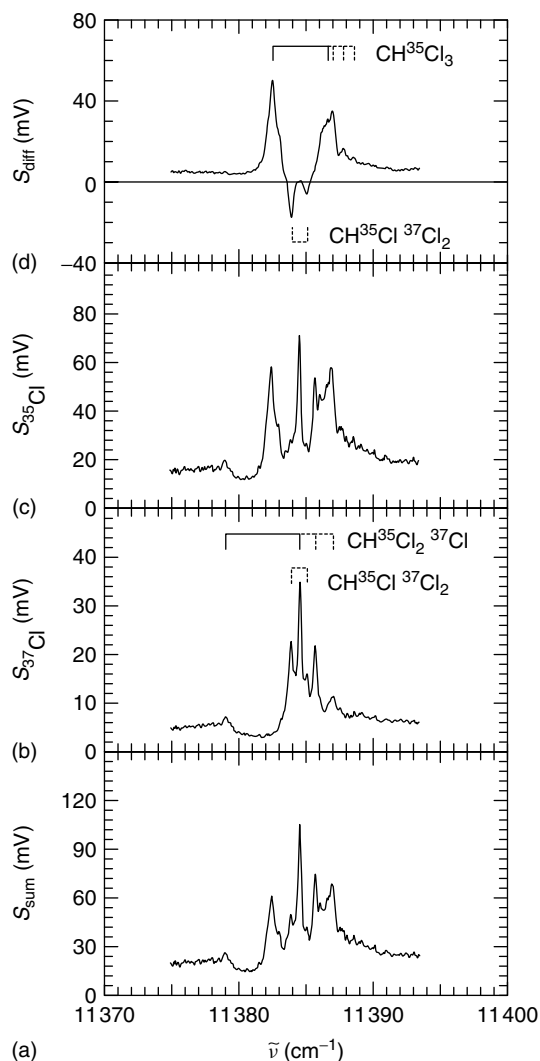


Figure 10 Central part of the $N_j = 4_1$ CH-chromophore absorption of CHCl_3 at room temperature, smoothed graphical resolution 0.08 cm^{-1} (actual resolution 0.02 cm^{-1}) (after Hippler and Quack 1996). (a) The OSVADPI spectrum without mass selection as reference plot. (b)–(d) The corresponding isotope-selective OSVADPI spectra (ISOS) with assignments to Cl-isotopomers. Hot-band sequences are indicated by dashed lines, the splitting due to the local anharmonic resonance is indicated by solid lines (see also text).

operating at 235.32 nm (corresponding to a $(2 + 1)$ REMPI transition of Cl), OSVADPI spectra have been obtained as already described. The OSVADPI spectrum, where all ions are collected without mass selection, corresponds to the chloroform isotopomer mixture. It is essentially identical with photoacoustic and FTIR reference spectra, although they have been obtained using completely different detection schemes. Mass gating the detection in the TOF to ^{35}Cl and ^{37}Cl fragment ions and applying the subtraction scheme (Figure 10d), all major peaks in the complex room-temperature spectrum have been assigned to

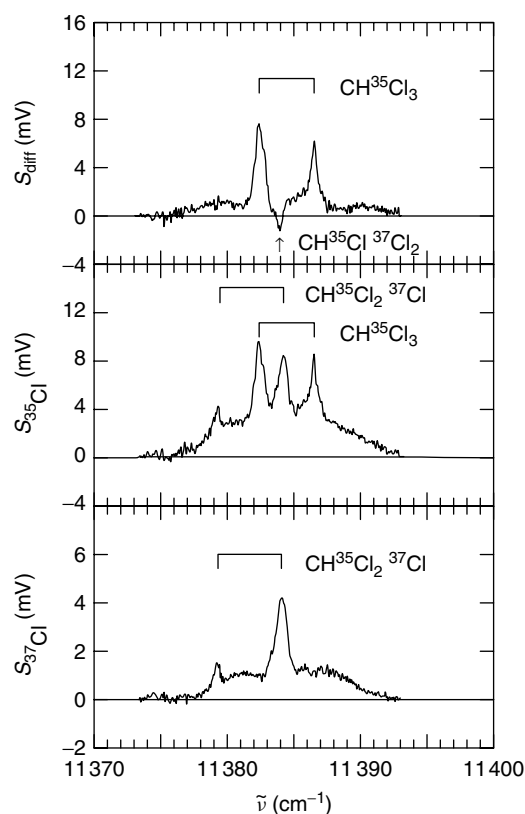


Figure 11 Isotope-selective OSVADPI spectra (ISOS) of the jet-cooled $N_j = 4_1$ CH-chromophore absorption of CHCl_3 with assignment of Q -branches to the three major Cl-isotopomers (after Hippler and Quack 1996). The brackets indicate the splitting due to the local anharmonic resonance.

Cl-isotopomers as indicated in Figure 10 and summarized in Hippler and Quack (1996).

Hot-band transitions have been identified by comparison with jet-cooled spectra (Figure 11) where the subtraction procedure has been applied to separate the Cl-isotopomers. The P - and R -branches have an FWHM of only ca 5 cm^{-1} , which indicates a very cold rotational temperature of the jet spectra. By comparison with simulated rotational band contours, a rotational temperature of about 5 K is estimated. No vibrational hot-band transitions are apparent in the expansion of chloroform seeded into Ar. Using He or N_2 as seeding gas, hot-band transitions with ν_6 were just emerging corresponding to slightly higher vibrational temperatures of ca 140 and 180 K, respectively. Under these different expansion conditions, however, no changes in band contours or position are apparent, which indicates that the jet-cooled spectra are not affected noticeably by cluster formation. Compared to the room-temperature spectrum, an interesting change of the rotational contour in the Q -branch of jet-cooled $\text{CH}^{35}\text{Cl}_2^{37}\text{Cl}$ is noted: the peak maximum is shifted 0.5 cm^{-1} to lower wavenumbers, and the FWHM of the contour increases to 1.3 cm^{-1} compared

to 0.4 cm^{-1} at room temperature. This effect is genuine and not an experimental artifact due to insecure wavelength calibration or insufficient resolution, since jet-cooled and room-temperature reference spectra were always recorded simultaneously using the same IR laser. Presumably, a band head is formed at high J values at room temperature, which is removed at very low temperatures, thus changing the rotational contour. In the assignment, hot-band transitions arise from ν_6 , $2\nu_6$, ν_3 , or $3\nu_6$. The intensities in this assignment are consistent with the thermal population, and the shifts are compatible with the anharmonicity constants $\tilde{x}'_{16} = 0.32 \text{ cm}^{-1}$ and $\tilde{x}'_{13} = 0.98 \text{ cm}^{-1}$ (Ruoff and Bürger 1970, Fuß and Weizbauer 1995, Hippler and Quack 1997).

After removing all vibrational hot bands and isotopomer congestion in the isotopomer-selected jet spectra, the splitting of Q -branches of the isotopomers $\text{CH}^{35}\text{Cl}_3$ and $\text{CH}^{35}\text{Cl}_2^{37}\text{Cl}$ is striking, which indicates a local anharmonic resonance (see Figure 11). For $\text{CH}^{35}\text{Cl}_3$, the Q -branch is split into two components of nearly equal intensity. In this case, the local resonance of the 4_1 state with a second vibrational state is almost perfect. In the isotopomer $\text{CH}^{35}\text{Cl}_2^{37}\text{Cl}$, the Q -branch is split into two components of different intensities, which indicates a detuning of the resonance due to a shift of vibrational frequencies in the different isotopomers. In the Q -branch of the third major Cl-isotopomer, $\text{CH}^{35}\text{Cl}^{37}\text{Cl}_2$, no splitting is apparent. Presumably, the local resonance is detuned even further and thus not as effective as for the other two isotopomers. In the vibrational hot-band transitions of the room-temperature spectra, no such resonance splittings are apparent, which is presumably because the resonance is detuned in the combination band of 4_1 with the hot-band vibration. Assuming a two-level model for the local resonance, where the unperturbed state 4_1 carries all absorption intensity, a deperturbation for $\text{CH}^{35}\text{Cl}_3$ yields 11384.1 cm^{-1} as unperturbed position of 4_1 and 11384.7 cm^{-1} for the perturbing vibrational state. For the interaction energy, $|\tilde{W}| = 2.0 \text{ cm}^{-1}$ is found (the sign is undetermined). A similar deperturbation for $\text{CH}^{35}\text{Cl}_2^{37}\text{Cl}$ gives the same interaction energy and 11383.1 cm^{-1} and 11380.2 cm^{-1} as unperturbed positions of 4_1 and of the perturber, respectively. Apparently, the same vibrational level is the perturber of 4_1 in both isotopomers. An assignment of the perturbing state may appear impossible at first glance: the density of vibrational states, which have A_1 symmetry, as has 4_1 and which can thus, in principle, interact via an anharmonic resonance, is about $340 \text{ states per cm}^{-1}$ at the energy of 4_1 . The count of vibrational states and their assignment was performed by a computer program, which calculates all possible vibrational combination bands within a given energy interval using experimental anharmonic spectroscopic constants and experimental or estimated isotopomer shifts (Ruoff and

Bürger 1970, Dübal *et al.* 1989, Fuß and Weizbauer 1995). To calculate positions of CH-stretching/bending modes within a Fermi-resonance polyad, the program diagonalizes the corresponding effective Hamiltonian matrix with experimental parameters (Dübal *et al.* 1989). Most of the vibrational background states involve many quanta of CCl₃ frame modes, and thus have an isotopomer shift much larger than found in the experiment. At the 4₁ energy, only about 0.7 states per cm⁻¹ of A₁ symmetry have an estimated isotopomer shift of less than 10 cm⁻¹ between CH³⁵Cl₃ and CH³⁵Cl₂³⁷Cl, estimating the shift by the sum of the observed isotopomer shifts of fundamentals multiplied by the number of the corresponding vibrational quanta in the combination band. Among these few states, the likely perturber seems to be the combination of the second Fermi-resonance component $N_j = 4_2$ and the C–Cl₃ “umbrella” vibration ν_3 . It is the only combination band of A₁ symmetry within a 30 cm⁻¹ interval, which could interact via a quartic anharmonic resonance with 4₁; all other bands would involve the change of more than four vibrational quanta relative to 4₁. A coupling of CH-stretching and bending vibrations with the C–Cl₃ umbrella vibration also appeals to physical intuition. The ν_3 fundamental has been observed before at 367.296 cm⁻¹ for the isotopomer CH³⁵Cl₃, at 364.52 cm⁻¹ for CH³⁵Cl₂³⁷Cl, and at 361.68 cm⁻¹ for CH³⁵Cl³⁷Cl₂ (Pietilä *et al.* 1999), in good agreement with our own FTIR measurements (Hippler and Quack 1996). With large isotopomer shifts, the availability of rotationally resolved spectra and no apparent perturbations, an assignment to isotopomers was relatively unproblematic in this case. For the $N_j = 4_2$ overtone absorption, an assignment would be less obvious, since the room-temperature spectra are not rotationally resolved. With ISOS, however, the following peak positions of *Q*-branches were obtained (see Section 6.2): 11 018.7 cm⁻¹ for the isotopomer CH³⁵Cl₃, 11 017.2 cm⁻¹ for CH³⁵Cl₂³⁷Cl, and 11 015.0 cm⁻¹ for CH³⁵Cl³⁷Cl₂; they may serve as good estimation for the band origins. Taking the sum of the ν_3 and 4₂ positions as estimation for the unperturbed position of the combination band 4₂ + ν_3 , almost perfect agreement with the values for the perturber in the local resonance in $N_j = 4_1$ is found. Estimated positions are only 1.4 cm⁻¹ higher, and the estimated isotopomer shift equals the deperturbed value. The 4 cm⁻¹ almost perfect resonance splitting indicates a redistribution time of 4 ps to the CCl₃ frame mode, independent of the particular assignment. This is to be compared with the ultrafast ($\cong 50$ fs) redistribution between CH-stretching and bending modes in CHCl₃ and generally in CHX₃ compounds (Dübal and Quack 1984, Peyerimhoff *et al.* 1984, Amrein *et al.* 1985, Lewerenz and Quack 1986, Baggott *et al.* 1986, Wong *et al.* 1987, William *et al.* 1987, Segall *et al.* 1987, Lewerenz and Quack 1988, Dübal *et al.*

1989, Ha *et al.* 1990, Hollenstein *et al.* 1990a, Quack 1990, 1993, Marquardt and Quack 1991, Hollenstein *et al.* 1993, Marquardt *et al.* 1995). The present result for the local anharmonic resonance in CHCl₃ thus indicates a clear separation of timescales in IVR by almost a factor 100. Assuming further that the bandwidth of possible homogeneous structures, $\tilde{\Gamma}$ (in wavenumber units), is caused by exponential decay to background states, further redistribution of vibrational excitation with decay time $\tau = h/(2\pi\Gamma) = 1/(2\pi c\tilde{\Gamma})$ is calculated. Taking as upper bound of $\tilde{\Gamma}$ the 0.4 cm⁻¹ FWHM of the sharpest feature in the $N_j = 4_1$ overtone spectrum (the *Q*-branch of CH³⁵Cl₂³⁷Cl at 11 384.64 cm⁻¹), $\tau \geq 13$ ps is thus obtained as lower bound.

In summary, the following hierarchy of timescales in IVR emerges for the observed overtone $N_j = 4_1$: the $\nu = 4$ CH-stretching overtone is the chromophore state coupled to the IR field. It is the “antenna” to receive vibrational energy from the radiation field. With a redistribution time of ca 50 fs, vibrational energy is redistributed to the CH-stretching/bending manifold by the strong Fermi resonance, resulting in the polyad state 4₁. This state is in local resonance with a CCl₃ frame mode with redistribution time $\tau = 4$ ps, which then further “decays” into the background of vibrational states with redistribution time $\tau \geq 13$ ps. The resulting spectroscopic states are observable by high-resolution spectroscopy; they will eventually decay back to the ground state by spontaneous IR emission with decay times of the order of 1 ms (see also Segall *et al.* 1987 and Albert *et al.* 2011a: **Fundamentals of Rotation–Vibration Spectra**, this handbook, for the case of CHF₃).

7 ISOTOPE-SELECTIVE OVERTONE SPECTROSCOPY (ISOS) BY RESONANTLY ENHANCED TWO-PHOTON IONIZATION OF VIBRATIONALLY EXCITED MOLECULES

The OSVADPI technique introduced in the previous section is based on a photofragment ionization scheme that requires molecules to have a dissociative excited electronic state. Here, a new variant of ISOS will be introduced, which can also be applied to molecules with a bound excited electronic state, employing the same experimental equipment: RE2PI of vibrationally excited molecules. ISOS and IRSIMS are thus truly general experimental techniques for the gas-phase infrared spectroscopy, which have a wide range of possible applications.

7.1 Overview

After providing a discussion on the scheme of excitation and the mechanism of RE2PI of vibrationally excited molecules, we introduce, as a selected application example, the spectroscopy and intramolecular dynamics of aniline isotopomers after excitation of the first NH-stretching overtone. In aniline, the influence of different isotopes on IVR and on the internal tunneling motion of the NH₂-group (inversion) can be studied by high-resolution spectroscopy. Tunneling or inversion motions are an important topic in intramolecular dynamics (von Puttkamer and Quack 1989, Quack 1989b, 1991, 1993, 1999, 1995b, Klopper *et al.* 1998, Fehrensen *et al.* 1998, 1999a,c, Kuhn *et al.* 1999). The inversion at the N-atom with pyramidal threefold substitution represents one prototype system, where ammonia has been a textbook example for a long time (Herzberg 1945, Luckhaus 2000, Marquardt *et al.* 2003, Snels *et al.* 2003). Owing to its low barrier to inversion of the amino group (Fehrensen *et al.* 1999a, Quack and Stockburger 1972, Kleibömer and Sutter 1988, Jiang and Lin 1997), aniline is particularly well suited to study inversion processes. In the past, the theoretical treatment and the analysis of experimental spectra have been mainly limited to effective one-dimensional models (Quack and Stockburger 1972, Larsen *et al.* 1976, Kydd and Krueger 1977, Hollas *et al.* 1983, Fehrensen *et al.* 1999a, Lopez-Tocon *et al.* 2000) or to the two-dimensional subspace including torsional motion (Pyka and Kreglewski 1985, Bludský *et al.* 1996), thus neglecting the influence of different excited vibrational modes on the inversion dynamics. Although the exact full-dimensional quantum mechanical treatment of such interactions is not feasible at present for molecules as large as aniline, the theoretical study of the vibrational mode-selective inversion motion has been possible within some approximations with the recent development of a reaction path Hamiltonian approach (Fehrensen *et al.* 1999a,c). The partially N-deuterated C₆H₅NHD is a particularly interesting isotopomer of aniline, since it is chiral in its equilibrium structure; the structure with defined handedness, however, is not an eigenfunction of the Hamiltonian and thus not stable (Quack 1989b, 1995b, 1999). The inversion motion corresponds, in this case, to a stereomutation, i.e., to the isomerization between enantiomers of different handedness (Quack 1989b, 1995b, 1999), and the analysis of stereomutation tunneling spectra can provide stereomutation times and their dependence on excitation of various vibrational modes for this prototypical, elementary chemical reaction. Aniline has two high-frequency IR chromophores, the CH-chromophore similar to benzene and the NH-chromophore. Their absorptions are, in general, well separated in the IR spectrum. The study of overtone spectroscopy will give information on anharmonic resonances and IVR. Aniline

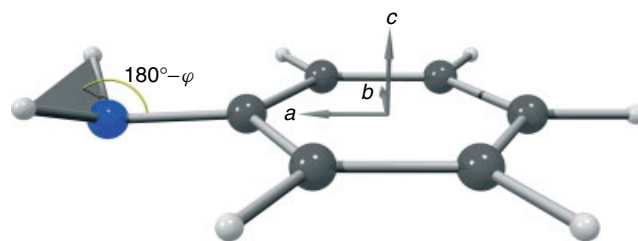


Figure 12 The equilibrium structure of aniline (from Hippler and Quack 2006). The inversion angle φ is defined as the angle between the NH₂ plane and the CN bond.

C₆H₅NHD is particularly suited to study IVR processes, since it has an isolated NH-chromophore, which facilitates a detailed analysis of its absorption spectrum.

The nonplanar equilibrium structure of aniline is shown schematically in Figure 12. The dihedral angle between the benzene ring and the NH₂-plane decreases from $\varphi_{\text{eq}} \approx 42^\circ$ in the electronic ground state S₀ to about 20° or less in the quasi-planar S₁ state (Quack and Stockburger 1972, Kleibömer and Sutter 1988, Sinclair and Pratt 1996, Jiang and Lin 1997). Owing to tunneling splitting with a relatively low effective barrier to NH₂-inversion of about 450 cm⁻¹ in the electronic ground state, the vibrational ground state is split into two components with energy difference $\Delta E_{\pm} = 40.9 \text{ cm}^{-1}$ for C₆H₅NH₂ and $\Delta E_{\pm} = 23.8 \text{ cm}^{-1}$ for C₆H₅NHD (Fehrensen *et al.* 1999a). These spectroscopic eigenstates have well-defined parity, but no well-defined geometry and handedness (Quack 1989b, 1995b, 1999). C₆H₅NH₂ levels are classified by the Longuet-Higgins symmetry group M_{S4} for nonrigid molecules, which is isomorphous to the point group C_{2v}, and C₆H₅NHD by M_{S2} , which is isomorphous to C_s (Longuet-Higgins 1963, Quack and Stockburger 1972, Fehrensen *et al.* 1999a) (*see also* Quack 2011: **Fundamental Symmetries and Symmetry Violations from High-resolution Spectroscopy**, this handbook). The torsional motion of the amino group is also a large-amplitude motion, which could, in principle, be included in the symmetry classification, since it effects a permutation of atoms. Owing to a high effective torsional barrier, however, the corresponding tunneling splittings are expected to be very small and not resolvable under the present experimental conditions. Therefore the torsional motion has been neglected in the symmetry classification as not feasible (Longuet-Higgins 1963). In principle, the weak nuclear force will introduce a small asymmetry in the inversion potential of the chiral C₆H₅NHD (Quack 1989b, 1995b, 1999). This effect, however, is extremely small compared to the much larger splittings induced by the low barrier to inversion and has also been neglected in the symmetry classification. Vibrational bands have a transition moment along the *a*, *b*, or *c* axis of the lowest, medium, or highest

moment of inertia, respectively (see Figure 12), with a corresponding type *A*, *B* or *C* rotational contour. In the IR spectrum of “in-plane” vibrations (e.g., NH-chromophore), type-*B* bands with a characteristic central minimum or type-*A* bands with a strong central peak are prevailing. Owing to the interaction of the inversion motion with vibrational excitation, energy differences ΔE_{\pm} of tunneling components in the ground and vibrationally excited state are, in general, different. At room temperature, both tunneling components of the ground state are almost equally populated. Vibrational transitions of “in-plane” vibrations have then satellites at a distance, which corresponds to the difference of the tunneling splittings in the ground and excited vibrational states. Vibrations of A_1 symmetry (e.g., symmetric NH-stretching vibrations) have, in addition to strong type *A* transitions, much weaker *c*-polarized bands with satellites at a distance corresponding to the sum of tunneling splittings. With a known energy difference ΔE_{\pm} in the vibrational ground state (Fehrensens *et al.* 1999a), the observation of “tunneling satellites” in the IR spectrum allows the calculation of the tunneling splitting in the vibrationally excited state.

7.2 Mechanism of Resonantly Enhanced Two-photon Ionization of Vibrationally Excited Molecules

We shall discuss the absorption mechanism, which allows the observation of IR + UV double-resonance signals with aniline serving as example: aniline has a first UV absorption band with origin at $34\,029\text{ cm}^{-1}$ (293.87 nm) corresponding to the $S_1 \leftarrow S_0$ one-photon transition to the stable intermediate 1B_2 (S_1) electronic state (Brand *et al.* 1966, Christoffersen *et al.* 1969, Quack and Stockburger 1972, Leutwyler and Even 1981, Sinclair and Pratt 1996). While the adiabatic ionization limit is at 7.720 eV or $62\,265\text{ cm}^{-1}$ (Hager *et al.* 1985, Lias *et al.* 1988), the more relevant vertical ionization limit for efficient ionization is about 8.05 eV (Lias *et al.* 1988) or $64\,900\text{ cm}^{-1}$. Since both absorption cross sections for resonant electronic excitation $S_1 \leftarrow S_0$ and for the ionization of electronically excited aniline are large and comparable (Boesl *et al.* 1981), strong $(1 + 1)$ REMPI (“RE2PI”) signals resonantly enhanced by the S_1 state are obtained for UV absorption above $34\,029\text{ cm}^{-1}$ (Brand *et al.* 1966, Christoffersen *et al.* 1969, Quack and Stockburger 1972, Leutwyler and Even 1981, Sinclair and Pratt 1996). Applying UV radiation only, a very low background level of ions is observed at wavenumbers below $32\,400\text{ cm}^{-1}$ (about half the vertical ionization limit). Owing to nonresonant two-photon ionization, the ionization yield increases above that threshold, and above $34\,029\text{ cm}^{-1}$, the origin of the $S_1 \leftarrow S_0$ one-photon

transition, very strong ion signals are finally obtained by $(1 + 1)$ REMPI.

If a vibrational level of the electronic ground state has been excited first by IR radiation, an enhancement of the ionization yield by several orders of magnitude is observed with UV radiation between about $30\,000$ and $32\,400\text{ cm}^{-1}$. Since ionization with UV radiation is very inefficient at these wavenumbers, the IR + UV double-resonance ionization signals are virtually background free. For example, peak IR + UV ionization signals for the $N = 2$ NH-chromophore absorption of $\text{C}_6\text{H}_5\text{NH}_2$ at 6738 cm^{-1} are ca 25 mV compared with a nonresonant UV background of ca 0.1 mV , only. The ion yield is easily saturated by the UV pulse energies employed, and no variation in the ion yield is then apparent when leaving the IR radiation resonant to a vibrational transition and scanning the UV laser over an extensive range. The ionization yield therefore mirrors the IR excitation, and by scanning the IR laser, infrared spectra are obtained. Spectra obtained under room-temperature conditions, where aniline was leaking through a needle valve into the ionization chamber, are essentially identical to FTIR reference spectra, without any apparent distortions. Compared to ionization depletion detection schemes, the spectra are almost background free and have an excellent signal-to-noise ratio, even for the reduced number densities in a skimmed supersonic jet expansion.

Concerning the laser excitation mechanism, we propose a new absorption scheme to explain the enhancement in the UV ionization yield by IR excitation in our aniline or benzene experiments, as summarized in Figure 13 (Fehrensens *et al.* 1998, Hippler *et al.* 2003, Hippler 2001): Without vibrational excitation, the UV radiation does not have sufficient energy to promote the transition to the electronically excited state S_1 , which could resonantly enhance ionization ($(1 + 1)$ REMPI), and nonresonant two-photon ionization is also energetically not possible. After IR excitation, however, Franck–Condon factors for hot-band transitions

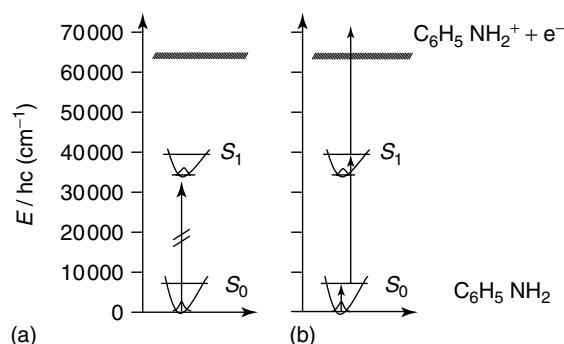


Figure 13 Scheme of excitation, with aniline $\text{C}_6\text{H}_5\text{NH}_2$ serving as example (after Fehrensens *et al.* 1998). (a) UV excitation only is not efficient for ionization. (b) Resonantly enhanced two-photon ionization of vibrationally excited molecules.

are much more favorable for the one-photon transitions to the S_1 state and the UV energy is sufficient to ionize vibrationally excited aniline or benzene molecules by RE2PI via vibrational hot bands on the $S_1 \leftarrow S_0$ transition. For aniline with IR excitation at 6750 cm^{-1} and UV radiation at 31220 or 32100 cm^{-1} in the double-resonance experiment, the excess energy in S_1 is 3940 or 4820 cm^{-1} , respectively. At these excitation energies, the vibrational density of states in S_1 is estimated to be roughly similar to the S_0 ground state density calculated as $\text{ca } 1.0 \times 10^3$ states per cm^{-1} at 4000 cm^{-1} , using the Beyer–Swinehart algorithm (Beyer and Swinehart 1973) with a set of harmonic frequencies from ab initio calculations (B3LYP with 6-31G** basis set (Frisch *et al.* 1995); the inversion mode is approximated by an effective harmonic oscillator with wavenumber 350 cm^{-1} ; a more detailed calculation including anharmonicity and large-amplitude torsional motion would be straightforward, but would not change the order of magnitude). For benzene with IR excitation at 6000 cm^{-1} and UV radiation at 37600 cm^{-1} , the excess energy in S_1 is about 5500 cm^{-1} . At this energy, the vibrational density of states in the ground state S_0 is about 700 states per cm^{-1} , as calculated by the Beyer–Swinehart algorithm (Beyer and Swinehart 1973) using a set of observed fundamental frequencies compiled in Miani *et al.* (2000). A similar density can be expected for the S_1 state. In both cases, this corresponds to a dense set of states, which is accessible to one-photon excitation from the vibrationally excited ground state. Compared to previous schemes, such a quasi-continuum of resonance-enhancing intermediate states has the distinct advantage that the UV laser does not need to be scanned simultaneously with the IR laser during an infrared scan, since the resonance condition is always fulfilled. RE2PI of vibrationally excited molecules is similar to the OSVADPI scheme introduced before; it is its natural extension to molecules, which have bound intermediate electronically excited states.

We have investigated the dependence of the ion yield on the UV and IR pulse energy and effectively fluence for aniline (Fehrensens *et al.* 1998). The dependence on the UV radiation is consistent with the proposed resonant ionization mechanism, which involves two one-photon UV steps. The dependence is described satisfactorily assuming a kinetic two-step photoionization model (Letokhov 1987). The relative absorption cross sections obtained by this fit for the resonant excitation and ionization are in good agreement with literature values (Boesl *et al.* 1981). At low fluence, the dependence is quadratic, at medium fluence, the $S_1 \leftarrow S_0$ transition is saturated, but not the ionization, and therefore a linear dependence is effective. At higher fluences, both one-photon steps are saturated. In a recent study of ionization-detected IR excitation of phenol and

some other aromatic molecules under very similar experimental conditions, a nonresonant two-photon ionization mechanism of vibrationally excited molecules was suggested (Omi *et al.* 1996, Ishiuchi *et al.* 1998). However, in a UV scan with the IR kept at a vibrational transition, these authors observed distinct features in the ion yield, which they attributed to vibrational resonances in S_1 (Ishiuchi *et al.* 1998). This would imply that ionization occurs also in these experiments via RE2PI as suggested here for benzene and aniline.

Aniline ionized by the IR+UV double-resonance scheme has a characteristic mass spectrum that is dominated by the parent ion and some weaker fragment ion peaks ranging from $\text{C}_{x=2-6}\text{H}_{y=0-5}$ to C (see Figure 14). Obviously, fragmentation occurs after ionization, since the UV wavelength chosen is not efficient to ionize neutral C atoms or other fragments. By gating ionization-detected IR excitation to the parent ion mass peak, mass-selective IR spectra are obtained.

With a natural abundance of 1.1% ^{13}C , the aniline isotopomers with one ^{13}C atom have 6.2% abundance in the natural isotopomer mixture. For the aniline isotopomer $^{13}\text{C}^{12}\text{C}_5\text{H}_5\text{NH}_2$, no shift of vibrational bands compared to $^{12}\text{C}_6\text{H}_5\text{NH}_2$ is observed for the NH-chromophore, and therefore the ^{13}C -isotopomer shift must be less than 1 cm^{-1} . This is not unexpected, since the NH-stretching and bending vibrations are not affected much by the benzene ring. In a mixture of undeuterated, partially and fully N-deuterated aniline, gating the mass detection to $m/z = 93$ u and 94 u yields the separate vibrational spectra of $^{12}\text{C}_6\text{H}_5\text{NH}_2$ and $^{12}\text{C}_6\text{H}_5\text{NHD}$ in a single scan. $^{13}\text{C}^{12}\text{C}_5\text{H}_5\text{NH}_2$ is also present at $m/z = 94$ u to a minor extent, but its transitions are easily discernible.

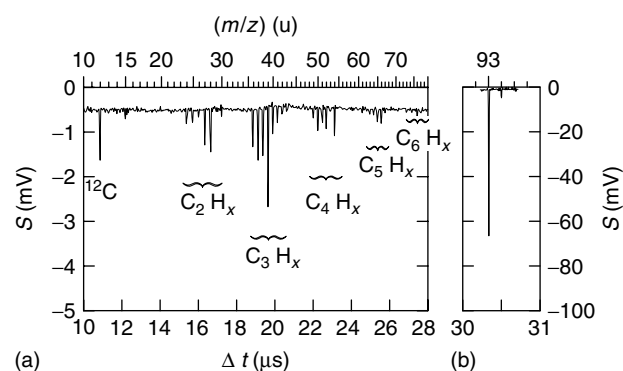


Figure 14 TOF mass spectrum after UV ionization (311.5 nm) of vibrationally excited jet-cooled aniline $\text{C}_6\text{H}_5\text{NH}_2$ ($N = 2$ NH-chromophore at 6738 cm^{-1}) (from Hippler and Quack 2006). S denotes the ion signal, Δt the flight time in the time-of-flight mass spectrometer; m/z the corresponding nonlinear mass scale. Note the different scales of the panel (a) fragment spectrum and (b) parent peaks, $^{12}\text{C}_6\text{H}_5\text{NH}_2$ and $^{13}\text{C}^{12}\text{C}_5\text{H}_5\text{NH}_2$.

7.3 The $N = 2$ and 3 NH-chromophore Absorption of Aniline Isotopomers: Isotope Effects and Vibrational Mode Specificity in IVR and Tunneling Processes

In Figure 15, the $N = 2$ NH-chromophore absorption between 6500 and 7100 cm^{-1} of $\text{C}_6\text{H}_5\text{NH}_2$ shows overtone and combination bands of symmetric (ν_s) and anti-symmetric (ν_{as}) NH-stretching vibrations and anharmonic resonances with them. In Figure 15(c), the mass-gated jet spectrum in a very cold Ar expansion is shown. The rotational contours are characterized by a very low rotational temperature, and no vibrational hot bands are apparent. Figure 15(b) displays the corresponding spectrum in an expansion with N_2 as seeding gas. Compared to the Ar expansion, the rotational contours are broader due to a somewhat higher rotational temperature, and some bands clearly exhibit tunneling splitting. Figure 15(a) shows for

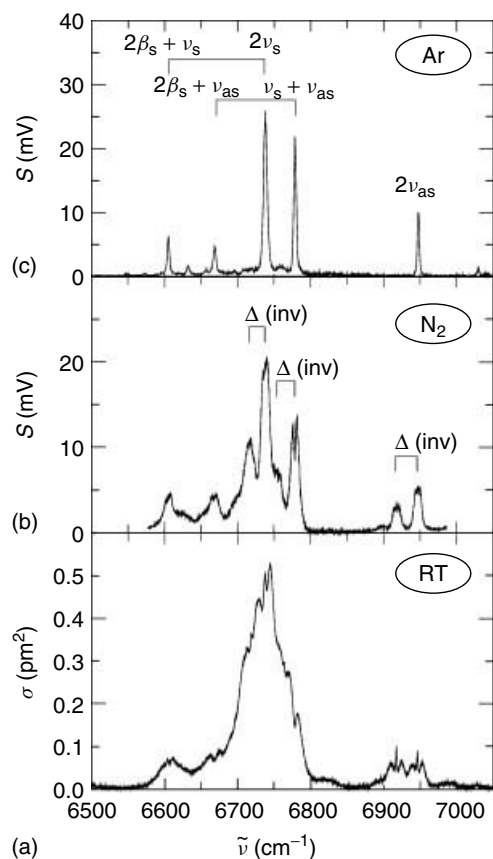


Figure 15 $N = 2$ NH-chromophore absorption spectra of $\text{C}_6\text{H}_5\text{NH}_2$ (from Fehrens *et al.* 1998). (a) The FTIR reference spectrum of 0.34 mbar aniline at room temperature ($l = 28\text{ m}$, resolution 0.1 cm^{-1}). (b) and (c) Ionization-detected ISOS spectra of jet-cooled aniline, mass gated at $m/z = 93\text{ u}$ ($^{12}\text{C}_6\text{H}_5\text{NH}_2$), trace (b) in a jet expansion with 1 bar of N_2 , and trace (c) with 1 bar of Ar. Brackets indicate the Fermi-resonance splitting (c) and the tunneling splitting due to NH_2 -inversion (b).

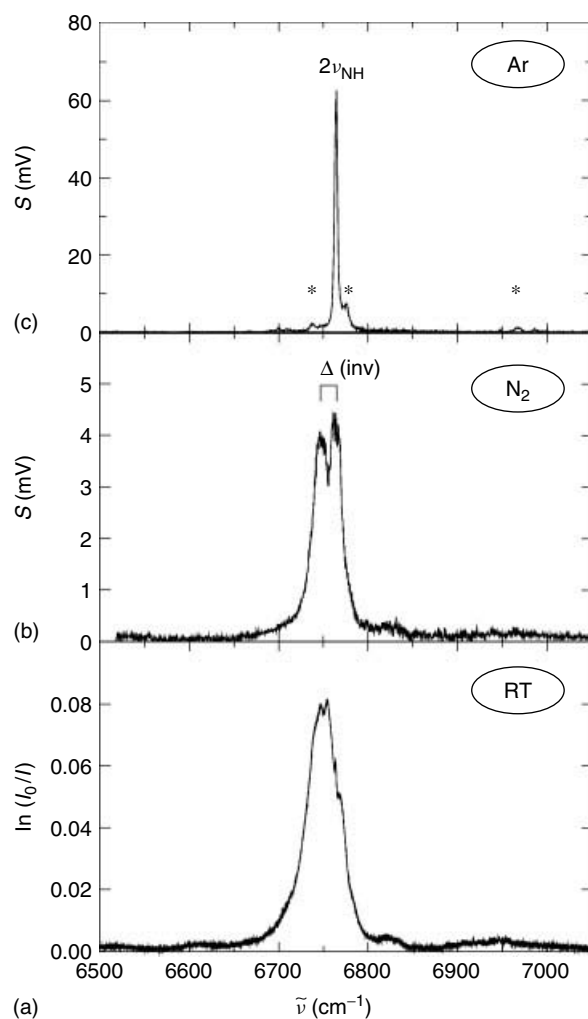


Figure 16 $N = 2$ NH-chromophore absorption of $\text{C}_6\text{H}_5\text{NHD}$ (from Fehrens *et al.* 1998). (a) FTIR reference spectrum of 0.4 mbar N-deuterated aniline ($\text{C}_6\text{H}_5\text{ND}_2$) at room temperature ($l = 49\text{ m}$, resolution 0.1 cm^{-1}). The transitions observed in this region are expected to arise from small amounts of $\text{C}_6\text{H}_5\text{NHD}$, due to incomplete deuteration. (b) and (c) Ionization-detected ISOS spectra of jet-cooled aniline, mass gated at $m/z = 94\text{ u}$ ($^{12}\text{C}_6\text{H}_5\text{NHD}$), (b) in a jet expansion with 1 bar of N_2 , and (c) with 1 bar of Ar. The bracket in (b) indicates the tunneling splitting due to NHD-inversion. The stars in (c) mark transitions, which are due to small amounts of $^{13}\text{C}^{12}\text{C}_5\text{H}_5\text{NH}_2$ present (compare Figure 15 and discussion in the text).

comparison an FTIR spectrum at room temperature. In Figure 16, the corresponding absorption spectrum of the $N = 2$ NH-chromophore of $\text{C}_6\text{H}_5\text{NHD}$ is displayed, which is dominated by the NH-stretching overtone $2\nu_{\text{NH}}$. Mass-gated ionization detection of the IR excitation allowed isotopomer-selective spectroscopy of $\text{C}_6\text{H}_5\text{NHD}$ in the isotopomer mixture with about 25% $\text{C}_6\text{H}_5\text{ND}_2$ and $\text{C}_6\text{H}_5\text{NH}_2$, respectively. Without isotopomer selection, no separated FTIR spectrum of $\text{C}_6\text{H}_5\text{NHD}$ can be obtained. The absorptions between 6500 and 7100 cm^{-1} in a $\text{C}_6\text{H}_5\text{ND}_2$ sample

are expected to arise from small amounts of C_6H_5NHD due to incomplete deuteration; the ND-chromophore of $C_6H_5ND_2$ has strong absorptions in a different spectral region. A contour fit of $2\nu_{as}$ band of $C_6H_5NH_2$ with extrapolated rotational constants (Fehrensens *et al.* 1999a) yields a rotational temperature $T_{rot} \approx 5$ K for the Ar expansion and $T_{rot} \approx 60$ K for the N_2 expansion. From the absence of transitions from the upper tunneling ground state level, which is higher in energy, $T_{inv} < 15$ K is estimated as a bound for the inversion vibrational temperature in the Ar expansion of both isotopomers. The tunneling splitting becomes apparent in the N_2 expansion. From the intensity ratio of “tunneling satellites”, $T_{inv} \approx 100$ K is estimated.

Three main transitions dominate the $C_6H_5NH_2$ jet spectrum in the very cold Ar expansion. By extrapolation from the fundamentals (Fehrensens *et al.* 1999a) and consistent with the band contours, they are tentatively assigned as the first overtones of the symmetric and antisymmetric NH-stretching vibrations $2\nu_s$ and $2\nu_{as}$, respectively, and as the combination band $\nu_s + \nu_{as}$. The NH-stretching modes act as IR chromophores. Some of the weaker observed transitions presumably obtain their intensity by anharmonic resonance coupling with the NH-stretching modes. The two strongest transitions among them are assigned as combination bands $\nu_s + 2\beta_s$ and $\nu_{as} + 2\beta_s$, which are coupled to $2\nu_s$ and $\nu_s + \nu_{as}$, respectively, by a strong Fermi-resonance exchanging two quanta of the symmetric NH-bending vibration β_s (“scissor”) with one quantum of the symmetric NH-stretching vibration ν_s . NH-stretching and bending vibrations are expected to be coupled by a Fermi resonance, as has previously been observed for other hydrides, whenever the 2:1 resonance condition is approximately fulfilled (Dübal and Quack 1984, Peyerimhoff *et al.* 1984, Amrein *et al.* 1985, Lewerenz and Quack 1986, Baggott *et al.* 1986, Wong *et al.* 1987, William *et al.* 1987, Segall *et al.* 1987, Lewerenz and Quack 1988, Dübal *et al.* 1989, Ha *et al.* 1990, Hollenstein *et al.* 1990a, 1993, Quack 1990, 1993, Marquardt and Quack 1991, Luckhaus and Quack 1992, Luckhaus *et al.* 1993, Marquardt *et al.* 1995). With an observed position of the fundamental β_s at 1610 cm^{-1} and ν_s at 3421 cm^{-1} (Fehrensens *et al.* 1999a), the Fermi-resonance coupling is quite effective. A harmonic approximation to estimate the unperturbed, zeroth-order positions of $\nu_s + 2\beta_s$ yields 6640 cm^{-1} and for $\nu_{as} + 2\beta_s$ gives 6730 cm^{-1} . The true zeroth-order positions will have somewhat lower wavenumbers because of anharmonicity. The corresponding bands in the experimental jet spectrum at 6605 cm^{-1} and 6670 cm^{-1} appear at even lower wavenumbers because of the Fermi resonance.

In the analysis of the anharmonic resonance system, the Fermi resonance exchanging one quantum of the symmetric NH-stretching vibration (ν_s) with two quanta of the symmetric NH-bending vibration (ν_b) and the

Darling–Dennison resonance exchanging two quanta of the symmetric NH-stretching with two quanta of the antisymmetric NH-stretching vibration (ν_{as}) have to be considered. Zeroth-order basis states $|v_s, \nu_{as}, \nu_b\rangle$ of one symmetry group, which have the common polyad quantum number $N = \nu_s + \nu_{as} + 0.5\nu_b$, are thus coupled and mixed. The interaction is described by an effective Hamiltonian with the usual matrix elements by equations (22)–(24):

$$\begin{aligned} \tilde{H}_{v_s, \nu_{as}, \nu_b; v_s, \nu_{as}, \nu_b}^N &= \tilde{v}'_s v_s + \tilde{v}'_{as} \nu_{as} + \tilde{v}'_b \nu_b + \tilde{x}'_{s,s} v_s^2 \\ &+ \tilde{x}'_{as,as} \nu_{as}^2 + \tilde{x}'_{b,b} \nu_b^2 + \tilde{x}'_{s,as} \nu_s \nu_{as} \\ &+ \tilde{x}'_{s,b} \nu_s \nu_b + \tilde{x}'_{as,b} \nu_{as} \nu_b \end{aligned} \quad (22)$$

$$\tilde{H}_{v_s, \nu_{as}, \nu_b; (v_s-1), \nu_{as}, (\nu_b+2)}^N = \frac{1}{2} k_{sbb} \left\{ \frac{1}{2} \nu_s (\nu_b+1) (\nu_b+2) \right\}^{1/2} \quad (23)$$

$$\begin{aligned} \tilde{H}_{v_s, \nu_{as}, \nu_b; (\nu_s-2), (\nu_{as}+2), \nu_b}^N &= \frac{1}{4} \gamma_{s,s,as,as} \left\{ \nu_s (\nu_s - 1) \right. \\ &\times (\nu_{as} + 1) (\nu_{as} + 2) \left. \right\}^{1/2} \end{aligned} \quad (24)$$

Matrix diagonalization gives the perturbed positions, which are observed in the experiment. For convenience, the matrix for the $N = 2$ polyad of A_1 symmetry is given explicitly in equation (25), and the matrix of B_2 symmetry in equation (26), where G denotes the term values of unperturbed states (for axis conventions and symmetry operations in the B_2 symmetry classification *see* Fehrensens *et al.* (1999a)).

$N = 2$, A_1 symmetry:

$$\begin{pmatrix} |2, 0, 0\rangle & |0, 2, 0\rangle & |1, 0, 2\rangle & |0, 0, 4\rangle \\ \left(\begin{array}{cccc} G(2\nu_s) & \gamma_{s,s,as,as} & \frac{1}{\sqrt{2}} k_{sbb} & 0 \\ & G(2\nu_{as}) & 0 & 0 \\ & & G(\nu_s + 2\nu_b) & \frac{\sqrt{6}}{2} k_{sbb} \\ & & & G(4\nu_b) \end{array} \right) \end{pmatrix} \quad (25)$$

$N = 2$, B_2 symmetry:

$$\begin{pmatrix} |1, 1, 0\rangle & |0, 1, 2\rangle \\ \left(\begin{array}{cc} G(\nu_s + \nu_{as}) & \frac{1}{2} k_{sbb} \\ & G(\nu_{as} + 2\nu_b) \end{array} \right) \end{pmatrix} \quad (26)$$

In the jet spectrum of $C_6H_5NH_2$, both B_2 states in the $N = 2$ polyad have been observed. Assuming that the whole band strength arises from the chromophore state $\nu_s + \nu_{as}$, while the combination band $\nu_{as} + 2\beta_s$ carries no oscillator strength, the unperturbed positions and the coupling matrix element can be determined from the observed perturbed positions and their relative intensity. The deperturbation yields zeroth-order positions at 6693 cm^{-1} for $\nu_{as} + 2\beta_s$ and 6754 cm^{-1} for $\nu_s + \nu_{as}$. The A_1 -polyad with $N = 2$ comprises four states, of which three have been

observed. The effective Hamiltonian predicts, in addition, a very weak polyad component of A_1 symmetry around 6400 cm^{-1} (approximately $4\beta_s$), which we could not observe. At this stage, only a preliminary “two-state” analysis of the Fermi resonance between $2\nu_s$ and $\nu_s + 2\beta_s$ can be attempted for the A_1 -polyad. In this model, $2\nu_s$ as bright state is coupled to the dark state $\nu_s + 2\beta_s$. The approximate deperturbation gives zeroth-order positions at 6626 cm^{-1} for $\nu_s + 2\beta_s$ and 6718 cm^{-1} for $2\nu_s$. In both symmetry groups, the off-diagonal coupling matrix element is about 47 cm^{-1} . k_{sbb} is thus ca 100 cm^{-1} (equation 26), corresponding to similar couplings for the CH-chromophore and timescales of about 100 fs for IVR in CHX_3 or CHXY_2 compounds, for example (Dübal and Quack 1984, Peyerimhoff *et al.* 1984, Amrein *et al.* 1985, Lewerenz and Quack 1986, 1988, 1992, Baggott *et al.* 1986, Wong *et al.* 1987, William *et al.* 1987, Segall *et al.* 1987, Dübal *et al.* 1989, Hollenstein *et al.* 1990a, 1993, Ha *et al.* 1990, Quack 1990, 1993, Marquardt and Quack 1991, Luckhaus *et al.* 1993, Marquardt *et al.* 1995). In the jet spectrum of $\text{C}_6\text{H}_5\text{NHD}$, no resonance splitting is evident in the $2\nu_{\text{NH}}$ overtone region (Figure 16). The Fermi resonance is expected to be weak here, because the NH-bending fundamental frequency is much lower (1445 cm^{-1}) and the resonance will only become relevant at higher overtones.

Jet-cooled aniline bands observed in the Ar expansion have an FWHM between 3 and 5 cm^{-1} . Assuming a homogeneous rovibronic line width between 1 and 2 cm^{-1} , the rotational contour of $2\nu_{\text{as}}$ is very satisfactorily reproduced for room temperature and jet conditions. The quasi-homogeneous line width might be explained by the exponential decay of vibrational excitation into the quasi-continuum of background states near the statistical limit (Bixon and Jortner 1968, Dübal and Quack 1980). In the 6740 cm^{-1} region of $\text{C}_6\text{H}_5\text{NH}_2$, a vibrational density of states of ca 1.7×10^5 per cm^{-1} is estimated with the Beyer–Swinehart algorithm (Beyer and Swinehart 1973) with harmonic frequencies from ab initio calculations (B3LYP, 6-31G** basis set (Frisch *et al.* 1995); the inversion mode is approximated by an effective harmonic oscillator with wavenumber 350 cm^{-1}). The upper bound for the homogeneous bandwidth $\tilde{\Gamma} < 2\text{ cm}^{-1}$ provides $\tau_{\text{d}} > 2.5\text{ ps}$ as a bound for the decay time of vibrational excitation into the dense background manifold. By these rough estimates, we do not imply that all background states are equally involved in the redistribution process. Some vibrational bands in the N_2 expansion have a satellite at lower wavenumbers due to the hot-band transition from the upper component of the ground state tunneling doublet, which is significantly populated compared to the very cold Ar expansion. The observed satellite shift corresponds to the difference of tunneling splittings in the ground and vibrationally excited NH-stretching states. A

shift to lower wavenumbers indicates a smaller ΔE_{\pm} in the excited vibrational state. If no separate satellite is noticeable, ΔE_{\pm} is similar to the ground state. In the $\text{C}_6\text{H}_5\text{NH}_2$ ground state, ΔE_{\pm} is 40.9 cm^{-1} (Fehrens *et al.* 1999a), and a tunneling splitting of $20 \pm 2.5\text{ cm}^{-1}$ in $2\nu_s$, $17 \pm 2.5\text{ cm}^{-1}$ in $\nu_s + \nu_{\text{as}}$, and $11 \pm 1\text{ cm}^{-1}$ in $2\nu_{\text{as}}$ is thus found. No satellites are apparent for $\nu_s + 2\beta_s$ and $\nu_{\text{as}} + 2\beta_s$. These bands presumably have a tunneling splitting close to the ground state value, approximately within $40 \pm 10\text{ cm}^{-1}$. Since ΔE_{\pm} decreases in the NH-stretching overtone bands, the NH-stretching is an inhibiting mode for the inversion, and the effective barrier height for inversion has therefore increased relative to the vibrational ground state. This result is in agreement with the previous analysis of the NH-stretching fundamentals (Fehrens *et al.* 1999a). From an analysis of the NH-bending fundamental β_s of $\text{C}_6\text{H}_5\text{NH}_2$, the promoting nature of this mode has been established, since the tunneling splitting increases from $\Delta E_{\pm} = 40.9\text{ cm}^{-1}$ in the vibrational ground state to 63.3 cm^{-1} in the β_s fundamental (Fehrens *et al.* 1999a). In the NH-bending/stretching combination bands $\nu_s + 2\beta_s$ and $\nu_{\text{as}} + 2\beta_s$ observed here, the inhibiting character of the NH-stretching apparently balances the promoting character of the NH-bending vibration.

With a ground state value ΔE_{\pm} of 23.8 cm^{-1} for $\text{C}_6\text{H}_5\text{NHD}$ (Fehrens *et al.* 1999a), $\Delta E_{\pm} = 6.5 \pm 2.5\text{ cm}^{-1}$ is calculated for $2\nu_{\text{NH}}$. The time of stereomutation in $\text{C}_6\text{H}_5\text{NHD}$ is calculated as $\tau_s = h/(2\Delta E_{\pm})$. NH-stretching excitation increases the effective barrier height for stereomutation relative to the vibrational ground state and therefore inhibits the stereomutation. Previously, values $\tau_s = 700\text{ fs}$ for the ground state and $\tau_s = 1.33\text{ ps}$ for the NH-stretching fundamental were determined (Fehrens *et al.* 1999a). With the present value $\tau_s = 2.6\text{ ps}$ for $2\nu_{\text{NH}}$, an increase of approximately a factor of 2 for each quantum of NH-stretching is thus found. At these energies and timescales, stereomutation is adiabatically separated from the vibrational motion, as theoretically analyzed in Fehrens *et al.* (1999a). A simple explanation for the inhibition of stereomutation by NH-stretching is provided by the increase of the effective adiabatic barrier due to the increased NH-stretching frequency in the sp^2 -hybridized planar transition structure. Other, dynamical effects such as the increase of the mean N–H bond length by vibrational excitation are also important in a quantitative analysis, as this leads to an increase of the effective moment of inertia for the tunneling process.

We have recently been able to extend this work to higher overtones and Figure 17 shows the result for the second NH-stretching overtone ($N = 3$ polyad) of $\text{C}_6\text{H}_5\text{NHD}$ (Miloglyadov *et al.* 2010).

One can very clearly see the tunneling splitting in the spectrum obtained under expansion conditions leading to a

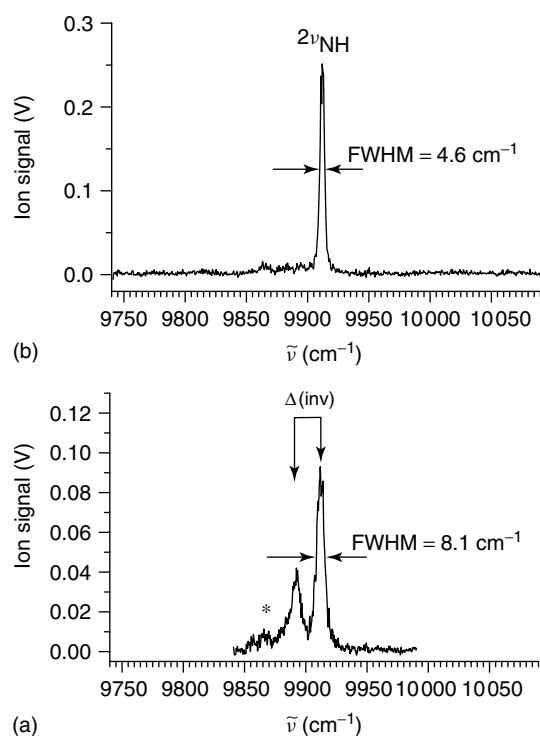


Figure 17 Second overtone ISOS spectra of aniline $^{12}\text{C}_6\text{H}_5\text{NHD}$ measured in the molecular beam with an instrumental resolution 0.15 cm^{-1} , as an ion signal mass gated at $m/z = 94\text{ u}$. (a) Spectrum obtained in a jet expansion with 0.35 bar of Ar. (b) Spectrum obtained in a jet expansion with 0.8 bar of Ar. The bracket in panel (a) indicates the tunneling splitting due to NHD-inversion. The appearance of the band corresponding to the lower tunneling doublet component in the trace (a) indicates a higher vibrational temperature estimated to be about 40 K . The star denotes the absorption bands of the $^{13}\text{C}^{12}\text{C}_5\text{H}_5\text{NH}_2$ isotopomers present in small amounts. (after Miloglyadov *et al.* 2010).

somewhat higher effective temperature of about 40 K in the supersonic jet, thus allowing the upper level of the ground state tunneling doublet (at 24 cm^{-1}) to be populated. At lower temperatures, only the vibrational-tunneling ground state is appreciably populated, thus resulting in a single, rather narrow, band where the total width (FWHM) of about 4.6 cm^{-1} , including some contribution from the rotational band contour, provides a bound on the IVR relaxation time ($\tau > 1.2\text{ ps}$).

Table 2 summarizes the current knowledge of tunneling splittings and stereomutation times $\tau_s = h/(2\Delta E)$ defined to be the time of change from the R to the S enantiomer. One can very clearly see the continuous inhibition of the stereomutation process with increasing NH-stretching excitation. We should point out that the phenomenon summarized in Table 2 corresponds to an extremely interesting process of mode-selective quasi-adiabatic channel above barrier-tunneling stereomutation. This phenomenon,

Table 2 Assignment of NH-stretching fundamental and overtone bands of $\text{C}_6\text{H}_5\text{NHD}$, aniline. The transition wavenumber connects upper, upper (u, u) and lower, lower (l, l) inversion sublevels. $\Delta\tilde{\nu}$ is the inversion splitting of the vibrational state, theory in parentheses (Fehrensens *et al.* 1999a).

Assignment	$\tilde{\nu}/\text{cm}^{-1}$	$\Delta\tilde{\nu}/\text{cm}^{-1}$	τ/ps
Ground state		23.8 (23.7)	0.7
$\nu_{\text{NH}}(u, u)$	3450.1 ^(a)	12.5	1.3
$\nu_{\text{NH}}(l, l)$	3461.4 ^(a)		
$2\nu_{\text{NH}}(u, u)$	6747 ^(b)	6.6	2.5
$2\nu_{\text{NH}}(l, l)$	6764.2 ^(b)		
$3\nu_{\text{NH}}(u, u)$	9891.6(5) ^(c)	3.5	4.8
$3\nu_{\text{NH}}(l, l)$	9911.9(2) ^(c)		

^(a)Fehrensens *et al.* (1999a).

^(b)Fehrensens *et al.* (1998).

^(c)Miloglyadov *et al.* (2010).

now well established, is in complete contradiction to statistical theories of unimolecular reaction, which assume fast intramolecular microcanonical quasiequilibrium and reaction rates above the barrier. This mode-selective process persists here in a large polyatomic molecule at very high densities of vibrational states and an energy exceeding the barrier for the reaction process by about a factor of 20. For a more detailed theoretical discussion of this type of process in the case of the smaller molecule H_2O_2 , where full-dimensional quantum dynamical calculations were carried out, we refer to Fehrensens *et al.* (2007) and Marquardt and Quack 2011: **Global Analytical Potential Energy Surfaces for High-resolution Molecular Spectroscopy and Reaction Dynamics**, this handbook.

We should note here also the results on the somewhat more complex situation in aniline- NH_2 isotopomer for which supersonic jet (Miloglyadov *et al.* 2010) and room temperature results (Howard *et al.* 2004) are available for the higher overtones.

8 ISOTOPE-SELECTIVE OVERTONE SPECTROSCOPY (ISOS) OF BENZENE ISOTOPOMERS

Owing to its high symmetry and as the archetypical aromatic compound, benzene occupies a special position in chemical physics. It has become a textbook example of an intermediate-sized molecule to study structure (Angus *et al.* 1936, Wilson *et al.* 1955, Tamagawa *et al.* 1976, Hollenstein *et al.* 1990b, Plíva *et al.* 1991, Riedle *et al.* 1994, Snels *et al.* 1997, Gauss and Stanton 2000), force fields (Wilson *et al.* 1955, Pulay *et al.* 1981, Maslen *et al.* 1992, Miani *et al.* 2000), IVR (Bray and Berry 1979, Reddy *et al.* 1982, Sibert *et al.* 1984a,c, Shi and Miller 1985, Page *et al.*

1987, 1988a,c, Lu and Hase 1988, Scotoni *et al.* 1991a,b, Zhang and Marcus 1992, Iung and Wyatt 1993, Callegari *et al.* 1997, Rashev *et al.* 1998a,b, Minehardt and Wyatt 1998, 1999, Minehardt *et al.* 1999, Callegari *et al.* 2000, 2001), and normal mode/local mode behavior in the CH-chromophore absorption (Rumpf and Mecke 1939, Henry and Siebrand 1968, Hayward *et al.* 1973, Halonen 1982, Reddy *et al.* 1982, Page *et al.* 1987, 1988b). The benzene vibrational spectroscopy has thus a long tradition (*see* Hippler *et al.* 2003 for a short review). The study of dynamic IVR processes in benzene started with the pioneering work of Berry and coworkers on the overtone spectroscopy of benzene in a room-temperature cell (Bray and Berry 1979, Reddy *et al.* 1982). After an approximate deconvolution to correct for the rotational band contour, the remaining broadening of overtone bands was attributed to ultrafast IVR decay processes. This broadening was then explained by Sibert *et al.*, (1984a,b) assuming strong Fermi resonances between the CH-stretching oscillator and CH-bending modes as the main mechanism of IVR following the basic scheme proposed by von Puttkamer *et al.* (1983a) and Dübäl and Quack (1984) for CHF₃ (*see*, however, also (Shi and Miller 1985)), and more recent classical and quantum calculations have established the dominant role of these Fermi resonances for IVR on very fast timescales (Sibert *et al.* 1984a,b, Shi and Miller 1985, Lu and Hase 1988, Zhang and Marcus 1992, Iung and Wyatt 1993, Rashev *et al.* 1998a,b, Minehardt and Wyatt 1998, 1999, Minehardt *et al.* 1999). In ¹²C₆H₆, an analysis of the IR-active CH-stretching fundamental ν_{20} (Wilson notation, Wilson *et al.* 1955) has confirmed the presence of strong Fermi-resonance splittings (Plíva and Pine 1982, 1987, Snaveley *et al.* 1984, Page *et al.* 1987, 1988a,b). The calculations predict even finer details of IVR in ¹²C₆H₆, and a whole sequence of timescales of redistribution of vibrational excitation among different modes has been suggested in recent publications (Sibert *et al.* 1984a,b, Shi and Miller 1985, Lu and Hase 1988, Zhang and Marcus 1992, Iung and Wyatt 1993, Rashev *et al.* 1998a,b, Minehardt and Wyatt 1998, 1999, Minehardt *et al.* 1999). A comparison of calculated spectra with the few available jet overtone spectra of ¹²C₆H₆, however, shows at most qualitative but no quantitative agreement. Recent jet measurements have also clearly shown that room-temperature spectra are heavily affected by inhomogeneous rotational and vibrational hot-band congestion (Snaveley *et al.* 1984, Page *et al.* 1987, 1988a,b, Callegari *et al.* 1997, Merker *et al.* 1999, Scotoni *et al.* 1991a,b, Hippler *et al.* 2003).

Compared to ¹²C₆H₆, only few spectra of the isotopomer ¹³C¹²C₅H₆ are reported (Brodersen *et al.* 1965, Painter and Koenig 1977, Thakur *et al.* 1986, Hollenstein *et al.* 1990b), and, to our knowledge, our spectra in Hippler *et al.* (2003) are the first overtone spectra to be published. Experimental

data for ¹³C¹²C₅H₆ are relevant for structural studies, since the isotopic substitution in the carbon ring will provide structural information not available by deuterium labeling, and experimental ¹³C-isotope shifts are thus useful for force-field determinations. In a recent time-dependent quantum mechanical study on IVR from the second CH-stretching overtone in ¹²C₆H₆, nonstatistical energy redistribution has been attributed to the influence of the symmetry of the molecule (Iung and Wyatt 1993). It is thus interesting to study the effect of the reduced symmetry in ¹³C¹²C₅H₆ on IVR. The shift of vibrational states in ¹³C¹²C₅H₆ compared to ¹²C₆H₆ will also affect Fermi and other anharmonic resonances and thus influence IVR processes.

8.1 ¹³C-isotope Effects in the IVR of Vibrationally Excited Benzene

With the ISOS technique described, we have observed isotopomer-resolved overtone spectra of ¹²C/¹³C-isotopomers (at natural abundance) of benzene (Hippler 2001, Hippler *et al.* 2003). In this case, two-photon (1 + 1) REMPI ionization occurs via the $\tilde{6}_0^1$ band in the $\tilde{A} \leftarrow \tilde{X}$ transition and other vibronic levels of the S₁ \tilde{A} state above 38 606 cm⁻¹ (Boesl *et al.* 1980, Page *et al.* 1987, 1988a,b, Boesl 1991) (*see* Hippler *et al.* 2003 for a more detailed discussion of the absorption mechanism in the ISOS scheme of benzene). For the benzene spectra shown below, a UV wavelength of 266 nm was chosen for the IR + UV double-resonance experiment. This particular UV frequency is easily accessible and available as a multiple of a Nd:YAG laser frequency. With a natural abundance of 1.1% ¹³C, the benzene isotopomers with one ¹³C atom have 6.2% abundance in the natural isotopomer mixture. Mass gating the ionization detection in the IR + UV double-resonance experiment to the corresponding masses $m/z = 78$ and 79 u allows us to obtain the separate vibrational spectra of both isotopomers in a single scan of the natural isotopomer mixture. For the jet experiments, 500 mbar of Ar as seed gas is flowing over frozen benzene at 0 °C, which has a measured vapor pressure of 35 mbar. Certain experimental conditions promote the formation of clusters, for example, high partial benzene sample pressure, high Ar stagnation pressure, or probing molecules in the middle or the end of the jet pulse train. Cluster formation made itself conspicuous by additional mass peaks in the TOF spectra and specific peaks in the UV spectrum of the S₁ \leftarrow S₀ transition in benzene (Page *et al.* 1988b, Weber *et al.* 1990, Weber and Neusser 1991, Henson *et al.* 1992). IR spectra of benzene clusters differ greatly from the monomer spectra (Page *et al.* 1988b, Sugawara *et al.* 1996). Care was therefore taken that the spectra displayed here are not affected by cluster formation.

Isotopically pure benzene $^{12}\text{C}_6\text{H}_6$ (depleted benzene, Cambridge Isotope Laboratories, $^{12}\text{C}_6$ 99.95%) is also used for some FTIR measurements.

Benzene $^{12}\text{C}_6\text{H}_6$ (D_{6h} symmetry) has 20 normal vibrations, of which 10 are doubly degenerate (Wilson 1934a). In D_{6h} symmetry, only perpendicular IR transitions from the ground state to E_{1u} vibrational states are allowed with an in-plane electric dipole moment, or parallel IR transitions to A_{2u} vibrational states with an out-of-plane dipole moment (Wilson *et al.* 1955). Seven fundamental vibrations are Raman active and four are IR active (Wilson 1934b). Benzene has four fundamental normal modes (essentially CH stretching modes) between 3048 and 3074 cm^{-1} , which are ν_2 (A_{1g} symmetry), ν_7 (E_{2g}), ν_{13} (B_{1u}) and the only IR-active CH-stretching fundamental ν_{20} (E_{1u}) (in the Wilson notation). In the region of the first CH-stretching overtone near 6000 cm^{-1} , only the three combination bands of CH-stretching modes ($\nu_{20} + \nu_7$, $\nu_7 + \nu_{13}$ and $\nu_2 + \nu_{20}$) have E_{1u} symmetry components with allowed IR transitions from the ground state. All other combinations including the overtone $2\nu_{20}$ are IR inactive (owing to the center of symmetry, no overtone frequencies with ν even can occur in the IR spectrum (Wilson *et al.* 1955)). A normal mode description of vibrational overtone bands is, however, not entirely satisfactory, since all IR-active CH-stretching normal mode combination bands are strongly coupled by Darling–Dennison and related anharmonic resonances. The resultant mixed states probably resemble local mode excitations. In the local mode picture, each CH-stretching overtone is dominated by one dominant absorption feature corresponding to one local CH-oscillator with all vibrational excitation. For the first overtone region, a recent calculation of the CH-stretching absorption spectrum by Iachello and Oss based on the algebraic “vibron” model has given three IR absorptions, at 6004 cm^{-1} , 6113 cm^{-1} , and 6128 cm^{-1} , with relative intensity 1, 0.0017, and 0.006, respectively (Iachello and Oss 1992). A pure local mode description of overtones, however, is also not satisfactory: theoretical studies (Sibert *et al.* 1984a,b, Shi and Miller 1985, Lu and Hase 1988, Zhang and Marcus 1992, Iung and Wyatt 1993, Rashev *et al.* 1998a,b, Minehardt and Wyatt 1998, 1999, Minehardt *et al.* 1999) and the analysis of the spectrum of the CH-stretching fundamental (Plíva and Pine 1982, 1987, Snavely *et al.* 1984, Page *et al.* 1987, 1988a,b) show that CH-stretching modes are, in addition, strongly coupled with CH-bending modes by Fermi resonances exchanging one quantum of CH-stretching excitation with two quanta of CH-bending excitation. All vibrational modes of a given symmetry with common polyad quantum number N are thus strongly coupled and mixed by Fermi, Darling–Dennison and related anharmonic

resonances, where $N = \nu_s + 0.5 \times \nu_b$; ν_s represents all CH-stretching and ν_b all CH-bending quantum numbers. We therefore refer to the IR absorption near 6000 cm^{-1} as the $N = 2$ CH-chromophore absorption, instead of the more common “first CH-stretching overtone”.

The benzene isotopomer $^{13}\text{C}^{12}\text{C}_5\text{H}_6$ is an asymmetric top of the point group C_{2v} . The asymmetry parameter $\kappa = 0.916$ is close to 1 (Brodersen *et al.* 1965); the replacement of one ^{12}C by the ^{13}C isotope introduces only a small perturbation. In C_{2v} symmetry, many more normal modes are formally IR allowed: Among the 30 normal mode vibrations, 27 vibrations of A_1 , B_1 , and B_2 symmetry species are IR active, and all modes are Raman allowed. Isotopic labeling will also cause, in principle, an alteration of normal mode characters (mode scrambling). The perturbation of the ^{13}C , however, is so small that intensities in $^{13}\text{C}^{12}\text{C}_5\text{H}_6$ cannot be expected to deviate much from the corresponding transitions in $^{12}\text{C}_6\text{H}_6$, despite the relaxed IR selection rules, and the character of corresponding vibrational modes will also be similar. The ^{13}C isotopic substitution will introduce a minor frequency shift to lower wavenumbers, if no perturbations apply. If only the one carbon atom in question moves in a hypothetical vibration, a relative energy shift of -4.1% will occur due to the change in the reduced mass. The overtone vibrations of the CH-chromophore will probably resemble local diatomic CH-oscillators. The relative energy shift of ^{13}CH -harmonic oscillator vibrations compared to a ^{12}CH -harmonic oscillator is about -0.3% .

The $N = 2$ CH-chromophore absorption spectrum of benzene obtained by FTIR spectroscopy at room temperature is shown in Figure 18. The spectrum of $^{12}\text{C}_6\text{H}_6$ is obtained in an isotopically pure sample. Depleted benzene $^{12}\text{C}_6\text{H}_6$ is readily available, since it is a solvent used in NMR spectroscopy. For $^{13}\text{C}^{12}\text{C}_5\text{H}_6$, no isotopically pure sample was available. To obtain its spectrum, the depleted spectrum is subtracted from the normal benzene spectrum using appropriate weights and rescaled. The difference spectrum is essentially due to the $^{13}\text{C}^{12}\text{C}_5\text{H}_6$ isotopomer. This manipulation, however, is prone to noise and possibly also to systematic errors and distortions. The difference spectrum can therefore only be considered as an approximation to the proper $^{13}\text{C}^{12}\text{C}_5\text{H}_6$ spectrum, in particular, the absorption cross sections indicated are only approximate. The room-temperature spectra improve previously published spectra of the natural benzene isotopomer mixture, which had been obtained at much lower instrumental bandwidth ($6\text{--}12 \text{ cm}^{-1}$) (Reddy *et al.* 1982).

The general appearances of both isotopomer spectra are similar. A main broad feature with FWHM of ca 40 cm^{-1} with a distinct central peak and some diffuse structure dominates the spectrum. The central peak is at $6005.3 \pm 0.4 \text{ cm}^{-1}$ for $^{12}\text{C}_6\text{H}_6$ and at $5991 \pm 1 \text{ cm}^{-1}$ for $^{13}\text{C}^{12}\text{C}_5\text{H}_6$. Higher CH-stretching overtones of $^{12}\text{C}_6\text{H}_6$ are

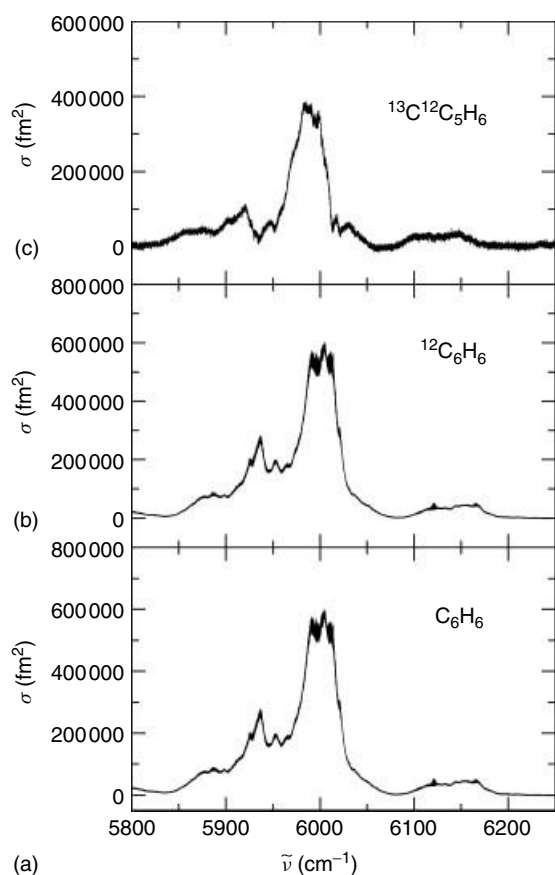


Figure 18 FTIR spectra of the $N = 2$ CH-chromophore absorption of benzene at room temperature (from Hippler *et al.* 2003). (a) Spectrum of benzene ($p = 2.20$ mbar, natural isotopomer mixture). (b) The corresponding spectrum of depleted benzene ($^{12}\text{C}_6\text{H}_6$, $^{12}\text{C}_6$ 99.95%) at room temperature ($p = 2.14$ mbar, $l = 28$ m, resolution 0.015 cm^{-1}). (c) The depleted spectrum has been subtracted from the normal benzene spectrum using appropriate weights, and rescaled. This difference spectrum is essentially due to the $^{13}\text{C}^{12}\text{C}_5\text{H}_6$ isotopomer (note that absorption cross sections for $^{13}\text{C}^{12}\text{C}_5\text{H}_6$ are only approximate).

well described by a Morse oscillator with $\omega_m = 3163\text{ cm}^{-1}$ and $x_m = 57.7\text{ cm}^{-1}$, which has been interpreted as the local mode ^{12}CH -oscillator absorption (Reddy *et al.* 1982, Scotoni *et al.* 1991a). The ^{12}CH -Morse oscillator vibration for $v = 2$ is then calculated at 5980 cm^{-1} , and at 5963 cm^{-1} for the ^{13}CH -Morse oscillator taking into account the change of reduced masses (Reddy *et al.* 1982), the shift of -17 cm^{-1} being comparable to the -14 cm^{-1} for band maxima mentioned above, although one must note that the spectrum should be dominated by the five ^{12}CH local mode absorptions in the $^{13}\text{CH}^{12}\text{C}_5\text{H}_5$ isotopomer (see below). A closer examination of the experimental spectra reveals some differences in relative intensities and rotational band contours of corresponding transitions, for example, in the wing at higher wavenumbers of the main feature, where two additional features are apparent for $^{13}\text{C}^{12}\text{C}_5\text{H}_6$. A further

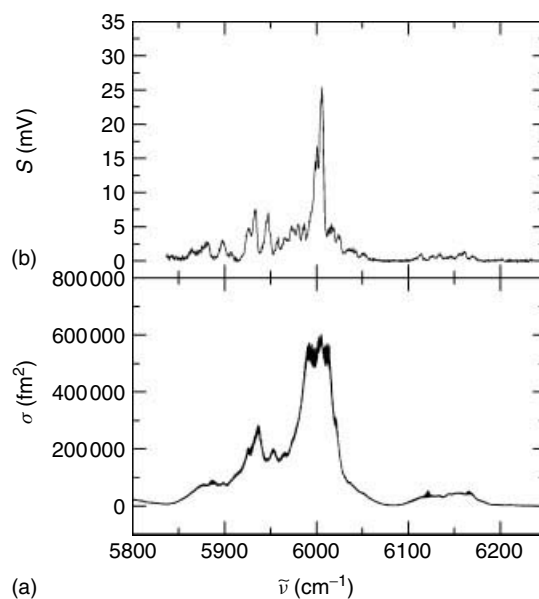


Figure 19 $N = 2$ CH-chromophore absorption of $^{12}\text{C}_6\text{H}_6$ near 6000 cm^{-1} (after Hippler *et al.* 2003). (a) FTIR reference spectrum of depleted benzene ($^{12}\text{C}_6\text{H}_6$, $^{12}\text{C}_6$ 99.95%) at room temperature ($p = 2.14$ mbar, $l = 28$ m, resolution 0.015 cm^{-1}). (b) Ionization-detected ISOS spectrum of jet-cooled benzene, mass gated at $m/z = 78\text{ u}$ ($^{12}\text{C}_6\text{H}_6$), in a jet expansion with 500 mbar of Ar.

assignment or interpretation of the spectra is not possible due to inhomogeneous congestion. In addition to broad rotational contours, room-temperature spectra are heavily affected by vibrational hot-band transitions, since about 40% of benzene molecules are in vibrationally excited states.

In Figures 19 and 20, the ionization-detected, jet-cooled ISOS spectra of benzene are displayed and compared with the corresponding FTIR room-temperature spectra. In the natural benzene isotopomer mixture, mass gating the ionization detection at $m/z = 78$ and 79 u yields simultaneously the separated spectra of $^{12}\text{C}_6\text{H}_6$ and $^{13}\text{C}^{12}\text{C}_5\text{H}_6$ isotopomers, respectively. In comparable jet experiments (for example on aniline, see previous section), rotational temperatures of about 5 K have been obtained, and vibrational hot-band transitions have been almost completely suppressed; similar conditions are expected to apply here. The spectral simplification afforded by jet cooling is striking. The FWHM of vibrational band contours decreases from about 40 cm^{-1} at room temperature to about $4\text{--}5\text{ cm}^{-1}$ for $^{12}\text{C}_6\text{H}_6$, and distinct resolved or partly resolved vibrational transitions become apparent. Line positions and intensities of observed transitions in the jet-cooled $N = 2$ CH-chromophore absorption spectra of the $^{12}\text{C}_6\text{H}_6$ and $^{13}\text{C}^{12}\text{C}_5\text{H}_6$ isotopomers are summarized in Hippler *et al.* 2003). The $^{12}\text{C}_6\text{H}_6$ spectrum (Figure 19) is essentially in good agreement with the previously published jet spectrum

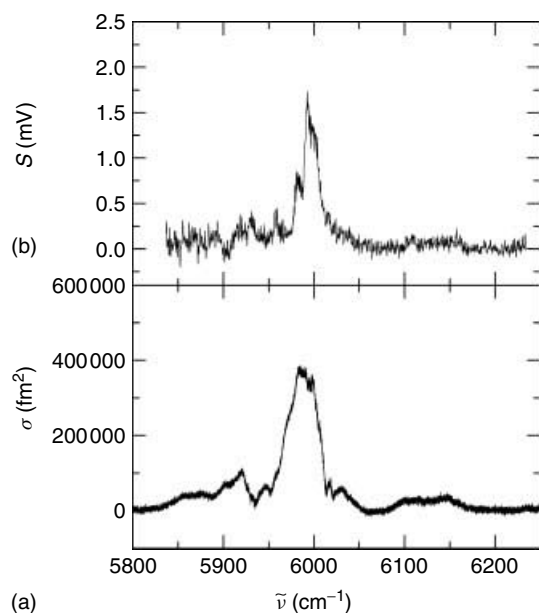


Figure 20 $N = 2$ CH-chromophore absorption of $^{13}\text{C}^{12}\text{C}_5\text{H}_6$ near 6000 cm^{-1} (from Hippler *et al.* 2003). (a) A manipulated spectrum, where the FTIR spectrum of 2.14 mbar depleted benzene ($^{12}\text{C}_6\text{H}_6$, $^{12}\text{C}_6$ 99.95%) at room temperature has been subtracted from the FTIR spectrum of 2.20 mbar benzene (natural isotopomer mixture) and rescaled ($l = 28$ m, resolution 0.015 cm^{-1}). The difference spectrum is essentially due to the $^{13}\text{C}^{12}\text{C}_5\text{H}_6$ isotopomer (as in Figure 18). (b) The ionization-detected ISOS spectrum of jet-cooled benzene, mass gated at $m/z = 79$ u ($^{13}\text{C}^{12}\text{C}_5\text{H}_6$), in a jet expansion with 500 mbar of Ar.

of Page *et al.* (1987, 1988a,b), but it is not affected by saturation and has a better signal-to-noise ratio (*see* Hippler *et al.* 2003 for a detailed comparison). The spectrum of the $^{13}\text{C}^{12}\text{C}_5\text{H}_6$ isotopomer in Figure 20 demonstrates that the 6.2% abundance in the natural isotopomer mixture of benzene is sufficient to obtain jet spectra with the ISOS technique. The strongest peak in the $^{12}\text{C}_6\text{H}_6$ jet spectrum is located at $6006.0 \pm 0.5\text{ cm}^{-1}$, and the corresponding strongest peak in the $^{13}\text{C}^{12}\text{C}_5\text{H}_6$ jet spectrum at $5993 \pm 1\text{ cm}^{-1}$. These peak positions provide good estimates for the band origins, giving a ^{13}C -isotopomer shift of -13 cm^{-1} or a relative shift of -0.22% . This is close to the estimation from the room-temperature spectrum, but is more reliable, since the value has been obtained from vibrational bands with much reduced inhomogeneous congestion. In $^{12}\text{C}_6\text{H}_6$, the main absorption feature and other features have an FWHM of about $4\text{--}5\text{ cm}^{-1}$, whereas spectral contours in $^{13}\text{C}^{12}\text{C}_5\text{H}_6$ are much broader, with an FWHM of about 15 cm^{-1} , but the features have sharp edges with a halfwidth of about 4 cm^{-1} , only. It is thus likely that part of the broadening is due to spectral congestion, for example, by the different rotational contour of the asymmetric rotor or by the presence of additional vibrational bands that are IR active in the C_{2v} symmetry. A

degenerate E_{1u} IR-active vibrational band in D_{6h} symmetry correlates to two IR-active bands of A_1 and B_1 species in C_{2v} symmetry (Wilson *et al.* 1955), which may be affected by a strong Coriolis perturbation (Brodersen *et al.* 1965). This effect may also give rise to an anomalous intensity distribution.

Previous theoretical studies provide some guidelines for a first tentative statistical interpretation of the $^{12}\text{C}_6\text{H}_6$ jet spectrum in terms of IVR processes: the calculations of Iachello and Oss have shown that one strong pure CH-stretching transition prevails in the IR spectrum of this region, which is calculated to occur at 6004 cm^{-1} by Iachello and Oss (1992). This CH-stretching mode is coupled to the IR field as a chromophore state. By anharmonic coupling, its vibrational excitation will be redistributed among many vibrational modes, giving rise to the observed vibrational bands in the IR jet spectrum. At 6000 cm^{-1} , the vibrational density of states is about 1560 states per cm^{-1} , as counted in the harmonic approximation by the Beyer–Swinehart algorithm (Beyer and Swinehart 1973) using an experimental set of fundamental vibrations compiled in Miani *et al.* (2000) and Hollenstein *et al.* (1990b). E_{1u} symmetry is required for an allowed anharmonic coupling with the E_{1u} CH-stretching overtone level. In the regular limit (Quack 1985), the density of E_{1u} states is $2/24 = 1/12$ of the total density, about 130 states per cm^{-1} . Instead of the one-step coupling of the bright state to the bath, a sequential “tier” picture (Quack 1981a,b, Dübal and Quack 1984, Sibert *et al.* 1984a,b, Gruebele and Bigwood 1998) appears to provide a better description of IVR in benzene. In the first tier, the bright CH-stretching state is strongly coupled with a subset of vibrational states. A broad Lorentzian curve obtained by a visual fit envelops all absorption features observed in the experimental jet spectrum (Figure 21, dotted curve) with FWHM $\tilde{\Gamma} = 45\text{ cm}^{-1}$ corresponding to a decay time of vibrational excitation into the first tier of vibrational states of $\tau \approx 120$ fs. Since CH-stretching and bending modes are known to be coupled by strong Fermi resonances (Plíva and Pine 1982, 1987, Snavely *et al.* 1984, Sibert *et al.* 1984a,b, Shi and Miller 1985, Page *et al.* 1988a,b, 1988b, Lu and Hase 1988, Zhang and Marcus 1992, Iung and Wyatt 1993, Rashev *et al.* 1998a,b, Minehardt and Wyatt 1998, 1999, Minehardt *et al.* 1999), the first tier presumably involves the CH-stretching/bending combination bands of E_{1u} symmetry species in the absorption region. The inferred decay time is compatible with theoretical calculations (Sibert *et al.* 1984a,b, Shi and Miller 1985, Lu and Hase 1988, Zhang and Marcus 1992, Rashev *et al.* 1998a,b, Iung and Wyatt 1993, Minehardt and Wyatt 1998, 1999, Minehardt *et al.* 1999) and with typical redistribution times found, e.g., for CH-stretching/bending Fermi resonances in CHX_3 or CHXY_2 compounds (Dübal and Quack 1984, Peyerimhoff *et al.* 1984, Amrein *et al.* 1985,

Lewerenz and Quack 1986, Baggott *et al.* 1986, Wong *et al.* 1987, William *et al.* 1987, Segall *et al.* 1987, Lewerenz and Quack 1988, Dübal *et al.* 1989, Quack 1990, 1993, Hollenstein *et al.* 1990a, 1993, Ha *et al.* 1990, Marquardt and Quack 1991, Luckhaus and Quack 1992, Luckhaus *et al.* 1993, Marquardt *et al.* 1995). The Lorentzian is centered at 5988 cm^{-1} , which corresponds to the position of the chromophore state. It is interesting to note that the Morse oscillator level $v = 2$ is calculated at 5980 cm^{-1} , close to the position found here for the chromophore state in the $N = 2$ polyad absorption. The main absorption feature at 6006 cm^{-1} has accompanying weaker satellite lines. A second Lorentzian obtained by a visual fit envelops these absorption features (Figure 21, dashed curve) with $\tilde{\Gamma} = 15\text{ cm}^{-1}$ corresponding to a decay time $\tau \approx 0.35\text{ ps}$ of vibrational excitation into a second tier of vibrational states. This tier could be composed of vibrational states coupled by weaker higher order anharmonic resonances to the CH-stretching/bending manifold. The two-tier statistical model proposed here for IVR in the $N = 2$ CH-chromophore absorption is compatible with the experiment and with expectation. The analysis of the CH-stretching fundamental has provided a similar coupling scheme (Plíva and Pine 1982, 1987, Snavely *et al.* 1984, Page *et al.* 1987, 1988a,b): the IR-active CH-stretching fundamental ν_{20} is coupled to the IR field. By strong Fermi resonances with CH-stretching/bending combination bands, vibrational excitation is redistributed to an absorption triad, ν_{20} , $\nu_{18} + \nu_{19}$, and $\nu_1 + \nu_6 + \nu_{19}$. The latter band is, in addition, coupled by weaker anharmonic resonances with $\nu_3 + \nu_6 + \nu_{15}$. The 4 cm^{-1} width (FWHM) of features in the jet spectrum of the $N = 2$ absorption is an upper bound for the homogeneous bandwidth $\tilde{\Gamma}$ giving a lower bound $\tau > 1.3\text{ ps}$ for the decay time of further redistribution of vibrational excitation. Callegari *et al.* have obtained the “eigenstate-resolved” benzene spectrum between 6004 and 6008 cm^{-1} by IR–IR double resonance with cw-laser systems and bolometric detection (Callegari *et al.* 1997, 2000, 2001). From the observed clustering of eigenstates, the authors deduced further timescales for IVR ranging from 100 ps to 2 ns .

The integral of a Lorentzian curve with FWHM $\tilde{\Gamma}$ centered around $\tilde{\nu}_0$ has its half height at $\tilde{\nu}_0$, and $\tilde{\Gamma}$ extends from $1/4$ to $3/4$ of its height. This suggests another useful and more quantitative analysis (Quack 1981a, Hippler *et al.* 2003) of the spectra considering the integral $S(\tilde{\nu})$,

$$S(\tilde{\nu}) = \int_{\tilde{\nu}_0}^{\tilde{\nu}} \sigma(\tilde{\nu}') d\tilde{\nu}' \quad (27)$$

or more appropriately, but almost equivalently

$$G(\tilde{\nu}) = \int_{\tilde{\nu}_0}^{\tilde{\nu}} \sigma(\tilde{\nu}') \tilde{\nu}'^{-1} d\tilde{\nu}' \approx \frac{1}{\tilde{\nu}_G} S(\tilde{\nu}) \quad (28)$$

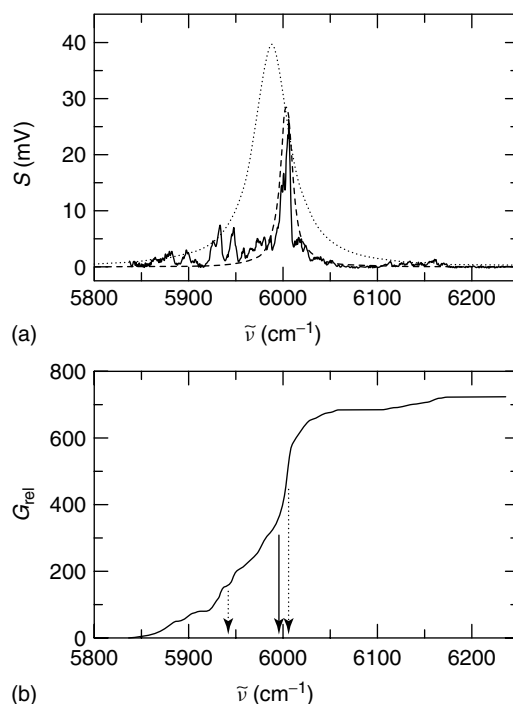


Figure 21 (a) Jet-cooled, isotopomer-selective overtone spectrum of the $N = 2$ CH-chromophore absorption of $^{12}\text{C}_6\text{H}_6$ (as in Figure 19). The dotted curve is a Lorentzian function with 45 cm^{-1} FWHM centered at 5988 cm^{-1} , the dashed curve a Lorentzian function with 15 cm^{-1} FWHM centered at 6003 cm^{-1} . (b) Relative $G_{\text{rel}}(\tilde{\nu})$ (integral of the absorption cross section) corresponding to the jet-cooled $N = 2$ CH-chromophore absorption of $^{12}\text{C}_6\text{H}_6$, in arbitrary units. The position of the half height (solid arrow) and of the $1/4$ - and $3/4$ -heights (dotted arrows) are indicated (see text for a discussion) (from Hippler *et al.* 2003).

$\sigma(\tilde{\nu})$ is the absorption cross section. The lower integration limit $\tilde{\nu}_0$ is near 5850 cm^{-1} , outside the absorption range, and $\tilde{\nu}_G$ is the center of gravity or effective band center. The integral $G(\tilde{\nu})$ corresponding to the jet-cooled $N = 2$ CH-chromophore absorption of $^{12}\text{C}_6\text{H}_6$ is shown in Figure 21. The effective band center obtained from the half height of this function is $\tilde{\nu}_G = 5995\text{ cm}^{-1}$, whereas the effective width $\tilde{\Gamma} = 60\text{ cm}^{-1}$ is obtained from the $1/4$ - and $3/4$ -heights, in reasonable agreement with the visual fit shown in Figure 21. We thus finally quote $\tilde{\Gamma} = (50 \pm 10)\text{ cm}^{-1}$ and a resulting approximate decay time of vibrational excitation $\tau \approx 100\text{ fs}$ combining both approaches. The basis of this dynamic analysis is the assumption of one single chromophore absorption carrying all the oscillator strength in the integration range. This assumption has had some theoretical basis for a long time (Quack 1981a,b, 1990, Mecke 1955) and has been justified again more recently, e.g., by the “vibron” model calculations of Iachello and Oss (1992). For $^{12}\text{C}_6\text{H}_6$, this chromophore absorption probably resembles the excitation of local ^{12}CH Morse-oscillators.

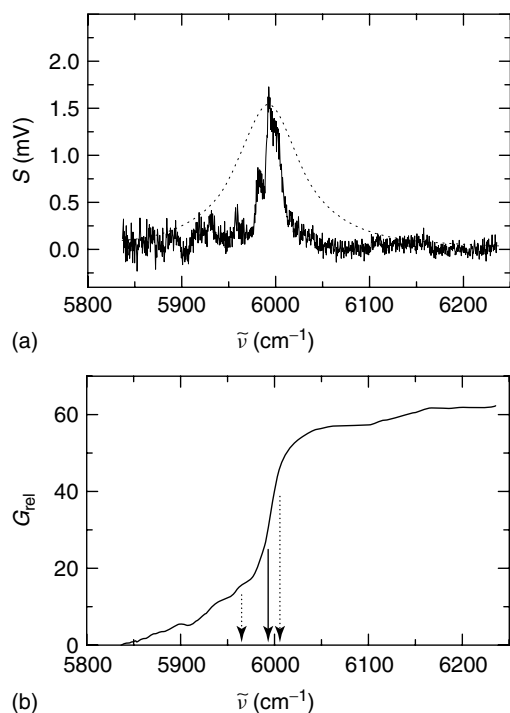


Figure 22 (a) Jet-cooled, isotopomer-selective overtone spectrum of the $N = 2$ CH-chromophore absorption of $^{13}\text{C}^{12}\text{C}_5\text{H}_6$ (as in Figure 20). The dotted curve is a Lorentzian function with 40 cm^{-1} FWHM centered at 5993 cm^{-1} . (b) Relative $G_{\text{rel}}(\tilde{\nu})$ (integral of the absorption cross section) corresponding to the jet-cooled $N = 2$ CH-chromophore absorption of $^{13}\text{C}^{12}\text{C}_5\text{H}_6$, in arbitrary units. The position of the half height (solid arrow) and of the 1/4- and 3/4-heights (dotted arrows) are indicated (see text for a discussion) (from Hippler *et al.* 2003).

Owing to the similarities in the general appearance of the jet spectra, the $N = 2$ CH-chromophore absorption of $^{13}\text{C}^{12}\text{C}_5\text{H}_6$ can probably be interpreted on similar general lines as outlined here for $^{12}\text{C}_6\text{H}_6$. Since no theoretical calculations exist to our knowledge to guide the assignment, only a preliminary analysis of the IVR dynamics can be made at this stage using some simple models. On the basis of a local mode picture, one could expect two chromophore absorptions for $^{13}\text{C}^{12}\text{C}_5\text{H}_6$ in this overtone region, a strong absorption due to local ^{12}CH Morse-oscillators, and a weaker absorption due to the local ^{13}CH Morse oscillator. Assuming now that the absorption of the local ^{12}CH Morse oscillators is dominating, one can attempt a similar quantitative analysis as before for the $^{12}\text{C}_6\text{H}_6$ isotopomer. In Figure 22, $G(\tilde{\nu})$ is shown for the jet-cooled $N = 2$ CH-chromophore absorption of $^{13}\text{C}^{12}\text{C}_5\text{H}_6$. The effective band center is obtained at $\tilde{\nu}_G = 5993\text{ cm}^{-1}$ with width $\tilde{\Gamma} = 40\text{ cm}^{-1}$, and a corresponding Lorentzian curve envelopes indeed all absorption features of the $^{13}\text{C}^{12}\text{C}_5\text{H}_6$ jet spectrum. The center of gravity of the band is shifted by only -2 cm^{-1} compared to the value for $^{12}\text{C}_6\text{H}_6$ (Hippler *et al.* 2003), presumably

because the dominating chromophore absorption is in both cases due to ^{12}CH Morse-oscillators (as detailed before, the ^{13}CH Morse oscillator has an expected shift of -17 cm^{-1}). Since the inherent assumption of one single chromophore absorption in this analysis is presumably not strictly valid for $^{13}\text{C}^{12}\text{C}_5\text{H}_6$, the actual $\tilde{\Gamma}$ due to IVR will be somewhat smaller than the 40 cm^{-1} obtained by the integration method. We thus estimate $\tilde{\Gamma} \leq 40\text{ cm}^{-1}$ and a resulting approximate decay time of vibrational excitation $\tau \geq 130\text{ fs}$. This very fast decay of initial vibrational excitation is most likely due to strong anharmonic Fermi resonances between CH-stretching and CH-bending modes, since similar resonances and redistribution times have been found for $^{12}\text{C}_6\text{H}_6$ (see above) and CHX_3 or CHXY_2 compounds (Dübal and Quack 1984, Peyerimhoff *et al.* 1984, Amrein *et al.* 1985, Baggott *et al.* 1986, Lewerenz and Quack 1986, 1988, 1992, William *et al.* 1987, Wong *et al.* 1987, Segall *et al.* 1987, Dübal *et al.* 1989, Quack 1990, 1993, Hollenstein *et al.* 1990a, 1993, Ha *et al.* 1990, Marquardt and Quack 1991, Luckhaus *et al.* 1993, Marquardt *et al.* 1995).

Zhang and Marcus (1992) have calculated the absorption spectrum of $^{12}\text{C}_6\text{H}_6$ in the 6000 cm^{-1} region using an anharmonic force field together with dipole moment derivatives (Pulay *et al.* 1981). More recently, Rashev *et al.* (1998a) have also published a calculated spectrum based on anharmonic force fields (Pulay *et al.* 1981, Maslen *et al.* 1992) and symmetrized complex coordinates. Relative intensities were calculated assuming local CH-oscillators as zeroth-order “bright” states. A comparison with our experimental jet spectrum shows qualitative but no quantitative agreement; furthermore, both calculations differ markedly (see Hippler *et al.* 2003 for more details). Further progress in the understanding of IVR in the important model molecule benzene could be achieved by alternative theoretical models to be developed in close comparison with experimental jet spectra.

8.2 Isotope-selective Overtone Spectroscopy (ISOS) of the CH-stretching Vibration in $^{12}\text{C}_6\text{HD}_5$ and of $^{13}\text{C}^{12}\text{C}_5\text{HD}_5$

One of the promising candidates for further experimental and theoretical studies is the isotopomer $\text{C}_6\text{D}_5\text{H}$ (Miloglyadov *et al.* 2008). It has a lower C_{2v} -symmetry (Wilson 1934a, Brodersen and Langseth 1959, Thakur *et al.* 1986), as compared to the D_{6h} -symmetry for C_6H_6 and only one “localized” CH-stretching vibration that reduces the number of strongly coupled states and simplifies the spectrum. Measurements of ^{13}C -isotope shifts are also useful for the determination of an accurate force field for benzene. It is also interesting to study the effect of the changes in mass

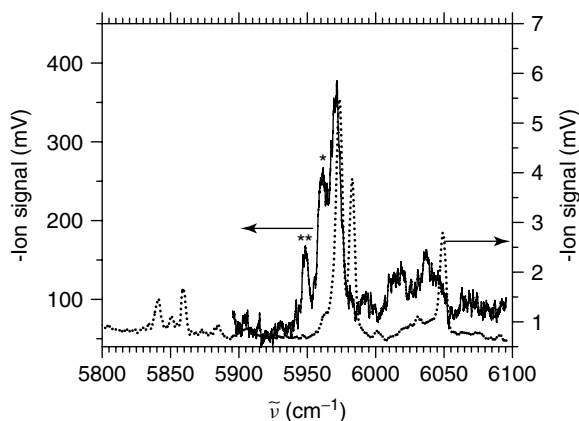


Figure 23 Molecular beam spectra of the first overtone of the CH-stretching vibration for $^{12}\text{C}_6\text{HD}_5$ (· · ·) and $^{13}\text{C}^{12}\text{C}_5\text{HD}_5$ (—). The spectrum of the ^{13}C -isotopomers is scaled by a factor 60. The expected wavenumber shift of 22.3 cm^{-1} (***) for the isomer with the ^{13}CH -chromophore with respect to the other ^{13}C -isotope-isomers is indicated. The peak shifted by 10.3 cm^{-1} (*) is assumed to result from a not yet identified resonantly coupled level (after Miloglyadov *et al.* 2008).

and of the reduced symmetry in $^{13}\text{C}^{12}\text{C}_5\text{HD}_5$ on IVR, as the shift of vibrational states in $^{13}\text{C}^{12}\text{C}_5\text{HD}_5$ relative to the ones in $^{12}\text{C}_6\text{HD}_5$ will affect Fermi and other anharmonic resonances. We present the first overtone spectra of the CH-stretching vibration of rotationally cooled C_6HD_5 and the isotope-isomers of $^{13}\text{C}^{12}\text{C}_5\text{HD}_5$.

The spectrum of the first overtone of the CH-stretching vibration for C_6HD_5 is presented in Figure 23. The main band responsible for the first overtone of the CH-stretching vibration is centered at 5975 cm^{-1} and has a width of about 35 cm^{-1} at room temperature (Reddy *et al.* 1982). At a rotational temperature $T \cong 3\text{ K}$, it is split into two peaks: one at $5973 \pm 0.2\text{ cm}^{-1}$ with a width of about 6 cm^{-1} (about 48% of the integral intensity of the spectrum) and one at $5982.9 \pm 0.2\text{ cm}^{-1}$ (about 28%). Together with the band at 6049 cm^{-1} , (about 24%) these three bands form a triad resulting presumably from strongly coupled states. The weak band at 5847.5 cm^{-1} in the room-temperature spectra is resolved into three bands at 5841, 5850.3, and 5859.1 cm^{-1} in the molecular beam spectrum. There are also a number of additional weak bands in the spectrum.

The strongest band at 5973 cm^{-1} corresponds to the first overtone of CH-stretching vibration $2\nu_2$ (in Wilson notation). To find possible candidates for the assignment of the other bands we might consider the “three-quantum combination bands” falling in the measured spectral range from 5750 to 6100 cm^{-1} . There are 11 such states of A_1 -symmetry with one quantum of CH-stretching in the range of the measurement. The main candidates for the assignment are $\nu_2 + 2\nu_{19b}$ for one of the bands (5841,

5850.3 , and 5859.1 cm^{-1}), and $\nu_2 + \nu_{19b} + \nu_{8b}$ and $\nu_2 + \nu_{19a} + \nu_{8a}$ for the bands at 6049 cm^{-1} and 5982.9 cm^{-1} respectively (Brodersen and Langseth 1959).

There are four distinguishable isotope-isomers of C_6HD_5 with one ^{13}C atom and all of them have to be present in the spectrum of the natural mixture. The only isomer that is expected to have a noticeable CH-stretching shift with respect to the others is the one with the ^{13}CH -chromophore and the rough overall spectrum without consideration of the resonances would consist of two bands with an expected intensity ratio of approximately 1 : 5. The relative isotopic shift of all ^{13}C -substituted isomers of pentadeuterated benzene can be estimated using quantum chemical calculations. The harmonic frequencies for C_6HD_5 and all its isotope-isomers with one ^{13}C were calculated with ab initio methods with full optimization at the MP2/aug-cc-pVTZ level of theory. The calculations show that only one harmonic frequency is shifted significantly, the frequency of the isomer with the ^{13}CH -chromophore. It has a calculated isotope shift of about -10.2 cm^{-1} relative to the other isomers for the fundamental vibration and a frequency shift of around -20 cm^{-1} may be expected for the first overtone, neglecting the influence of vibrational couplings. The overtone spectrum of C_6HD_5 substituted with one ^{13}C atom (Figure 23) is presented together with the spectrum of $^{12}\text{C}_6\text{HD}_5$. If we assume that the intensity of the transitions is given by the relative abundance of the isomers, we can identify the two relevant peaks in the spectra: the main peak at 5970.5 cm^{-1} and one at 5948.2 cm^{-1} (**), separated by 22.3 cm^{-1} . The third peak at 5960.2 cm^{-1} (*) may correspond to the strongly shifted coupled state, which is found for $\text{C}_6\text{D}_5\text{H}$ at 5982.9 cm^{-1} . It is clear, however, that the situation remains quite complex and at present such an analysis must be preliminary.

9 CONCLUSIONS AND OUTLOOK

In the present review we have stressed on the developments in mass and isotope selective infrared spectroscopy that have been carried out by us over the last two decades in the framework of our studies of intramolecular dynamics as derived from high-resolution spectroscopy. We have tried to relate this effort to alternative approaches by other research groups, wherever possible, and apologize for any possible omissions in the citation of work from our colleagues worldwide that may have occurred because of limited information on our side, due to the necessary restrictions being imposed on the length of our review, or that might have occurred inadvertently.

We have demonstrated in the foregoing sections the power of the methods developed in their application to various aspects of isotope effects in high-resolution

spectroscopy. It should be clear that the methods described here open new avenues for high-resolution spectroscopy. The selective ionization of vibrationally excited molecules in the IR + UV double-resonance schemes allows indirect, but extremely sensitive, detection of the IR excitation. The technique has been applied to overtone spectroscopy in supersonic jet expansions, where the cooling of vibrational and rotational degrees of freedom greatly reduces hot-band congestion and simplifies spectra, which is often essential for a reliable assignment. Ionization detection of the IR excitation can be coupled very efficiently with a TOF mass spectrometer, which allows the separation of spectral contributions of different components in a mixture. Mass spectrometry is thus added as a second dimension to IR spectroscopy, which greatly increases the selectivity. The IR excitation can also increase the selectivity of mass spectrometry, since it allows the separation of species, which have nearly the same mass (isobars). Through their different IR spectra, isotope-isomers can be distinguished in principle, and the application of the technique to $^{13}\text{C}^{12}\text{C}_5\text{HD}_5$ in Section 8.2 provides an example. With these mass- and isotopomer-selective spectroscopic techniques, it is possible to study isotope effects in intramolecular dynamics and energy redistribution (Marquardt and Quack 2001) with isotopomers in mixtures of natural abundance or enriched only to a limited extent.

An application of great physical significance concerns the study of intramolecular primary processes in a variety of isotopomers of polyatomic molecules by means of high-resolution spectroscopy. Here we have summarized some of these results for IVR in CHCl_3 , aniline, and benzene, among others. The study of quasi-adiabatic channel above barrier-tunneling stereomutation in the “large” chiral molecule aniline-NHD provides an exemplary case as this isotopomer can hardly be studied separately by other techniques because of the fast H/D isotope exchange leading always to mixtures with aniline- NH_2 and $-\text{ND}_2$ isotopomers. The demonstration of the mode-selective inhibition of stereomutation by NH-stretching

excitation discussed in Section 7.3 is a most striking result in opposition to some of the classic dogmas of unimolecular rate theory. In considering the power of the presently discussed isotope-selective techniques of OSVADPI, ISOS, and IRSIMS, it may be useful to compare these with other powerful current techniques of high-resolution molecular spectroscopy as summarized in Table 3 (Quack 2003). As measures of spectroscopic power, we use here, firstly, the obvious resolving power $\nu/\delta\nu$, and the effective resolution or instrumental bandwidth $\delta\nu$. Given the present limitations of our pulsed laser light sources, the current implementations of IRSIMS/ISOS perform only moderately well compared to FTIR spectroscopy, midinfrared diode laser spectroscopy, or near-infrared cw-diode laser cavity ring down (CRD) spectroscopy. There is clearly room for improvement in this area and, in the future, powerful cw-optical parametric oscillators may be able to fill this gap and generate resolving powers larger than 10^8 with instrumental resolutions in the megahertz or even sub-megahertz range in combination with Doppler-free methods (Dietiker *et al.* 2010). The scanning range $\Delta\tilde{\nu}$ and scanning power of ISOS/IRSIMS is already excellent today (Table 3). The sensitivity is not to be measured by effective absorption length l , as absorption signals are not measured directly, but rather by an ionization signal. While this detection scheme has the usual disadvantage of lacking information about absolute absorption intensities, it is outstandingly sensitive, which more than compensates for the disadvantage. But clearly the largest advantage in detection is the additional discrimination through the mass selectivity. The combination of the several techniques in Table 3 obviously provides additional possibilities (see articles by Albert *et al.* 2011b: **High-resolution Fourier Transform Infrared Spectroscopy** and by Snels *et al.* 2011: **High-resolution FTIR and Diode Laser Spectroscopy of Supersonic Jets**, in the present handbook). An interesting future development might be the combination of this advantage with the interferometric techniques, thus providing hypothetical mass-selective interferograms

Table 3 Powerful spectroscopic techniques to apply to atmospheric analysis and quantum chemical kinetics^(a).

	$R_P^{(b)}$	$S_P^{(c)}$	$\delta\nu/\text{MHz}^{(d)}$	$\Delta\tilde{\nu}/\text{cm}^{-1(e)}$	$l/\text{m}^{(f)}$
FTIR	$\leq 2 \times 10^6$	$\sim 10^7$	20–70	20 000	100
Diode laser, direct absorption	$\geq 2 \times 10^6$	$< 5 \times 10^4$	20–30	20 (2500)	100
NIR-diode laser, cw-CRD	$\geq 2 \times 10^8$	$< 10^7$	~ 1	500	1000–10 000
ISOS/IR	$\geq 6 \times 10^5$	$\geq 30\,000$ ($\geq 10^6$)	~ 500	500 (20 000)	10^{-3}

^(a)After Quack (2003).

^(b)Resolving power, $R_P = \nu/\delta\nu$.

^(c)Scanning power, $S_P = \Delta\nu/\delta\nu$.

^(d)Effective resolution or instrumental bandwidth, $\delta\nu$.

^(e)Effective scanning range, $\Delta\tilde{\nu}$.

^(f)Effective absorption length, l .

as already proposed some time ago (Quack 1990). This would combine the great scanning power, scanning ranges, and high resolving powers of interferometric FTIR spectroscopy with the additional mass and isotope selectivity. However, the efficient implementation of such an experimental technique is highly nontrivial and very demanding, indeed.

Besides an overview and outlook on possible extensions of the present techniques and their alternatives, we should discuss also some further applications. Beyond the applications concerning molecular spectroscopy and dynamics already discussed in some detail in this article, one can also conceive of mere analytical applications. One could think of ordinary analyses making use just of mass-selected infrared spectra of ordinary chemical mixtures (for instance, in environmental or industrial applications). The application to mixtures of aromatic compounds including polycyclic aromatic hydrocarbons following the lines discussed here for aniline and benzene isotopomers would be straightforward. The isotopomer-selected infrared spectra could also be used in special analyses studying isotope fractionation in natural processes or even in dating with isotopes. Here, infrared molecular spectroscopy would provide the additional dimension to isotope analysis.

Another obvious application of ISOS/IRSIMS is in a preparatory phase of laser isotope separation. Laser isotope separation by molecular infrared multiphoton absorption had been discovered already in 1975–1976 (Ambartsumyan *et al.* 1975, Lyman *et al.* 1975) and is now a well-established technique (Ambartsumyan *et al.* 1975, Lyman *et al.* 1975, Quack 1978, 1989a, 1995a, 1998, Outhouse *et al.* 1985, Lupo and Quack 1987, Letokhov 1987, Fuß *et al.* 1994, Chen *et al.* 1995). Traditionally, spectroscopic techniques have been employed in optimizing the overall process, or else the laser isotope separation is optimized by simple trial of the laser frequencies used with respect to effective separation. ISOS/IRSIMS is obviously ideally suited to test for optimum frequency selection in appropriate laser isotope separation schemes. A particularly useful application of ISOS/IRSIMS would be in planning two-step laser isotope separation schemes (Kowalczyk 2000, Boyarkin *et al.* 2003). As there is now renewed interest in possible medical applications of stable isotopes (Quack 1989a, 1995a, Widmer 1989, Krumbiegel 1991, Fuß *et al.* 1994, de Meer *et al.* 1999), this application might become more important in the future. In a more general context, laser isotope-isomer separation of organic molecules might also become of interest as demonstrated in Groß *et al.* (1998).

A further future application might concern spectroscopic studies of molecules aiming at problems of fundamental physics. In this context, possible spectroscopic investigations of the new isotope effects based on differences

in electroweak charges of isotopes in enantiomeric isotopomers (Sieben *et al.* 2003) discussed in the introduction are obvious applications. ISOS/IRSIMS can be used here for preparatory spectroscopic studies of possible molecular candidates. If combined with appropriate additional experiments, it could also be used to study the effects of the weak nuclear interaction on energy differences of isotopic enantiomers, similar to the case of other enantiomers (Quack 1986, 1989b, 1995b, 2002, Gottselig *et al.* 2004). There is clearly room for many exciting

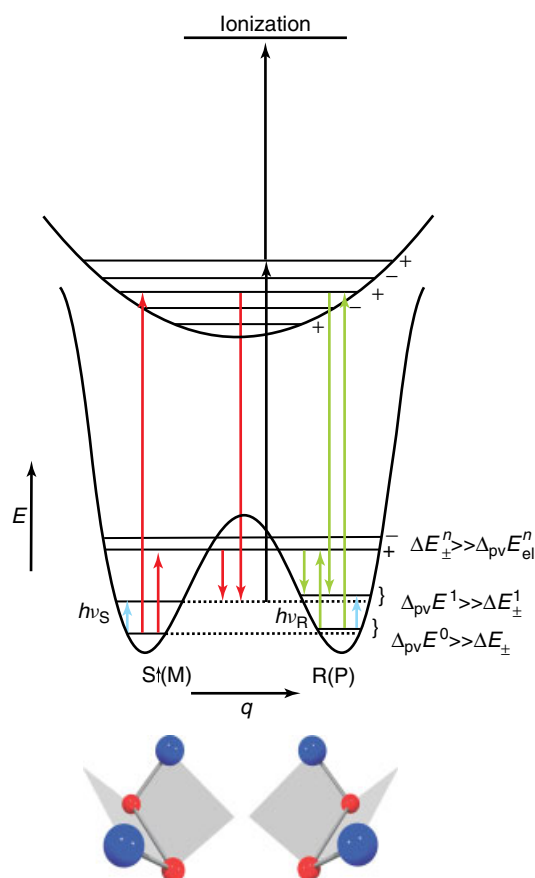


Figure 24 Enantiomers of chiral molecules of the general type X–Y–Y–X and scheme for the experiment to measure $\Delta_{pv}E$ (red arrows for time-dependent experiment) and $\Delta_{pv}v/v$ (blue arrows). The combination of red and green arrows in the scheme leads to a measurement of $\Delta_{pv}E$ in the frequency domain. The excited state of well-defined parity (plus signs) can be in an electronically excited state or in an excited vibrational state as shown (Quack and Willeke 2006). The red arrow in absorption corresponds to a transition between an S and a positive parity level (energy $h\nu_{S+}$). The green arrow in absorption corresponds to a transition between an R and a positive parity level (energy $h\nu_{R+}$). The difference is $(h\nu_{S+} - h\nu_{R+}) = \Delta_{pv}E^0$. The energy difference between the two blue absorption lines within R and S, $(h\nu_S - h\nu_R) = \Delta_{pv}E^1 - \Delta_{pv}E^0$, is the difference of parity-violating energy differences. The black arrows correspond to the detection step in the ISOS scheme.

developments of isotope-selective infrared spectroscopy in the future. In conclusion, we might also note that the detection scheme ISOS/IRSIMS by ionization and mass selection can be also directly used in the experimental scheme for measuring the parity-violating energy difference $\Delta_{\text{pv}}E$ of enantiomers of chiral molecules. This is illustrated in Figure 24. Instead of the initial one-photon infrared excitation, one then has a sequential two-photon absorption/stimulated emission preparation of “parity isomers” of chiral molecules (red arrows) and subsequent probing by UV/VIS excitation and ionization (black arrows). For details of this interesting application, we refer to the article Quack 2011: **Fundamental Symmetries and Symmetry Violations from High-resolution Spectroscopy**, this handbook.

ACKNOWLEDGMENTS

We are grateful to Sieghard Albert, Karen K. Albert, Benjamin Fehrensen, Hans Hollenstein, David Luckhaus, Veronika Horka-Zelenkova, Robert Pfab, Robert Prentner, Jürgen Stohner, and Martin Willeke for help and discussions. Our work is supported financially by the ETH Zürich (including C4 and CSCS), the Schweizerischer Nationalfonds, and had some initial support also from the AGS project (Alliance for Global Sustainability).

ABBREVIATIONS AND ACRONYMS

BBO	β -barium borate
CRD	cavity ring down
FTIR	Fourier transform infrared
FWHM	full width at half maximum
IRLAPS	infrared laser-assisted photofragment spectroscopy
IR-REMPI	infrared resonance enhanced multiphoton ionization
IRSIMS	infrared spectroscopy with isotope and mass selection
ISOS	isotopomer-selective overtone spectroscopy
IVR	intramolecular vibrational redistribution
LIF	laser-induced fluorescence
NMR	nuclear magnetic resonance
OSVADPI	overtone spectroscopy by vibrationally assisted dissociation and photofragment ionization
OPA	optical parametric amplifier
RE2PI	resonantly enhanced two-photon ionization
REMPI	resonantly enhanced multiphoton ionization
SEP	stimulated emission pumping
SRE	stimulated Raman excitation

TOF	time-of-flight
UHV	ultrahigh vacuum
VUV	vacuum ultraviolet

REFERENCES

- Albert, S. and Quack, M. (2007) High resolution rovibrational spectroscopy of chiral and aromatic compounds. *ChemPhysChem*, **8**, 1271–1281.
- Albert, S., Albert, K.K., Hollenstein, H., Tanner, C.M., and Quack, M. (2011a) Fundamentals of rotation–vibration spectra, in *Handbook of High-resolution Spectroscopy*, Quack, M. and Merkt, F. (eds), John Wiley & Sons, Ltd., Chichester, UK.
- Albert, S., Albert, K.K., and Quack, M. (2011b) High resolution fourier transform infrared spectroscopy, in *Handbook of High-resolution Spectroscopy*, Quack, M. and Merkt, F. (eds), John Wiley & Sons, Chichester, UK.
- Ambarsumyan, R.V., Gorokhov, Y.A., Letokhov, V.S., and Makarov, G.N. (1975) Separation of sulfur isotopes with enrichment coefficient $>10^3$ through action of CO₂-laser radiation on SF₆ molecules. *JETP Letters*, **21**(6), 171–172.
- Amirav, A., Even, U., and Jortner, J. (1980) Cooling of large and heavy molecules in seeded supersonic beams. *Chemical Physics*, **51**(1–2), 31–42.
- Amrein, A., Dübal, H.R., and Quack, M. (1985) Multiple anharmonic resonances in the vibrational overtone spectra of CHClF₂. *Molecular Physics*, **56**(3), 727–735.
- Amrein, A., Quack, M., and Schmitt, U. (1988) High-resolution interferometric Fourier transform infrared absorption spectroscopy in supersonic free jet expansions: carbon monoxide, nitric oxide, methane, ethyne, propyne, and trifluoromethane. *Journal of Physical Chemistry*, **92**(19), 5455–5466.
- Andresen, P., Beushausen, V., Häusler, D., Lülfi, H.W., and Rothe, E.W. (1985) Strong propensity rules in the photodissociation of a single rotational quantum state of vibrationally excited H₂O. *Journal of Chemical Physics*, **83**(3), 1429–1430.
- Angus, W.R., Bailey, C.R., Hale, J.B., Ingold, C.K., Leckie, A.H., Raisin, C.G., Thompson, J.W., and Wilson, C.L. (1936) Structure of Benzene. *Journal of Chemical Society London*, 912–987.
- Antonov, V.S. and Letokhov, V.S. (1981) Laser multiphoton and multistep photoionization of molecules and mass spectrometry. *Applied Physics*, **24**, 89–106.
- Arepalli, S., Presser, N., Robie, D., and Gordon, R.J. (1985) Detection of Cl atoms and HCl molecules by resonantly enhanced multiphoton ionization. *Chemical Physics Letters*, **118**(1), 88–92.
- Ayers, J.D., Pomerantz, A.E., Fernandez-Alonso, F., Ausfelder, F., Bean, B.D., and Zare, R.N. (2003) Measurement of the cross section for $\text{H} + \text{D}_2 \rightarrow \text{HD}(v' = 3, j'' = 0) + \text{D}$ as a function of angle and energy. *Journal of Chemical Physics*, **119**(9), 4662–4670.
- Baggott, J.E., Clase, H.J., and Mills, I.M. (1986) Overtone band shapes and IVR: C–H stretch overtones in CHCl₃. *Journal of Chemical Physics*, **84**(8), 4193–4195.

- Bahnmaier, A., Schmid, R., Zhang, B., and Jones, H. (1992) Highly sensitive infrared spectroscopy: IR-REMPI double resonance experiments. *Berichte der Bunsengesellschaft für Physikalische Chemie*, **96**(9), 1305–1308.
- Bakasov, A., Berger, R., Ha, T., and Quack, M. (2004) Ab initio calculation of parity-violating potential energy hypersurfaces of chiral molecules. *International Journal of Quantum Chemistry*, **99**(4), 393–407.
- Bakasov, A., Ha, T.K., and Quack, M. (1996) Ab initio calculation of molecular energies including parity violating interactions, in *Proceedings of the 4th Trieste Conference (1995), Chemical Evolution: Physics of the Origin and Evolution of Life*, Chela-Flores, J. and Raulin, F. (eds), Kluwer Academic Publishers, Dordrecht, pp. 287–296.
- Bakasov, A., Ha, T., and Quack, M. (1998) Ab initio calculation of molecular energies including parity violating interactions. *Journal of Chemical Physics*, **109**(17), 7263–7285.
- Bar, I., Cohen, Y., David, D., Rosenwaks, S., and Valentini, J.J. (1990) Direct observation of preferential bond fission by excitation of a vibrational fundamental: photodissociation of HOD (0,0,1). *Journal of Chemical Physics*, **93**(3), 2146–2148.
- Bauder, A. (2011) Fundamentals of rotational spectra, in *Handbook of High-resolution Spectroscopy*, Quack, M. and Merkt, F. (eds), John Wiley & Sons, Chichester, UK.
- Baumert, T., Helbing, J., Gerber, G., Woste, L., Zewail, A.H., Troe, J., Manz, J., Kobayashi, T., Letokhov, V.S., Even, U. *et al.* (1997) Coherent control with femtosecond laser pulses, in *Chemical Reactions and their control on the Femtosecond Time Scale XXth Solvay conference on chemistry*, Advances in Chemical Physics, Gaspard, P. and Burghardt, I. (eds), John Wiley & Sons, 47–82, vol. 101.
- Bean, B.D., Fernandez-Alonso, F., and Zare, R.N. (2001) Distribution of rovibrational product states for the “Prompt” reaction $H + D_2(v = 0, j = 0 - 4) \rightarrow HD(v' = 1, 2, j') + D$ near 1.6 eV collision energy. *Journal of Physical Chemistry A*, **105**(11), 2228–2233.
- Beil, A., Luckhaus, D., Marquardt, R., and Quack, M. (1994) Intramolecular energy transfer and vibrational redistribution in chiral molecules: experiment and theory. *Faraday Discussions*, **99**(99), 49–76.
- Beil, A., Luckhaus, D., and Quack, M. (1996) Fermi resonance structure and femtosecond quantum dynamics of a chiral molecule from the analysis of vibrational overtone spectra of CHBrClF. *Berichte der Bunsengesellschaft für Physikalische Chemie*, **100**(11), 1853–1875.
- Beil, A., Luckhaus, D., Quack, M., and Stohner, J. (1997) Intramolecular vibrational redistribution and unimolecular reaction: Concepts and new results on the femtosecond dynamics and statistics in CHBrClF. *Berichte der Bunsengesellschaft für Physikalische Chemie*, **101**(3), 311–328.
- Bell, R.P. (1980) *The Tunnel Effect in Chemistry*, University Press, Cambridge.
- Berger, R., Laubender, G., Quack, M., Sieben, A., Stohner, J., and Willeke, M. (2005) Isotopic chirality and molecular parity violation. *Angewandte Chemie (International ed. in English)*, **44**(23), 3623–3626.
- Berger, R. and Quack, M. (2000) Multiconfiguration linear response approach to the calculation of parity violating potentials in polyatomic molecules. *Journal of Chemical Physics*, **112**(7), 3148–3158.
- Bespalov, V.G., Krylov, V.N., Mikhailov, V.N., Parfenov, V.A., and Staselko, D.I. (1991) Generating tunable radiation with high spectral luminescence based on vibrational and rotational stimulated Raman scattering in gases. *Optics and Spectroscopy*, **70**(2), 193–196.
- Beyer, T. and Swinehart, D.F. (1973) Number of multiply-restricted partitions. *Communications of the ACM*, **16**, 379–385.
- Bigeleisen, J. (2006) Theoretical basis of isotope effects from an autobiographical perspective, chapter 1, in *Isotope Effects in Chemistry and Biology*, Kohen, A., Limbach, H.-H. (eds), Taylor & Francis, Boca Raton, FL, pp. 1–40.
- Bischel, W.K. and Dyer, M.J. (1986) Wavelength dependence of the absolute Raman gain coefficient for the Q (1) transition in H₂. *Journal of the Optical Society of America*, **3**(5), 677–682.
- Bixon, M. and Jortner, J. (1968) Intramolecular radiationless transitions. *Journal of Chemical Physics*, **48**(2), 715–726.
- Bludský, O., Šponer, J., Leszczynski, J., Špirko, V., and Hobza, P. (1996) Amino groups in nucleic acid bases, aniline, aminopyridines, and aminotriazine are nonplanar: results of correlated ab initio quantum chemical calculations and anharmonic analysis of the aniline inversion motion. *Journal of Chemical Physics*, **105**(24), 11042–11050.
- Boesl, U. (1991) Multiphoton excitation and mass-selective ion detection for neutral and ion spectroscopy. *Journal of Physical Chemistry*, **95**, 2949–2962.
- Boesl, U., Neusser, H.J., and Schlag, E.W. (1980) Visible and UV multiphoton ionization and fragmentation of polyatomic molecules. *Journal of Chemical Physics*, **72**(8), 4327–4333.
- Boesl, U., Neusser, H.J., and Schlag, E.W. (1981) Multi-photon ionization in the mass spectrometry of polyatomic molecules: Cross sections. *Chemical Physics*, **55**(2), 193–204.
- Boesl, U., Weinkauff, R., and Schlag, E.W. (1992) Reflectron time-of-flight mass spectrometry and laser excitation for the analysis of neutrals, ionized molecules and secondary fragments. *International Journal of Mass Spectrometry and Ion Processes*, **112**(2–3), 121–166.
- Boyarkin, O.V., Kowalczyk, M., and Rizzo, T.R. (2003) Collisionally enhanced isotopic selectivity in multiphoton dissociation of vibrationally excited CF₃H. *Journal of Chemical Physics*, **118**(1), 93–103.
- Boyarkin, O.V., Lubich, L., Settle, R.D.F., Perry, D.S., and Rizzo, T.R. (1997) Intramolecular energy transfer in highly vibrationally excited methanol. I. Ultrafast dynamics. *Journal of Chemical Physics*, **107**(20), 8409–8422.
- Boyarkin, O.V. and Rizzo, T.R. (1995) Rotational state selected vibrational overtone spectroscopy of jet-cooled molecules. *Journal of Chemical Physics*, **103**(5), 1985–1988.
- Boyarkin, O.V. and Rizzo, T.R. (1996) Secondary time scales of intramolecular vibrational energy redistribution in CF₃H studied by vibrational overtone spectroscopy. *Journal of Chemical Physics*, **105**(15), 6285–6292.
- Boyarkin, O.V., Rizzo, T.R., and Perry, D.S. (1999) Intramolecular energy transfer in highly vibrationally excited methanol. II.

- Multiple time scales of energy redistribution. *Journal of Chemical Physics*, **110**(23), 11346–11358.
- Boyarkin, O., Rizzo, T., Rueda, D., Quack, M., and Seyfang, G. (2002) Nonlinear intensity dependence in the infrared multiphoton excitation and dissociation of methanol pre-excited to different energies. *Journal of Chemical Physics*, **117**(21), 9793–9805.
- Brand, J.C.D., Williams, D.R., and Cook, T.J. (1966) Vibrational analysis of the first ultraviolet band system of aniline. *Journal of Molecular Spectroscopy*, **20**(4), 359–380.
- Bray, R.G. and Berry, M.J. (1979) Intramolecular rate processes in highly vibrationally excited benzene. *Journal of Chemical Physics*, **71**(12), 4909–4922.
- Brodersen, S. and Langseth, A. (1959) The fundamental frequencies of all the deuterated benzenes. *Matematisk-fysiske Skrifter udgivet af Det Kongelige Danske Videnskabernes Selskab*, **1**, 1–36.
- Brodersen, S., Christoffersen, J., Bak, B., and Nielsen, J.T. (1965) The infrared spectrum of mono-¹³C-substituted benzene. *Spectrochimica Acta*, **21**(12), 2077–2084.
- Bronner, W., Oesterlin, P., and Schellhorn, M. (1984) Ion-Dip Raman spectroscopy: a method to measure Raman spectra at $4 \cdot 10^{-9}$ bar. *Applied Physics B*, **34**, 11–15.
- Brouard, M., Martinez, M.T., O'Mahony, J., and Simons, J.P. (1988) Photofragment vector correlations in the vibrationally mediated photodissociation of H₂O₂. *Chemical Physics Letters*, **150**(1–2), 6–12.
- Brown, S.S., Berghout, H.L., and Crim, F.F. (1997) Raman spectroscopy of the ν_1 N–H stretch fundamental in isocyanic acid (HNCO): State mixing probed by photoacoustic spectroscopy and by photodissociation of vibrationally excited states. *Journal of Chemical Physics*, **106**(14), 5805–5815.
- Busker, M., Svartsov, Y.N., Häber, T., and Kleinermaans, K. (2009) IR-UV double resonance spectra of pyrazine dimers: competition between CH $\cdots\pi$, $\pi\cdots\pi$ and CH \cdots N interactions. *Chemical Physics Letters*, **467**(4–6), 255–259.
- Butler, L.J., Ticich, T.M., Likar, M.D., and Crim, F.F. (1986) Vibrational overtone spectroscopy of bound and predissociative states of hydrogen peroxide cooled in a supersonic expansion. *Journal of Chemical Physics*, **85**(4), 2331–2332.
- Callegari, A., Merker, U., Engels, P., Srivastava, H.K., Lehmann, K.K., and Scoles, G. (2000) Intramolecular vibrational redistribution in aromatic molecules. I. Eigenstate resolved CH stretch first overtone spectra of benzene. *Journal of Chemical Physics*, **113**(23), 10583–10596.
- Callegari, A., Merker, U., Engels, P., Srivastava, H.K., Lehmann, K.K., and Scoles, G. (2001) Erratum: “Intramolecular vibrational redistribution in aromatic molecules. I. Eigenstate resolved CH stretch first overtone spectra of benzene” [*Journal of Chemical Physics* **113**, 10583 (2000)]. *Journal of Chemical Physics*, **114**(7), 3344–3344.
- Callegari, A., Rebstein, J., Jost, R., and Rizzo, T.R. (1999) State-to-state unimolecular reaction dynamics of HOCl near the dissociation threshold: The role of vibrations, rotations, and IVR probed by time- and eigenstate-resolved spectroscopy. *Journal of Chemical Physics*, **111**(16), 7359–7368.
- Callegari, A., Srivastava, H.K., Merker, U., Lehmann, K.K., Scoles, G., and Davis, M.J. (1997) Eigenstate resolved infrared–infrared double-resonance study of intramolecular vibrational relaxation in benzene: first overtone of the CH stretch. *Journal of Chemical Physics*, **106**(1), 432–435.
- Carrington, T., Halonen, L., and Quack, M. (1987) Fermi resonance in CHX₃: a hamiltonian in symmetrized curvilinear internal coordinates. *Chemical Physics Letters*, **140**(5), 512–519.
- Chadwick, B.L. and Orr, B.J. (1992) Raman-ultraviolet double resonance in acetylene: rovibrational state preparation and spectroscopy. *Journal of Chemical Physics*, **97**(5), 3007–3020.
- Chen, G.C., Wu, B., Liu, J.L., Jing, Y., Chu, M.X., Xue, L.L., and Ma, P.H. (1995) Scaling-up ¹³C separation by infrared multiphoton dissociation of the CHClF₂/Br₂ system. *Applied Physics B*, **60**, 583–588.
- Cho, S.H., Huh, H., Kim, H.M., Kim, N.J., and Kim, S.K. (2005) Infrared-visible and visible-visible double resonance spectroscopy of 1-hydroxy-9,10-anthraquinone-(H₂O)_n ($n = 1, 2$) complexes. *Journal of Chemical Physics*, **122**(3), 034305.
- Chowdhury, P.K. (2006) Infrared depletion spectroscopy of the doubly hydrogen-bonded aniline-(tetrahydrofuran)₂ complex produced in supersonic jet. *Chemical Physics*, **320**(2–3), 133–139.
- Christoffersen, J., Hollas, J.M., and Kirby, G.H. (1969) Rotational band contours in the 2938 Å electronic system of aniline. *Molecular Physics*, **16**(5), 441–452.
- Cohen, E., Cvitaš, T., Frey, J., Holmström, B., Kuchitsu, K., Marquardt, R., Mills, I., Pavese, F., Quack, M., Stohner, J., et al. (2007) *Quantities, Units and Symbols in Physical Chemistry*, 3rd edition, IUPAC, RSC Publishing, Cambridge.
- Crane, J.C., Nam, H., Clauberg, H., Beal, H.P., Kalinowski, I.J., Shu, R.G., and Moore, C.B. (1998) Stimulated emission pumping spectra and intramolecular vibrational dynamics of DF₂(S₀) from 9000 to 20000 cm⁻¹. *Journal of Physical Chemistry A*, **102**, 9433–9444.
- Crim, F.F. (1993) Vibrationally mediated photodissociation: exploring excited-state surfaces and controlling decomposition pathways. *Annual Review of Physical Chemistry*, **44**, 397–428.
- Darling, B.T. and Dennison, D.M. (1940) The water vapor molecule. *Physical Review*, **57**(2), 128–139.
- Demtröder, W. (1981) *Laser Spectroscopy: Basic Concepts and Instrumentation*. Springer Series in Chemical Physics, Springer, Berlin. Vol. 5.
- Dietiker, P., Quack, M., Schneider, A., Seyfang, G., and Unlu, F. (2010) Cavity enhanced saturation spectroscopy of NH₃ in the near infrared, in *Proceedings of the 17th SASP 2010*, Milewski, I., Kendl, A. and Scheier, P. (eds), Innsbruck University Press (IUP), Innsbruck, pp. 161–164.
- Donaldson, P.M., Guo, R., Fournier, F., Gardner, E.M., Barter, L.M.C., Barnett, C.J., Gould, I.R., Klug, D.R., Palmer, D.J., and Willison, K.R. (2007) Direct identification and decongestion of Fermi resonances by control of pulse time ordering in two-dimensional IR spectroscopy. *Journal of Chemical Physics*, **127**(11), 114513.
- Dübal, H.R., Ha, T., Lewerenz, M., and Quack, M. (1989) Vibrational spectrum, dipole moment function, and potential energy surface of the CH chromophore in CHX₃ molecules. *Journal of Chemical Physics*, **91**(11), 6698–6713.

- Dübal, H.R. and Quack, M. (1980) Spectral bandshape and intensity of the C–H chromophore in the infrared spectra of CF₃H and C₄F₉H. *Chemical Physics Letters*, **72**(2), 342–347.
- Dübal, H.R. and Quack, M. (1981) High-resolution IR spectrum of fluoroform: a close resonance. *Chemical Physics Letters*, **80**(3), 439–444.
- Dübal, H.R. and Quack, M. (1984) Tridiagonal Fermi resonance structure in the IR spectrum of the excited CH chromophore in CF₃H. *Journal of Chemical Physics*, **81**(9), 3779–3791.
- Duncan, M.A. (2000) Frontiers in the spectroscopy of mass-selected molecular ions. *International Journal of Mass Spectrometry*, **200**(1–3), 545–569.
- Duncan, J.L. and Law, M.M. (1990) A study of vibrational anharmonicity, Fermi resonance interactions, and local mode behavior in CH₃Cl. *Journal of Molecular Spectroscopy*, **140**(1), 13–30.
- Duncan, M.D., Mahon, R., Tankersley, L.L., and Reintjes, J. (1991) Second Stokes generation in deuterium and hydrogen. *Optics Communications*, **86**(6), 538–546.
- Duperrex, R. and van den Bergh, H. (1979) Time resolved measurement of CF₂ formation in the infrared multiphoton dissociation of CF₂HCl. *Journal of Chemical Physics*, **71**(9), 3613–3619.
- Ebata, T., Fujii, A., and Mikami, N. (1998) Vibrational spectroscopy of small-sized hydrogen-bonded clusters and their ions. *International Reviews in Physical Chemistry*, **17**, 331–361.
- Ernst, R.R. (1992) Nuclear magnetic resonance fourier transform spectroscopy (Nobel Lecture). *Angewandte Chemie (International ed. in English)*, **31**(7), 805–823.
- Ernst, R.R., Bodenhausen, G., and Wokaun, A. (1997) *Principles of Nuclear Magnetic Resonance in One and Two Dimensions*, Clarendon Press, Oxford.
- Esherick, P. and Owyong, A. (1983) Ionization-detected stimulated Raman spectroscopy. *Chemical Physics Letters*, **103**(3), 235–240.
- Fehrensen, B., Hippler, M., and Quack, M. (1998) Isotopomer-selective overtone spectroscopy by ionization detected IR+UV double resonance of jet-cooled aniline. *Chemical Physics Letters*, **298**(4–6), 320–328.
- Fehrensen, B., Luckhaus, D., and Quack, M. (1999a) Inversion tunneling in aniline from high resolution infrared spectroscopy and an adiabatic reaction path Hamiltonian approach. *Zeitschrift für Physikalische Chemie*, **209**, 1–19.
- Fehrensen, B., Luckhaus, D., and Quack, M. (1999b) Mode selective stereomutation tunnelling in hydrogen peroxide isotopomers. *Chemical Physics Letters*, **300**(3–4), 312–320.
- Fehrensen, B., Luckhaus, D., and Quack, M. (2007) Stereomutation dynamics in hydrogen peroxide. *Chemical Physics*, **338**, 90–105.
- Fermi, E. (1931) Über den Ramaneffekt des Kohlendioxyds. *Zeitschrift für Physiotherapie*, **71**, 250–259.
- Fernandez-Alonso, F., Bean, B.D., Ayers, J.D., Pomerantz, A.E., Zare, R.N., Baares, L., and Aoiz, J. (2000) Evidence for scattering resonances in the H+D₂ reaction. *Angewandte Chemie (International ed. in English)*, **39**(15), 2748–2752.
- Frey, J.A., Müller, A., Frey, H.-M., and Leutwyler, S. (2004) Infrared depletion spectra of 2-aminopyridine · 2-pyridone, a Watson - Crick mimic of adenine · uracil. *Journal of Chemical Physics*, **121**(17), 8237–8245.
- Frisch, M.J., Trucks, G.W., Schlegel, H.B., Gill, P.M.V., Johnson, B.G., Robb, M.A., Cheeseman, J.R., Keith, T., Petersson, G.A., Montgomery, J.A. et al. (1995) GAUSSIAN 94, Gaussian Inc., Pittsburgh.
- Frost, R.K., Hagemester, F.C., Arrington, C.A., Zwier, T.S., and Jordan, K.D. (1996) Fluorescence-dip infrared spectroscopy of tropolone and tropolone-OD. *Journal of Chemical Physics*, **105**(7), 2595–2604.
- Fujii, A., Fujimaki, E., Ebata, T., and Mikami, N. (2000) Infrared spectroscopy of CH stretching vibrations of jet-cooled alkylbenzene cations by using the “messenger” technique. *Journal of Chemical Physics*, **112**(14), 6275–6284.
- Fujimaki, E., Matsumoto, Y., Fujii, A., Ebata, T., and Mikami, N. (2000) Autoionization-detected infrared spectroscopy of jet-cooled naphthol cations. *Journal of Physical Chemistry A*, **104**(31), 7227–7232.
- Fuß, W., Gothel, J., Ivanenko, M., Schmid, W.E., Hering, P., Kompa, K.L., and Witte, K. (1994) Macroscopic isotope-separation of C-13 by a CO₂-laser. *Isotopenpraxis*, **30**, 199–203.
- Fuß, W. and Weizbauer, S. (1995) Anharmonische Konstanten von SiHCl₃ und CHCl₃. *Berichte der Bunsengesellschaft für Physikalische Chemie*, **99**(3), 289–295.
- Gauss, J. and Stanton, J.F. (2000) The equilibrium structure of benzene. *Journal of Physical Chemistry A*, **104**, 2865–2868.
- Gentry, W.R. (1988) Low-energy pulsed beam sources, in *Atomic and Molecular Beam Methods*, Scoles, G. (ed), Oxford University Press, New York, Chapter 3. Vol. I.
- Gerber, R.B., McCoy, A.B., and Garcia-Vela, A. (1995) Dynamics of photoinduced reactions in the van der Waals and in the hydrogen-bonded clusters, in *Femtosecond Chemistry, Proceedings of the Berlin Conference on Femtosecond Chemistry (Berlin, March 1993)*, Manz, J. and Woeste, L. (eds), Verlag Chemie, Weinheim, pp. 499–531.
- Gerhards, M., Jansen, A., Unterberg, C., and Gerlach, A. (2005) Structures and rearrangement reactions of 4-aminophenol(H₂O)₁⁺ and 3-aminophenol(H₂O)₁⁺ clusters. *Journal of Chemical Physics*, **123**(7), 074320.
- Gerhards, M. and Unterberg, C. (2001) IR double-resonance spectroscopy applied to the 4-aminophenol(H₂O)₁ cluster. *Applied Physics A: Materials Science & Processing*, **72**(3), 273–279.
- Gohl, W., Kutscher, R., Laue, H.J., and Wollnik, H. (1983) Time-of-flight mass spectrometry for ions of large energy spread. *International Journal of Mass Spectrometry and Ion Processes*, **48**, 411–414.
- Gottselig, M., Quack, M., Stohner, J., and Willeke, M. (2004) Mode-selective stereomutation tunneling and parity violation in HOClH⁺ and H₂Te₂ isotopomers. *International Journal of Mass Spectrometry*, **233**(1–3), 373–384.
- Groß, H., Grassi, G., and Quack, M. (1998) The synthesis of [2-²H₁]Thiirane-1-oxide and [2,2-²H₂]Thiirane-1-oxide and the diastereoselective infrared laser chemistry of [2-²H₁]Thiirane-1-oxide. *Chemistry. A European Journal*, **4**(3), 441–448.
- Gruebele, M. and Bigwood, R. (1998) Molecular vibrational energy flow: beyond the Golden Rule. *International Reviews in Physical Chemistry*, **17**, 91–145.

- Ha, T., Lewerenz, M., Marquardt, R., and Quack, M. (1990) Overtone intensities and dipole moment surfaces for the isolated CH chromophore in CHD₃ and CHF₃: experiment and ab initio theory. *Journal of Chemical Physics*, **93**(10), 7097–7109.
- Hager, J., Smith, M.A., and Wallace, S.C. (1985) Autoionizing Rydberg structure observed in the vibrationally selective, two-color, threshold photoionization spectrum of jet-cooled aniline. *Journal of Chemical Physics*, **83**(9), 4820–4822.
- Halonen, L. (1982) Local mode vibrations in benzene. *Chemical Physics Letters*, **87**(3), 221–225.
- Halonen, L. (1988) Analysis of Fermi resonances in CH₂Cl₂ and CD₂Cl₂ using an internal coordinate Hamiltonian. *Journal of Chemical Physics*, **88**(12), 7599–7602.
- Halonen, L., Carrington, T., and Quack, M. (1988) Investigation of Fermi resonances in CHX₃ molecules with an internal-coordinate Hamiltonian. *Journal of Chemical Society, Faraday Transactions 2*, **84**, 1371–1388.
- Hamilton, C.E., Kinsey, J.L., and Field, R.W. (1986) Stimulated emission pumping: new methods in spectroscopy and molecular dynamics. *Annual Review of Physical Chemistry*, **37**, 493–524.
- Hayward, R.J., Henry, B.R., and Siebrand, W. (1973) Anharmonicity in polyatomic molecules: the problem of phase coincidence and applications to the CH-stretching overtone spectrum of benzene. *Journal of Molecular Spectroscopy*, **46**(2), 207–213.
- von Helden, G., Holleman, I., Knippels, G.M.H., van der Meer, A.F.G., and Meijer, G. (1997) Infrared resonance enhanced multiphoton ionization of fullerenes. *Physical Review Letters*, **79**(26), 5234–5237.
- von Helden, G., Holleman, I., Putter, M., van Roij, A.J.A., and Meijer, G. (1999) Infrared resonance enhanced multi-photon ionization spectroscopy of C₈₄. *Chemical Physics Letters*, **299**(2), 171–176.
- Henry, B.R. and Siebrand, W. (1968) Anharmonicity in polyatomic molecules. The CH-stretching overtone spectrum of Benzene. *Journal of Chemical Physics*, **49**(12), 5369–5376.
- Henson, B.F., Hartland, G.V., Venturo, V.A., and Felker, P.M. (1992) Raman-vibronic double-resonance spectroscopy of benzene dimer isotopomers. *Journal of Chemical Physics*, **97**(4), 2189–2208.
- Herman, M., Liévin, J., Vander, A.J., and Campargue, A. (eds.) (1999) Global and accurate vibration Hamiltonians from high-resolution molecular spectroscopy, in *Advances in Chemical Physics 108*, Wiley, New York.
- Herzberg, G. (1945) *Molecular Spectra and Molecular Structure. Vol. II. Infrared and Raman Spectra of Polyatomic Molecules*, Van Nostrand Reinhold Company Inc., New York, Cincinnati, Toronto, London and Melbourne.
- Herzberg, G. (1950) *Molecular Spectra and Molecular Structure. Vol. I. Spectra of Diatomic Molecules*, Van Nostrand Reinhold Company Inc., New York, Cincinnati, Toronto, London and Melbourne.
- Herzberg, G. (1966) *Molecular Spectra and Molecular Structure. Vol. III. Electronic Spectra of Polyatomic Molecules*, Van Nostrand Reinhold Company Inc., New York, Cincinnati, Toronto, London and Melbourne.
- Hippler, M. (1993) *Ultraviolet Laser Spectroscopy of Nitric Oxide: Analytical and Dynamical Applications*, Ph.D. Thesis, Heriot-Watt University, Edinburgh.
- Hippler, M. (2001) *New Experimental Techniques for the Infrared Spectroscopy of Molecules in the Gas Phase*, Habilitation thesis, ETH Zürich.
- Hippler, M. and Pfab, J. (1995) Detection and probing of nitric oxide (NO) by two-colour laser photoionisation (REMPI) spectroscopy on the A ← X transition. *Chemical Physics Letters*, **243**(5–6), 500–505.
- Hippler, M. and Quack, M. (1994) Overtone spectroscopy by vibrationally assisted dissociation and photofragment ionization. *Chemical Physics Letters*, **231**(1), 75–80.
- Hippler, M. and Quack, M. (1995) Overtone spectroscopy of Chloroform in a supersonic jet by vibrationally assisted dissociation and photofragment ionization. *Berichte der Bunsengesellschaft für Physikalische Chemie*, **99**(3), 417–421.
- Hippler, M. and Quack, M. (1996) Isotope selective overtone spectroscopy of CHCl₃ by vibrationally assisted dissociation and photofragment ionization. *Journal of Chemical Physics*, **104**(19), 7426–7430.
- Hippler, M. and Quack, M. (1997) Intramolecular energy transfer from isotope selective overtone spectroscopy by vibrationally assisted dissociation and photofragment ionization. *Berichte der Bunsengesellschaft für Physikalische Chemie*, **101**(3), 356–362.
- Hippler, M. and Quack, M. (2006) Isotope selective infrared spectroscopy and intramolecular dynamics, in *Isotope Effects in Chemistry and Biology*, Kohen, A., Limbach, H.-H. (eds), Taylor & Francis, Boca Raton, FL, pp. 305–359. Chapter 11.
- Hippler, M., Pfab, R., and Quack, M. (2003) Isotopomer-selective overtone spectroscopy of jet-cooled Benzene by ionization detected IR + UV double resonance: the N = 2 CH chromophore absorption of ¹²C₆H₆ and ¹³C¹²C₅H₆ near 6000 cm⁻¹. *Journal of Physical Chemistry A*, **107**(49), 10743–10752.
- Hippler, M., Quack, M., Schwarz, R., Seyfang, G., Matt, S., and Mark, T. (1997) Infrared multiphoton excitation, dissociation and ionization of C₆₀. *Chemical Physics Letters*, **278**(1–3), 111–120.
- Holland, J.K., Lawrance, W.D., and Mills, I.M. (1992) Perturbations in the infrared spectrum of monofluoroacetylene, and their relationship to intramolecular vibrational energy redistribution. *Journal of Molecular Spectroscopy*, **151**(2), 369–377.
- Hollas, J.M. (1982) *High Resolution Spectroscopy*, Butterworths, London.
- Hollas, J.M., Howson, M.R., Ridley, T., and Halonen, L. (1983) The NH₂-inversion potential function in the \tilde{A}^1B_2 electronic state of aniline: evidence for planarity. *Chemical Physics Letters*, **98**(6), 611–614.
- Hollenstein, H., Lewerenz, M., and Quack, M. (1990a) Isotope effects in the Fermi resonance of the CH chromophore in CHX₃ molecules. *Chemical Physics Letters*, **165**(2–3), 175–183.
- Hollenstein, H., Luckhaus, D., and Quack, M. (1993) Dynamics of the CH chromophore in CHX₃: a combined treatment for a set of isotopic species. *Journal of Molecular Structure*, **294**, 65–70.
- Hollenstein, H., Piccirillo, S., Quack, M., and Snels, M. (1990b) High-resolution infrared spectrum and analysis of the ν_{11} ,

- $A_{2u}(B_2)$ fundamental band of $^{12}C_6H_6$ and $^{13}C_{12}C_5H$. *Molecular Physics*, **71**(4), 759–768.
- Hollenstein, H., Quack, M., and Richard, E. (1994) Slit jet diode laser and FTIR spectroscopy of CF_3I and improved analysis of the symmetric CF_3 stretching chromophore absorption. *Chemical Physics Letters*, **222**(1–2), 176–184.
- Hollenstein, U., Seiler, R., Osterwalder, A., Wüest, M.S.A., Rupper, P., Willitsch, S., Greetham, G.M., and Merkt, B.B.-G.F. (2001) High-resolution vacuum ultraviolet photoelectron spectroscopy. *Chimia*, **55**, 759–762.
- Howard, D.L., Robinson, T.W., Fraser, A.E., and Kjaergaard, H.G. (2004) The effect of NH_2 -inversion tunneling splitting on the NH -stretching overtone spectra of aniline vapour. *Physical Chemistry Chemical Physics*, **6**, 719–724.
- Hubrich, C. and Stuhl, F. (1980) The ultraviolet absorption of some halogenated methanes and ethanes of atmospheric interest. *Journal of Photochemistry*, **12**(2), 93–107.
- Iachello, F. and Oss, S. (1992) Vibrational modes of polyatomic molecules in the vibron model. *Journal of Molecular Spectroscopy*, **153**(1–2), 225–239.
- Ishiyuchi, S., Shitomi, H., Takazawa, K., and Fujii, M. (1998) Nonresonant ionization detected IR spectrum of jet-cooled phenol. Ionization mechanism and its application to overtone spectroscopy. *Chemical Physics Letters*, **283**(3–4), 243–250.
- Lung, C. and Wyatt, R.E. (1993) Time-dependent quantum mechanical study of intramolecular vibrational energy redistribution in benzene. *Journal of Chemical Physics*, **99**(3), 2261–2264.
- Jiang, J.C. and Lin, C.E. (1997) Ab initio study of the ground and first excited singlet states of aniline. *Journal of Molecular Structure: THEOCHEM*, **392**, 181–191.
- Jones, H. (1979) Infrared-microwave double resonance techniques, in *Modern Aspects of Microwave Spectroscopy*, Chantry, G.W. (ed), Academic Press, London, pp. 123–216. Chapter 3.
- Jungen, C. and Raoult, M. (1981) Spectroscopy in the ionisation continuum: vibrational preionisation in H_2 calculated by multichannel quantum-defect theory. *Faraday Discussions of the Chemical Society*, **71**, 253–271.
- Karataev, V.I., Mamyry, B.A., and Shmikk, D.V. (1972) New method for focusing ion bunches in time-of-flight mass spectrometers. *Soviet Physics-Technical Physics*, **16**, 1177–1179.
- Kleibömer, B. and Sutter, D.H. (1988) The vibrational state dependence of the ^{14}N quadrupole coupling tensor in aniline. A microwave Fourier-transform study combined with semi-rigid bender calculations. *Zeitschrift für Naturforschung*, **43a**, 561–571.
- Klopper, W., Quack, M., and Suhm, M. (1998) HF dimer: Empirically refined analytical potential energy and dipole hypersurfaces from ab initio calculations. *Journal of Chemical Physics*, **108**(24), 10096–10115.
- Kohen, A. and Limbach, H.-H. (eds) (2006) *Isotope Effects in Chemistry and Biology*, Taylor & Francis, Boca Raton, FL.
- Kowalczyk, M. (2000) *Highly Selective Molecular Laser Isotope Separation of Carbon-13*, Ph.D. thesis, EPF Lausanne.
- Krumbiegel, P. (1991) *Stable Isotope Pharmaceuticals: for Clinical Research and Diagnosis*, Gustav Fischer Verlag, Jena, Stuttgart, New York.
- Kuhn, B., Rizzo, T., Luckhaus, D., Quack, M., and Suhm, M. (1999) A new six-dimensional analytical potential up to chemically significant energies for the electronic ground state of hydrogen peroxide. *Journal of Chemical Physics*, **111**(6), 2565–2587.
- Kydd, R.A. and Krueger, P.J. (1977) The far-infrared vapour phase spectra of aniline- ND_2 and aniline-NHD. *Chemical Physics Letters*, **49**(3), 539–543.
- Larsen, N.W., Hansen, E.L., and Nicolaisen, F.M. (1976) Far infrared investigation of aniline and 4-fluoroaniline in the vapour phase. Inversion and torsion of the amino group. *Chemical Physics Letters*, **43**(3), 584–586.
- Lehmann, K.K., Scoles, G., and Pate, B.H. (1994) Intramolecular dynamics from eigenstate-resolved infrared spectra. *Annual Review of Physical Chemistry*, **45**, 241–274.
- Letokhov, V.S. (1987) *Laser Photoionization Spectroscopy*, Academic Press, Orlando. Chapter 3.1.
- Leutwyler, S. and Even, U. (1981) Isotopically selective two-photon ionization of aniline in supersonic beams. *Chemical Physics Letters*, **81**(3), 578–581.
- Lewerenz, M. and Quack, M. (1986) Vibrational overtone intensities of the isolated CH and CD chromophores in fluoroform and chloroform. *Chemical Physics Letters*, **123**(3), 197–202.
- Lewerenz, M. and Quack, M. (1988) Vibrational spectrum and potential energy surface of the CH chromophore in CHD_3 . *Journal of Chemical Physics*, **88**(9), 5408–5432.
- Lias, S., Bartmess, J.E., Liebman, J.F., Holmes, J.L., Levin, R.D., and Mallard, W.G. (1988) *Ion Energetics Data, NIST Chemistry WebBook, NIST Standard Reference Database 69*, National Institute of Standards and Technology, Gaithersburg. (<http://webbook.nist.gov>).
- Limbach, H.H. (1990) Dynamic NMR spectroscopy in the presence of kinetic hydrogen/deuterium isotope effects, in *NMR Basic Principles and Progress*, Diehl, P., Fluck, E., Gunther, H., Kosteld, R., and Seelig, J. (eds), Springer-Verlag, Berlin, Heidelberg. Vol. 23.
- Limbach, H.H., Denisov, G.S., and Golubev, N.S. (2006) Hydrogen bond isotope effects studied by NMR, in *Isotope Effects in Chemistry and Biology*, Kohen, A., Limbach, H.-H. (eds), Taylor & Francis, Boca Raton, FL, pp. 193–230. Chapter 7.
- Longuet-Higgins, H.C. (1963) The symmetry groups of non-rigid molecules. *Molecular Physics*, **6**, 445–460.
- Lopez-Tocon, I., Valle, R.G.D., Becucci, M., Castellucci, E., and Otero, J.C. (2000) NH_2 inversion potential in the S_0 and S_1 electronic states of aniline: fit to the (ro-)vibrational data and comparison with ab initio and density functional results. *Chemical Physics Letters*, **327**(1–2), 45–53.
- Lu, D.H. and Hase, W.L. (1988) Classical trajectory calculation of the benzene overtone spectra. *Journal of Physical Chemistry*, **92**, 3217–3225.
- Lubich, L., Boyarkin, O.V., Settle, R.D.F., Perry, D.S., and Rizzo, T.R. (1995) Multiple timescales in the intramolecular vibrational energy redistribution of highly excited methanol. *Faraday Discussions*, **102**, 167–178.
- Luckhaus, D. (1997) The rovibrational spectrum of hydroxylamine: a combined high resolution experimental and theoretical study. *Journal of Chemical Physics*, **106**(20), 8409–8426.

- Luckhaus, D. (2000) 6D Vibrational quantum dynamics: generalized coordinate discrete variable representation and (a) diabatic contraction. *Journal of Chemical Physics*, **113**(4), 1329–1347.
- Luckhaus, D. and Quack, M. (1992) Spectrum and dynamics of the CH chromophore in CD₂HF. I. Vibrational Hamiltonian and analysis of rovibrational spectra. *Chemical Physics Letters*, **190**(6), 581–589.
- Luckhaus, D., Quack, M., and Stohner, J. (1993) Femtosecond quantum structure, equilibration and time reversal for the CH-chromophore dynamics in CHD₂F. *Chemical Physics Letters*, **212**(5), 434–443.
- Luo, X., Fleming, P.R., and Rizzo, T.R. (1992) Vibrational overtone spectroscopy of the $4\nu_{OH} + \nu_{OH'}$ combination level of HOOH via sequential local mode–local mode excitation. *Journal of Chemical Physics*, **96**(8), 5659–5667.
- Luo, X. and Rizzo, T.R. (1990) Rotationally resolved vibrational overtone spectroscopy of hydrogen peroxide at chemically significant energies. *Journal of Chemical Physics*, **93**(12), 8620–8633.
- Lupo, D. and Quack, M. (1987) IR-laser photochemistry. *Chemical Reviews*, **87**(1), 181–216.
- Lyman, J.L., Jensen, R.J., Rink, J., Robinson, C.P., and Rockwood, S.D. (1975) Isotopic enrichment of SF₆ in S³⁴ by multiple absorption of CO₂ laser radiation. *Applied Physics Letters*, **27**(2), 87–89.
- Mahjoub, A., Chakraborty, A., Lepere, V., Barbu-Debus, K.L., Guchhait, N., and Zehnacker, A. (2009) Chirality-dependent hydrogen bond direction in jet-cooled (*S*)-1,2,3,4-tetrahydro-3-isoquinoline methanol (THIQM): IR-ion dip vibrational spectroscopy of the neutral and the ion. *Physical Chemistry and Chemical Physics*, **11**, 5160–5169.
- Mamyrin, B.A., Karataev, V.I., Shmikk, D.V., and Zagulin, V.A. (1973) The mass-reflectron, a new nonmagnetic time-of-flight mass spectrometer with high resolution. *Soviet Physics-JETP*, **37**, 45–48.
- Marquardt, R., Gonçalves, N.S., and Sala, O. (1995) Overtone spectrum of the CH chromophore in CHI₃. *Journal of Chemical Physics*, **103**(19), 8391–8403.
- Marquardt, R. and Quack, M. (1991) The wave packet motion and intramolecular vibrational redistribution in CHX₃ molecules under infrared multiphoton excitation. *Journal of Chemical Physics*, **95**(7), 4854–4876.
- Marquardt, R. and Quack, M. (2001) Energy redistribution in reacting systems, in Moore, J., Spencer, N. (eds), *Encyclopedia of Chemical Physics and Physical Chemistry*, IOP Publishing, Bristol, pp. 897–936. Vol. 1 (Fundamentals) Chapter A.3.13.
- Marquardt, R. and Quack, M. (2011) Global analytical potential energy surfaces for high resolution molecular spectroscopy and reaction dynamics, in *Handbook of High-resolution Spectroscopy*, Quack, M. and Merkt, F. (eds), John Wiley & Sons, Chichester, UK.
- Marquardt, R., Quack, M., Thanopoulos, I., and Luckhaus, D. (2003) Tunneling dynamics of the NH chromophore in NHD₂ during and after coherent infrared excitation. *Journal of Chemical Physics*, **118**(2), 643–658.
- Maslen, P.E., Handy, N.C., Amos, R.D., and Jayatilaka, D. (1992) Higher analytic derivatives. IV. Anharmonic effects in the benzene spectrum. *Journal of Chemical Physics*, **97**(6), 4233–4254.
- Mecke, R. (1955) Dipolmoment und chemische Bindung. *Zeitschrift für Elektrochemie*, **54**, 38–42.
- de Meer, K., Roef, M.J., Kulik, W., and Jakobs, C. (1999) In vivo research with stable isotopes in biochemistry, nutrition and clinical medicine: An overview. *Isotopes in Environmental and Health Studies*, **35**, 19–37.
- Merker, U., Srivastava, H.K., Callegari, A., Lehmann, K.K., and Scoles, G. (1999) Eigenstate resolved infrared and millimeter-wave-infrared double resonance spectroscopy of methylamine in the N-H stretch first overtone region. *Physical Chemistry and Chemical Physics*, **1**, 2427–2433.
- Merkt, F. (1997) Molecules in high Rydberg States. *Annual Reviews in Physical Chemistry*, **48**, 675–709.
- Merkt, F. and Quack, M. (2011) Molecular quantum mechanics and molecular spectra, molecular symmetry, and interaction of matter with radiation, in *Handbook of High-resolution Spectroscopy*, Quack, M. and Merkt, F. (eds), John Wiley & Sons, Ltd., Chichester, UK.
- Meshulach, D. and Silberberg, Y. (1999) Coherent quantum control of multiphoton transitions by shaped ultrashort optical pulses. *Physical Review A*, **60**, 1287.
- Miani, A., Cané, E., Palmieri, P., Trombetti, A., and Handy, N.C. (2000) Experimental and theoretical anharmonicity for benzene using density functional theory. *Journal of Chemical Physics*, **112**(1), 248–259.
- Miller, D.R. (1988) Free jet sources. in *Atomic and Molecular Beam Methods*, Scoles, G. (ed), Oxford University Press, New York. Chapter 2. Vol. I.
- Mills, I.M. (1988) The interpretation of vibrational overtone spectra observed by Fourier transform and laser photoacoustic spectroscopy, in *Frontiers of Laser Spectroscopy of Gases*, Alves, A.C.P., Brown, J.M., Hollas, J.M. (eds), Kluwer Academic Publishers, Dordrecht, pp. 461–489.
- Miloglyadov, E., Kulik, A., Quack, M., and Seyfang, G. (2010) Supersonic jet isotope selective infrared spectroscopy of the second overtone polyad of the NH-stretching vibration in C₆H₅NH₂, C₆D₅NH₂ and C₆H₅NDH, in *Contributions of the 17th Symposium on Atomic, Cluster and Surface Physics 2010 (SASP 2010), Obergurgl Austria, 24 to 29 January 2010, ISBN 978-3-902719-52-2*, Milewski, I., Kendl, A., Scheier, P. (eds), Innsbruck University Press (IUP), Innsbruck, pp. 216–219.
- Miloglyadov, E., Quack, M., and Seyfang, G. (2008) Fundamental and first overtone spectra of the CH-stretching vibration of ¹²C₆HD₅ and of ¹³C¹²C₅HD₅ measured by the ISOS method. Contributions. 16th Symposium on Atomic and Surface Physics and related topics(SASP2008), Les Diablerets, January 20–25, ISBN 978-3-902571-31-1, pp. 184–187.
- Minck, R.W., Terhune, R.W., and Rado, W.G. (1963) Laser-stimulated Raman effect and resonant four-photon interactions in gases H₂, D₂, and CH₄. *Applied Physics Letters*, **3**(10), 181–184.
- Minehardt, T.J., Adcock, J.D., and Wyatt, R.E. (1999) Energy partitioning and normal mode analysis of IVR in 30-mode benzene: overtone relaxation for CH($\nu = 2$). *Chemical Physics Letters*, **303**, 537–546.

- Minehardt, T.J. and Wyatt, R.E. (1998) Quasi-classical dynamics of benzene overtone relaxation on an ab initio force field: 30-mode models of energy flow and survival probability for CH($v = 2$). *Chemical Physics Letters*, **295**, 373–379.
- Minehardt, T.J. and Wyatt, R.E. (1999) Quantum dynamics of intramolecular vibrational energy redistribution for initially excited CC ring modes in 30-mode benzene. *Chemical Physics Letters*, **312**, 485–493.
- Minejima, C., Ebata, T., and Mikami, N. (2002) C–H stretching vibrations of benzene and toluene in their S_1 states observed by double resonance vibrational spectroscopy in supersonic jets. *Physical Chemistry Chemical Physics*, **4**, 1537–1541.
- Muenter, J.S., Rebstein, J., Callegari, A., and Rizzo, T.R. (1999) Photodissociation detection of microwave transitions in highly excited vibrational states. *Journal of Chemical Physics*, **111**(8), 3488–3493.
- Nesbitt, D.J. and Field, R.W. (1996) Vibrational energy flow in highly excited molecules: role of intramolecular vibrational redistribution. *Journal of Physical Chemistry*, **100**, 12735–12756.
- Omi, T., Shitomi, H., Sekiya, N., Takazawa, K., and Fujii, M. (1996) Nonresonant ionization detected IR spectroscopy for the vibrational study in a supersonic jet. *Chemical Physics Letters*, **252**(3–4), 287–293.
- Ottiger, P., Frey, J.A., Frey, H.-M., and Leutwyler, S. (2009) Jet-cooled 2-Aminopyridine dimer: conformers and infrared vibrational spectra. *Journal of Physical Chemistry A*, **113**(18), 5280–5288.
- Outhouse, A., Lawrence, P., Gauthier, M., and Hackett, P.A. (1985) Laboratory scale-up of 2-stage laser chemistry separation of C-13 From CF_2HCl . *Applied Physics B*, **36**(2), 63–75.
- Page, R.H., Shen, Y.R., and Lee, Y.T. (1987) Highly resolved spectra of local modes of benzene. *Physical Review Letters*, **59**(12), 1293–1296.
- Page, R.H., Shen, Y.R., and Lee, Y.T. (1988a) Infrared–ultraviolet double resonance studies of benzene molecules in a supersonic beam. *Journal of Chemical Physics*, **88**(9), 5362–5376.
- Page, R.H., Shen, Y.R., and Lee, Y.T. (1988b) Local modes of benzene and benzene dimer, studied by infrared–ultraviolet double resonance in a supersonic beam. *Journal of Chemical Physics*, **88**(8), 4621–4636.
- Painter, P.C. and Koenig, J.L. (1977) Liquid phase vibrational spectra of ^{13}C -isotopes of benzene. *Spectrochimica Acta, Part A*, **33**(11), 1003–1018.
- Papoušek, D. and Aliev, M.R. (1982) *Molecular Vibrational-Rotational Spectra*, Elsevier Scientific Publishing Company, Prag.
- Peyerimhoff, S., Lewerenz, M., and Quack, M. (1984) Spectroscopy and dynamics of the isolated CH chromophore in CD_3H : experiment and theory. *Chemical Physics Letters*, **109**(6), 563–569.
- Pietilä, J., Horneman, V.M., and Anttila, R. (1999) High resolution infrared study of the parallel band ν_3 of chloroform $CH^{35}Cl_3$. *Molecular Physics*, **96**, 1449–1456.
- Plíva, J., Johns, J.W.C., and Goodman, L. (1991) Infrared bands of isotopic benzenes: ν_{13} and ν_{14} of $^{13}C_6D_6$. *Journal of Molecular Spectroscopy*, **148**(2), 427–435.
- Plíva, J. and Pine, A.S. (1982) The spectrum of benzene in the 3- μm region: The ν_{12} fundamental band. *Journal of Molecular Spectroscopy*, **93**(1), 209–236.
- Plíva, J. and Pine, A.S. (1987) Analysis of the 3- μm bands of benzene. *Journal of Molecular Spectroscopy*, **126**(1), 82–98.
- Pribble, R.N. and Zwier, T.S. (1994) Size-specific infrared spectra of Benzene-(H_2O) $_n$ clusters ($n = 1$ through 7): evidence for noncyclic (H_2O) $_n$ structures. *Science*, **265**, 75–79.
- Pulay, P., Fogarasi, G., and Boggs, J.E. (1981) Force field, dipole moment derivatives, and vibronic constants of benzene from a combination of experimental and ab initio quantum chemical information. *Journal of Chemical Physics*, **74**(7), 3999–4014.
- Putter, M., von Helden, G., and Meijer, G. (1996) Mass selective infrared spectroscopy using a free electron laser. *Chemical Physics Letters*, **258**(1–2), 118–122.
- von Puttkamer, K., Dübal, H.R., and Quack, M. (1983a) Temperature-dependent infrared band structure and dynamics of the CH chromophore in $C_4F_9-C\equiv C-H$. *Chemical Physics Letters*, **95**(4–5), 358–362.
- von Puttkamer, K., Dübal, H.R., and Quack, M. (1983b) Time-dependent processes in polyatomic molecules during and after intense infrared irradiation. *Faraday Discussions of the Chemical Society*, **75**(75), 197–210.
- von Puttkamer, K. and Quack, M. (1989) Vibrational spectra of $(HF)_2$, $(HF)_n$ and their D-isotopomers: Mode selective rearrangements and nonstatistical unimolecular decay. *Chemical Physics*, **139**(1), 31–53.
- Pyka, J. and Kreglewski, M. (1985) Vibration-inversion-torsion-rotation Hamiltonian for aniline. *Journal of Molecular Spectroscopy*, **109**(2), 207–220.
- Quack, M. (1977) Detailed symmetry selection rules for reactive collisions. *Molecular Physics*, **34**(2), 477–504.
- Quack, M. (1978) Theory of unimolecular reactions induced by monochromatic infrared radiation. *Journal of Chemical Physics*, **69**(3), 1282–1307.
- Quack, M. (1981a) Discussion contributions on high resolution spectroscopy. (On normal, local, and global vibrational states). *Faraday Discussions of the Chemical Society*, **71**, 359–364.
- Quack, M. (1981b) Statistical mechanics and dynamics of molecular fragmentation. *Nuovo Cimento della Società Italiana di Fisica, B*, **63**(1), 358–376.
- Quack, M. (1983a) Detailed symmetry selection rules for chemical reactions, in *Studies in Physical and Theoretical Chemistry*, Maruani, J. and Serre, J. (eds), *Symmetries and Properties of Non - Rigid Molecules: A Comprehensive Survey, Proceedings of an International Symposium, Paris, France, 1–7 July 1982*, Elsevier Scientific Publishing Company, Amsterdam, pp. 355–378, Vol. 23.
- Quack, M. (1983b) Some kinetic and spectroscopic evidence on intramolecular relaxation processes in polyatomic molecules, in *Energy Storage and Redistribution in Molecules*, Hinze, J. (ed), Plenum Publishing Corporation, New York, pp. 493–511.
- Quack, M. (1985) On the densities and numbers of rovibronic states of a given symmetry species: rigid and nonrigid molecules, transition states, and scattering channels. *Journal of Chemical Physics*, **82**(7), 3277–3283.

- Quack, M. (1986) On the measurement of the parity violating energy difference between enantiomers. *Chemical Physics Letters*, **132**(2), 147–153.
- Quack, M. (1989a) Infrared laser chemistry and the dynamics of molecular multiphoton excitation. *Infrared Physics*, **29**(2–4), 441–466.
- Quack, M. (1989b) Structure and dynamics of chiral molecules. *Angewandte Chemie (International ed. in English)*, **28**(5), 571–586.
- Quack, M. (1990) Spectra and dynamics of coupled vibrations in polyatomic molecules. *Annual Reviews in Physical Chemistry*, **41**, 839–874.
- Quack, M. (1993) Molecular quantum dynamics from high resolution spectroscopy and laser chemistry. *Journal of Molecular Structure*, **292**, 171–195.
- Quack, M. (1995a) IR laser chemistry. *Infrared Physical Technology*, **36**(1), 365–380.
- Quack, M. (1995b) Molecular femtosecond quantum dynamics between less than yoctoseconds and more than days: experiment and theory, in *Femtosecond Chemistry*, Manz, J., Woeste, L. (eds), Verlag Chemie, Weinheim, pp. 781–818.
- Quack, M. (1995c) Molecular infrared spectra and molecular motion. *Journal of Molecular Structure*, **347**, 245–266.
- Quack, M. (1998) Multiphoton excitation, in *Encyclopedia of Computational Chemistry*, Schleyer, P.v.R., Allinger, N., Clark, T., Gasteiger, J., Kollman, P.A., Schaefer, H.F. III, and Schreiner, P.R. (eds), John Wiley & Sons, Inc., pp. 1775–1791. Vol. 3.
- Quack, M. (1999) Intramolekulare Dynamik: Irreversibilität, Zeitumkehrsymmetrie und eine absolute Moleküluhr. *Nova Acta Leopoldina*, **NF 81**(314), 137–173.
- Quack, M. (2001) Molecules in motion. *Chimia*, **55**(10), 753–758.
- Quack, M. (2002) How important is parity violation for molecular and biomolecular chirality? *Angewandte Chemie (International ed. in English)*, **41**(24), 4618–4630.
- Quack, M. (2003) Molecular spectra, reaction dynamics, symmetries and life. *Chimia*, **57**(4), 147–160.
- Quack, M. (2011) Fundamental symmetries and symmetry violations from high resolution spectroscopy, in *Handbook of High-resolution Spectroscopy*, Quack, M. and Merkt, F. (eds), John Wiley & Sons, Chichester, UK.
- Quack, M. and Kutzelnigg, W. (1995) Molecular spectroscopy and molecular dynamics: theory and experiment. *Berichte der Bunsengesellschaft für Physikalische Chemie*, **99**(3), 231–245.
- Quack, M. and Stockburger, M. (1972) Resonance fluorescence of aniline vapour. *Journal of Molecular Spectroscopy*, **43**(1), 87–116.
- Quack, M. and Stohner, J. (2003) Combined multidimensional anharmonic and parity violating effects in CDBrClF. *Journal of Chemical Physics*, **119**(21), 11228–11240.
- Quack, M. and Stohner, J. (2005) Parity violation in chiral molecules. *Chimia*, **59**(7–8), 530–538.
- Quack, M. and Suhm, M. (1991) Potential energy surfaces, quasiadiabatic channels, rovibrational spectra, and intramolecular dynamics of (HF)₂ and its isotopomers from quantum Monte Carlo calculations. *Journal of Chemical Physics*, **95**(1), 28–59.
- Quack, M. and Willeke, M. (2006) Stereomutation tunneling switching dynamics and parity violation in chlorineperoxide Cl-O-O-Cl. *Journal of Physical Chemistry A*, **110**(9), 3338–3348.
- Quack, M., Humbert, P., and van den Bergh, H. (1980) The dependence of rate coefficients and product yields upon fluence, intensity, and time in unimolecular reactions induced by monochromatic infrared radiation. *Journal of Chemical Physics*, **73**(1), 247–255.
- Quack, M., Stohner, J., and Willeke, M. (2008) High-resolution spectroscopic studies and theory of parity violation in chiral molecules. *Annual Reviews in Physical Chemistry*, **59**, 741–769.
- Rabi, I.I. (1937) Space quantization in a gyrating magnetic field. *Physical Review*, **51**(8), 652–654.
- Rashev, S., Stamova, M., and Djambova, S. (1998a) A quantum mechanical description of vibrational motion in benzene in terms of a completely symmetrized set of complex vibrational coordinates and wave functions. *Journal of Chemical Physics*, **108**(12), 4797–4803.
- Rashev, S., Stamova, M., and Kancheva, L. (1998b) Quantum mechanical study of intramolecular vibrational energy redistribution in the second CH stretch overtone state in benzene. *Journal of Chemical Physics*, **109**(2), 585–591.
- Reddy, K.V., Heller, D.F., and Berry, M.J. (1982) Highly vibrationally excited benzene: overtone spectroscopy and intramolecular dynamics of C₆H₆, C₆D₆, and partially deuterated or substituted benzenes. *Journal of Chemical Physics*, **76**(6), 2814–2837.
- Reimann, B., Buchhold, K., Vaupel, S., and Brutschy, B. (2001) Blue-shift in the frequencies of the CH stretches of chloro- and fluoroform induced by C–H...π hydrogen bonding with Benzene derivatives: the influence of electron donating and withdrawing substituents. *Zeitschrift für Physikalische Chemie*, **215**, 777–793.
- Reisner, D.E., Field, R.W., Kinsey, J.L., and Dai, H.-L. (1984) Stimulated emission spectroscopy: a complete set of vibrational constants for \tilde{X}^1A_1 formaldehyde. *Journal of Chemical Physics*, **80**(12), 5968–5978.
- Riedle, E., Beil, A., Luckhaus, D., and Quack, M. (1994) Sub-Doppler supersonic jet spectra of the coupled 6a₁₀ and 6b₁₀ vibronic bands of the S₁(¹B_{2u}) ← S₀(¹A_{1g}) transition in monodeuterobenzene and their rovibrational analysis. *Molecular Physics*, **81**(1), 1–15.
- Rizzo, T.R., Hayden, C.C., and Crim, F.F. (1983) Product energy partitioning in the decomposition of state-selectively excited HOOH and HOOD. *Faraday Discussions of the Chemical Society*, **75**, 223–237.
- Rothman, L., Gamache, R., Tipping, R., Rinsland, C., Smith, M., Benner, D., Devi, V., Flaud, J.-M., Camy-Peyret, C. Perrin, A. et al. (1992) The HITRAN molecular database: editions of 1991 and 1992. *Journal of Quantitative Spectroscopy & Radiative Transfer*, **48**(5–6), 469–507. (special Issue Conference on Molecular Spectroscopic Databases).
- Rothman, L.S., Jacquemart, D., Barbe, A., Chris Benner, D., Birk, M., Brown, L.R., Carleer, M.R., Chackerian Jr., C., Chance, K., Coudert, L.H., et al. (2005) The HITRAN 2004 molecular spectroscopic database. *Journal of Quantitative Spectroscopy and Radiative Transfer*, **96**(2), 139–204.

- Rumpf, K. and Mecke, R. (1939) Über die Absorptionsspektren einiger Benzolderivate im nahen Ultraroten bei großen Schichtdicken. *Zeitschrift für Physikalische Chemie B*, **44**, 299–312.
- Ruoff, A. and Bürger, H. (1970) Schwingungsspektren und Kraftkonstanten symmetrischer Kreisel-I. HCCl_3 und DCCl_3 . *Spectrochimica Acta, Part A*, **26**(4), 989–997.
- Russell, B.R., Edwards, L.O., and Raymond, J.W. (1973) Vacuum ultraviolet absorption spectra of the chloromethanes. *Journal of the American Chemical Society*, **95**, 2129–2133.
- Sakai, M., Ueda, T., Yamanaka, T., and Fujii, M. (2003) Construction of a picosecond time-resolved IR dip spectrometer for studying structures and dynamics of solvated clusters. *Bulletin of the Chemical Society of Japan*, **76**, 509–514.
- Schug, K.P., Wagner, H.G., and Zabel, F. (1979) Gas phase α, α elimination of hydrogen halides from halomethanes. I. Thermal decomposition of CHClF_2 , CHF_3 and CHCl_3 behind shock waves. *Berichte der Bunsengesellschaft für Physikalische Chemie*, **83**, 167–175.
- Scotoni, M., Boschetti, A., Oberhofer, N., and Bassi, D. (1991a) The $3 \leftarrow 0$ CH stretch overtone of benzene: an optothermal study. *Journal of Chemical Physics*, **94**(2), 971–977.
- Scotoni, M., Leonardi, C., and Bassi, D. (1991b) Opto-thermal spectroscopy of the benzene $4 \leftarrow 0$ C–H stretch overtone. *Journal of Chemical Physics*, **95**(11), 8655–8657.
- Segall, J., Zare, R.N., Dübal, H.R., Lewerenz, M., and Quack, M. (1987) Tridiagonal Fermi resonance structure in the vibrational spectrum of the CH chromophore in CHF_3 . II. visible spectra. *Journal of Chemical Physics*, **86**(2), 634–646.
- Settle, R.D.F. and Rizzo, T.R. (1992) CO_2 laser assisted vibrational overtone spectroscopy. *Journal of Chemical Physics*, **97**(4), 2823–2825.
- Seurre, N., Barbu-Debus, K.L., Lahmani, F., Zehnacker-Rentien, A., and Sepiol, J. (2003) Electronic and vibrational spectroscopy of jet-cooled m-cyanophenol and its dimer: laser-induced fluorescence and fluorescence-dip IR spectra in the S_0 and S_1 states. *Chemical Physics*, **295**(1), 21–33.
- Shapiro, M. and Brumer, P.W. (2003) *Principles of the Quantum Control of Molecular Processes*, John Wiley & Sons, Inc., New York.
- Shi, S. and Miller, W.H. (1985) A semiclassical model for intramolecular vibrational relaxation of local mode overtone in polyatomic molecules. *Theoretica Chimica Acta*, **68**, 1–21.
- Shubert, V.A. and Zwier, T.S. (2007) IR-IR-UV Hole-Burning: Conformation Specific IR Spectra in the Face of UV Spectral Overlap. *Journal of Physical Chemistry A*, **111**(51), 13283–13286.
- Sibert, E.L., Hynes, J.T., and Reinhardt, W.P. III (1984a) Classical dynamics of highly excited CH and CD overtones in benzene and perdeuterobenzene. *Journal of Chemical Physics*, **81**(3), 1135–1144.
- Sibert, E.L., Reinhardt, W.P., and Hynes, J.T. III (1984b) Intramolecular vibrational relaxation and spectra of CH and CD overtones in benzene and perdeuterobenzene. *Journal of Chemical Physics*, **81**(3), 1115–1134.
- Sieben, A., Berger, R., Quack, M., and Willeke, M. (2003) Surprisingly large parity violating energy differences in enantiomers which are chiral by isotopic substitution: Theory and initial spectroscopic studies. *Proceedings of 18th Colloquium on High Resolution Spectroscopy (2003)*, Dijon, France, p. 161.
- Sigrist, M.W. (2011) High-resolution infrared laser spectroscopy and gas sensing applications, in *Handbook of High-resolution Spectroscopy*, Quack, M. and Merkt, F. (eds), John Wiley & Sons, Ltd., Chichester, UK.
- Sinclair, W.E. and Pratt, D.W. (1996) Structure and vibrational dynamics of aniline and aniline–Ar from high resolution electronic spectroscopy in the gas phase. *Journal of Chemical Physics*, **105**(18), 7942–7956.
- Snavely, D.L., Walters, V.A., Colson, S.D., and Wiberg, K.B. (1984) FTIR spectrum of benzene in a supersonic expansion. *Chemical Physics Letters*, **103**(5), 423–429.
- Snels, M., Beil, A., Hollenstein, H., and Quack, M. (1997) Excited vibrational states of benzene: High resolution FTIR spectra and analysis of some out-of-plane vibrational fundamentals of $\text{C}_6\text{H}_5\text{D}$. *Chemical Physics*, **225**(1–3), 107–130.
- Snels, M., Beil, A., Hollenstein, H., Quack, M., Schmitt, U., and Damato, F. (1995) Rotational analysis of the ν_1 band of trichlorofluoromethane from high resolution Fourier transform and diode laser spectra of supersonic jets and isotopically enriched samples. *Journal of Chemical Physics*, **103**(20), 8846–8853.
- Snels, M., Hollenstein, H., and Quack, M. (2003) The NH and ND stretching fundamentals of ($^{14}\text{ND}_2\text{H}$). *Journal of Chemical Physics*, **119**(15), 7893–7902.
- Snels, M., Horka-Zelenkova, V., Hollenstein, H., and Quack, M. (2011) High resolution FTIR and diode laser spectroscopy of supersonic jets, in *Handbook of High-resolution Spectroscopy*, Quack, M. and Merkt, F. (eds), John Wiley & Sons, Ltd., Chichester, UK.
- Stanca-Kaposta, E.C. and Simons, J.P. (2011) High-resolution infrared–ultraviolet (IR–UV) double-resonance spectroscopy of biological molecules, in *Handbook of High-resolution Spectroscopy*, Quack, M. and Merkt, F. (eds), John Wiley & Sons, Ltd., Chichester, UK.
- Stohner, J. and Quack, M. (2011) Conventions, symbols, quantities, units and constants for high-resolution molecular spectroscopy, in *Handbook of High-resolution Spectroscopy*, Quack, M. and Merkt, F. (eds), John Wiley & Sons, Ltd., Chichester, UK.
- Sugawara, K., Miyawaki, J., Nakanaga, T., Takeo, H., Lembach, G., Djafari, S., Barth, H.-D., and Brutschy, B. (1996) Infrared depletion spectroscopy of the aniline dimer. *Journal of Physical Chemistry*, **100**, 17145–17147.
- Suzuki, T., Hiroi, M., and Ito, M. (1988) Stimulated emission spectroscopy of jet-cooled polyatomics: $S_1 \rightarrow S_0$ two-color ionization dip spectra of m-fluorotoluene and aniline. *Journal of Physical Chemistry*, **92**, 3774–3778.
- Tamagawa, K., Iijima, T., and Kimura, M. (1976) Molecular structure of benzene. *Journal of Molecular Structure*, **30**(2), 243–253.
- Thakur, S.N., Goodman, L., and Ozkabak, A.G. (1986) The benzene ground state potential surface. I. Fundamental frequencies for the planar vibrations. *Journal of Chemical Physics*, **84**(12), 6642–6656.
- Ticich, T.M., Likar, M.D., Dübal, H.-R., Butler, L.J., and Crim, F.F. (1987) Vibrationally mediated photodissociation

- of hydrogen peroxide. *Journal of Chemical Physics*, **87**(10), 5820–5829.
- Toth, R.A. (1994) Extensive measurements of H₂¹⁶O line frequencies and strengths: 5750 to 7965 cm⁻¹. *Applied Optics*, **33**(21), 4851–4867.
- Tsubomura, H., Kimura, K., Kaya, K., Tanaka, J., and Nagakura, S. (1964) Vacuum ultraviolet absorption spectra of saturated organic compounds with non-bonding electrons. *Bulletin of the Chemical Society of Japan*, **37**, 417–423.
- Wal, R.L.V., Scott, J.L., Crim, F.F., Weide, K., and Schinke, R. (1991) An experimental and theoretical study of the bond selected photodissociation of HOD. *Journal of Chemical Physics*, **94**(5), 3548–3555.
- Warren, W.S., Rabitz, H., and Dahleh, M. (1993) Coherent control of quantum dynamics: the dream is alive. *Science*, **259**, 1581–1589.
- Weber, T. and Neusser, H.J. (1991) Structure of the benzene–Ar₂ cluster from rotationally resolved ultraviolet spectroscopy. *Journal of Chemical Physics*, **94**(12), 7689–7699.
- Weber, T., von Barga, A., Riedle, E., and Neusser, H.J. (1990) Rotationally resolved ultraviolet spectrum of the benzene–Ar complex by mass-selected resonance-enhanced two-photon ionization. *Journal of Chemical Physics*, **92**(1), 90–96.
- Weston, R.E. (1999) Anomalous or mass-independent isotope effects. *Chemical Reviews*, **99**(8), 2115–2136.
- Weston, R.E. (2006) Nonmass-dependent isotope effects, in *Isotope Effects in Chemistry and Biology*, Kohen, A., Limbach, H.-H. (eds), Taylor & Francis, Boca Raton, FL, pp. 361–386. Chapter 12.
- White, J.C. (1987) Stimulated raman scattering, in *Tunable Lasers. Vol. 59 of "Topics in Applied Physics"*, Mollenauer, L.F., White, J. (eds), Springer-Verlag, New York, pp. 115–207. Chapter 4.
- Widmer, R. (1989) *Quantitative Untersuchungen zur ¹²C/¹³C-Isotopentrennung mit Hilfe der Infrarot-Laserchemie*, Ph.D. thesis, ETH Zürich.
- Wiley, W.C. and McLaren, I.H. (1955) Time-of-flight mass spectrometer with improved resolution. *Review of Scientific Instruments*, **26**(12), 1150–1157.
- William, H., Green, J., Lawrance, W.D., and Moore, C.B. (1987) Kinetic anharmonic coupling in the trihalomethanes: a mechanism for rapid intramolecular redistribution of CH stretch vibrational energy. *Journal of Chemical Physics*, **86**(11), 6000–6011.
- Wilson, E.B. (1934a) The normal modes and frequencies of vibration of the regular plane hexagon model of the benzene molecule. *Physical Review*, **45**(10), 706–714.
- Wilson, E.B. (1934b) A partial interpretation of the Raman and infrared spectra of benzene. *Physical Review*, **46**(2), 146–147.
- Wilson, E.B. Jr, Decius, J., and Cross, P.C. (1955) *Molecular Vibrations. The Theory of Infrared and Raman Vibrational Spectra*, McGraw-Hill Inc., New York.
- Witte, T., Hornung, T., Windhorn, L., Proch, D., de Vivie-Riedle, R., Motzkus, M., and Kompa, K.L. (2003) Controlling molecular ground-state dissociation by optimizing vibrational ladder climbing. *Journal of Chemical Physics*, **118**(5), 2021–2024.
- Wolfsberg, M. (2006) Comments on selected topics in isotope theoretical chemistry, in *Isotope Effects in Chemistry and Biology*, Kohen, A., Limbach, H.-H. (eds), Taylor & Francis, Boca Raton, FL, pp. 89–118. Chapter 3.
- Wong, J.S., William, H., Green, J., Cheng, C., and Moore, C.B. (1987) Coupling of CH stretching and bending vibrations in trihalomethanes. *Journal of Chemical Physics*, **86**(11), 5994–5999.
- Wörner, H.J. and Merkt, F. (2011) Fundamentals of electronic spectroscopy, in *Handbook of High-resolution Spectroscopy*, Quack, M. and Merkt, F. (eds), John Wiley & Sons, Chichester, UK.
- Yang, X., Felder, P., and Huber, J.R. (1994) Photodissociation of the CHFCl₂ and CHCl₃ molecules and the CHCl₂ radical in a beam at 193 nm. *Chemical Physics*, **189**(1), 127–136.
- Zhang, Y. and Marcus, R.A. (1992) Intramolecular dynamics. III. Theoretical studies of the CH overtone spectra for benzene. *Journal of Chemical Physics*, **97**(8), 5283–5295.

RELATED ARTICLES

Albert *et al.* 2011a: **Fundamentals of Rotation–Vibration Spectra**

Albert *et al.* 2011b: **High-resolution Fourier Transform Infrared Spectroscopy**

Bauder 2011: **Fundamentals of Rotational Spectroscopy**
Marquardt and Quack 2011: **Global Analytical Potential Energy Surfaces for High-resolution Molecular Spectroscopy and Reaction Dynamics**

Merkt and Quack 2011: **Molecular Quantum Mechanics and Molecular Spectra, Molecular Symmetry, and Interaction of Matter with Radiation**

Quack 2011: **Fundamental Symmetries and Symmetry Violations from High-resolution Spectroscopy**

Sigrist 2011: **High-resolution Infrared Laser Spectroscopy and Gas Sensing Applications**

Snels *et al.* 2011: **High-resolution FTIR and Diode Laser Spectroscopy of Supersonic Jets**

Stanca-Kaposta and Simons 2011: **High-resolution Infrared–Ultraviolet (IR–UV) Double-resonance Spectroscopy of Biological Molecules**

Stohner and Quack 2011: **Conventions, Symbols, Quantities, Units and Constants for High-resolution Molecular Spectroscopy**

Wörner and Merkt 2011: **Fundamentals of Electronic Spectroscopy**